A Wind Tunnel and Computer Investigation of the Low Speed Aerodynamic Characteristics of the Prone Escape System (PRESS)

THESIS

Lonnie R. Dillon
Captain, USAF

AFIT/GAE/AA/88D-09

DEPARTMENT OF THE AIR FORCE
AIR UNIVERSITY
AIR FORCE INSTITUTE OF TECHNOLOGY

Wright-Patterson Air Force Base, Ohio

AFIT/GAE/AA/88D-09

A Wind Tunnel and Computer Investigation of the Low Speed Aerodynamic Characteristics of the Prone Escape System (PRESS)

THESIS

Lonnie R. Dillon
Captain, USAF

AFIT/GAE/AA/88D-09

Approved for public release; distribution unlimited

AFIT/GAE/AA/88D-09

A Wind Tunnel and Computer Investigation of the Low Speed Aerodynamic Characteristics of the Prone Escape System (PRESS)

THESIS

Presented to the Faculty of the School of Engineering

of the Air Force Institute of Technology

Air University

In Partial Fulfillment of the

Requirements for the Degree of

Master of Science in Aeronautical Engineering

Lonnie R. Dillon, B.S.

Captain, USAF

December, 1988

Acknowledgments

I would like to thank many people who helped me with my research, without whom this thesis would have been much shorter but much less complete. First and foremost I would like to thank my adviser, Lt Col Paul King, whose patience and guidance helped me through rough waters on many occasions, as well as allowing me the freedom of letting me learn from my own mistakes. Dave Driscoll's skill in the model shop helped make the experimental research a possibility, and Jay Anderson and Andy Riemenschneider assembled a brand new pressure measurement system to keep me on schedule in the wind tunnel. The exceptional programming skill of Frank Baxter provided the wind tunnel data acquisition and reduction software. The water tunnel work would have been impossible without the unflagging support of Lieutenant Francis Geiser in the Aeromechanics Division of the Flight Dynamics Laboratory. The computer support for QUADPAN provided by Norma Taylor of the Aircraft Dynamics Branch of the 4950 Test Wing proved indispensable to the analytical portion of this thesis. Finally, the support at home of my wife, [redacted] allowed me the time and motivation to put this thesis together.

Lonnie R. Dillon

Table of Contents

Page

Acknowledgments ii

Table of Contents iii

List of Figures vii

List of Tables ix

List of Symbols ix

Abstract xiii

I. Introduction 1-1

Background 1-1

G-Force Tolerance 1-1

Windblast Protection 1-2

PRESS Design Study 1-4

Research Objectives 1-5

Primary Objective 1-5

Secondary Objective 1-6

II. Experimental Model Designs 2-1

Wind Tunnel Model 2-1

Precision of Construction 2-1

Scale Requirements 2-2

Onboard Instrumentation 2-3

Tunnel Mounting 2-3

Materials 2-5

Page

Final Design 2-5

Water Tunnel Model 2-7

III. Wind Tunnel Testing
Procedures and Data Reduction 3-1

Facility Description 3-1

Instrumentation 3-1

Flow Angles and Coordinate System 3-2

Trim Attitude 3-4

Model Test Configurations 3-4

Model Orientation 3-6

Stability Fins 3-6

Pressure Port Layout 3-8

Test Procedure 3-9

Data Reduction 3-9

Velocity Scaling 3-10

Wind Tunnel Corrections 3-11

Dimensionless Coefficients 3-12

Center of Gravity Considerations 3-13

IV. Wind Tunnel Test Results 4-1

Force and Moment Data 4-1

Longitudinal Forces and Moments 4-1

Lateral Forces and Moments 4-6

Pressure Data 4-8

Stability Augmentation Effectiveness 4-11

Force Effects 4-11

Moment Effects 4-16

Center of Gravity Considerations 4-17

Page

V. Water Tunnel
Flow Visualization 5-1
Facility Description 5-1
Test Configurations 5-1
Data Collection 5-4
Test Procedure 5-4
Results 5-4
Flow Separation 5-7
Vortical Flow 5-7

VI. Computer Analysis 6-1
Modified Newtonian Method 6-1
Subsonic Aerodynamic Paneling Techniques 6-2
Apparent Body Analysis 6-4
QUADPAN Results 6-6
Pressure Data 6-6
Force And Moment Data 6-11

VII. Summary Of Results and Conclusions 7-1
Stability Characteristics of the PRESS 7-1
Computer Analysis Results 7-1
Conclusions 7-2

Bibliography BIB-1

A. Wind Tunnel Program Algorithm A-1
Calibration A-1
Balance Strain Gage Calibration A-1
Sting Bend Calibration A-2
Angle of Attack Calibration A-2

Page

Pressure Calibration A-3

Data Collection A-3

Tare Slope Calculation A-4

Data Reduction A-4

B. Tare Slope Corrections and Calculations B-1

General Form of Tare Equations B-1

Transformation Matrix and Tare Equations B-2

Tare Slope Calculation B-6

Vita VITA-1

List of Figures

Figure		Page
1.1.	Example of Semi-Prone Seating	1-3
1.2.	Prone Escape System (PRESS)	1-4
2.1.	PRESS Pressure port layout	2-4
2.2.	PRESS model design	2-6
3.1.	Body Axis and Flow Angles	3-3
3.2.	Body Axis Force and Moment Definitions	3-5
3.3.	Large Tail	3-7
3.4.	Yaw Fins	3-8
4.1.	PRESS Axial Force as a Function of Angle of Attack	4-2
4.2.	PRESS Normal Force as a Function of Angle of Attack	4-2
4.3.	PRESS Lift as a Function of Angle of Attack	4-3
4.4.	PRESS Drag as a Function of Angle of Attack	4-3
4.5.	PRESS Pitching Moment as a Function of Angle of Attack	4-4
4.6.	PRESS Side Force as a Function of Sideslip	4-7
4.7.	PRESS Rolling Moment as a Function of Sideslip	4-7
4.8.	PRESS Yawing Moment as a Function of Sideslip	4-8
4.9.	Cowling Pressures as a Function of Angle of Attack	4-10
4.10.	Upper Cowling Pressures as a Function of Angle of Attack	4-10
4.11.	Seat Pan Pressure as a Function of Angle of Attack	4-11
4.12.	Effect of Stability Augmentation Devices on Axial Force	4-12
4.13.	Effect of Stability Augmentation Devices on Normal Force	4-12
4.14.	Effect of Stability Augmentation Devices on Lift	4-13
4.15.	Effect of Stability Augmentation Devices on Drag	4-13

Figure Page

4.16. Effect of Stability Augmentation Devices on Pitching Moment 4-14

4.17. Effect of Stability Augmentation Devices on Side Force 4-14

4.18. Effect of Stability Augmentation Devices on Rolling Moment 4-15

4.19. Effect of Stability Augmentation Devices on Yawing Moment 4-15

4.20. Center of Gravity Forces and Moments 4-18

4.21. CG Locations to Trim PRESS at 35 Degrees 4-19

4.22. Effect of VaryingCG Locations on Pitch Stability (Baseline) 4-20

4.23. CG Locations to Trim PRESS at 35 Degrees with Short Tail 4-22

4.24. Effect of Varying CG Locations on Pitch Stability (Short Tail) 4-23

5.1. Dye Source Locations 5-3

5.2. PRESS Flow field, $\alpha = 52$ deg 5-5

5.3. PRESS Flow field, $\alpha = 70$ deg 5-6

5.4. Lateral Separation Vorticity 5-8

6.1. PRESS Apparent Body Computer Model 6-5

6.2. QUADPAN Pressure Output for Impact Surfaces 6-7

6.3. QUADPAN/Wind Tunnel Comparison of C_p for Front Cowling 6-8

6.4. QUADPAN/Wind Tunnel Comparison of C_p for Bottom Cowling . . . 6-9

6.5. QUADPAN/Wind Tunnel Comparison of C_p for Chamfer 6-10

B.1. Balance Coordinate System B-4

B.2. Weight Induced Moments (Body Coordinates) B-5

List of Tables

Table		Page
2.1.	PRESS Pressure port layout	2-5
A.1.	Angle Spline Tables	A-5

List of Symbols

Symbols

α	Angle of attack, deg
β	Angle of sideslip, deg
γ	Angle of sting prebend, deg
δ	Angle that flow makes with surface plane, deg
Δp	Pressure difference from atmospheric, psf
θ	Yoke pitch angle, deg
μ	Fluid viscosity, lb·sec/ft^2
ν	Fluid kinematic viscosity, μ/ρ, ft^2/sec
ρ	Fluid density, slugs/ft^3
ϕ	Model roll angle, deg
ψ	Yoke yaw angle, deg
a	Speed of sound, ft/sec
a	acceleration, ft/sec/sec
AX	Axial force/gage, lbs
C_D	Coefficient of drag
C_L	Coefficient of lift
C_l	Coefficient of rolling moment
C_M	Coefficient of pitching moment
C_N	Coefficient of yawing moment
C_P	Coefficient of Pressure, $(p - p_s)/q$
C_Y	Coefficient of sideforce
D	Drag

g	Acceleration due to gravity, ft/sec^2
g	Acceleration units measured in "gravities"
K	Modified Newtonian coefficient
L	Reference length, ft
L	Lift
m	Mass, slugs
M	Mach number, V/a
$N1$	Forward normal force/gage, lbs
$N2$	Rearward normal force/gage, lbs
p	pressure, $\frac{1}{2}\rho V^2$, psf
q	Dynamic pressure, $\frac{1}{2}\rho V^2$, psf
R_E	Reynolds number, $\rho V L/\mu$
RM	Rolling moment/gage, ft·lbs
S	Reference area, ft^2
V	Velocity, ft/sec
W	Weight of model, lbs
x	Distance of model CG from BMC along x-axis, ft
y	Distance of model CG from BMC along y-axis, ft
$Y1$	Forward side force/gage, lbs
$Y2$	Rearward side force/gage, lbs
z	Distance of model CG from BMC along z-axis, ft

Axis Systems

XYZ	Wind tunnel coordinates, (wind axes)
$X_B Y_B Z_B$	Balance coordinates, Body coordinates

$X_S Y_S Z_S$ . . . . . Stability axes

$X_W Y_W Z_W$ . . . . . Wind Axes

$X_1 Y_1 Z_1$ . . . . . Intermediate system

$X_2 Y_2 Z_2$ . . . . . Intermediate system

Subscripts

A . . . . . Aerodynamic (sub-subscript)

A . . . . . Axial force (balance)

C . . . . . Corrected

D . . . . . Drag

l . . . . . Roll moment

L . . . . . Lift

M . . . . . Pitch moment

N . . . . . Yaw moment

N . . . . . Normal force, (balance)

Q . . . . . Used when choice of axis unimportant i.e. derivations

S . . . . . Side force (balance)

T . . . . . Total

X . . . . . Axial force (Body)

X . . . . . Used when choice of axis unimportant i.e. derivations

Z . . . . . Normal force (body)

0 . . . . . Constant

Miscellaneous

ACES . . . . . Advanced Concept Ejection Seat

AGSM	Anti-g Straining Manuevers
BMC	Balance moment center
CG	Center of Gravity
CP	Center of Pressure
h-value	Vertical distance from aortic valve to eyes
PRESS	Prone Escape System

Abstract

Due to new design technology, future fighter aircraft will fly at higher g levels than ever before. As a result, a previous preliminary design study was conducted to develop an ejection seat providing higher g-tolerance for the crewmember during maneuvering as well as improved windblast protection during ejection. This seat utilized the crewmember in a prone, or leaning forward, position. The Prone Ejection System (PRESS) was computer simulated at supersonic conditions in the earlier report and found satisfactory. It was the purpose of this research to perform an experimental low speed study of the aerodynamic characteristics of the PRESS. Wind tunnel testing was performed to determine the static stability of the PRESS and measure pressures over the seat. It was determined that static pitch stability did not occur at the desired angle of attack, but could be easily corrected with aerodynamic fins and/or a shift in the center of gravity. Directional stability was also confirmed. In addition, an analytical experiment was performed to determine whether a potential paneling code could be modified to predict flow conditions about the PRESS. An apparent body was constructed by including the regions of flow separation as part of the seat itself. Water tunnel flow visualization was utilized to determine the shape of the apparent body. The computer analysis showed that a paneling code could accurately predict the pressure coefficients on the cowling.

A Wind Tunnel and Computer Investigation of the Low Speed Aerodynamic Characteristics of the Prone Escape System (PRESS)

I. Introduction

Background

The major goal of any air force is to obtain and keep control of the airspace over the land battle and other areas of tactical and strategic importance. Primarily, this means providing pilots with aircraft that are better than potential adversaries in terms of performance and maneuverability. For the United States air forces, the threat of facing a numerically superior enemy has made this goal even more imperative. This realization has driven the American industrial complex and military engineering researchers to develop new technologies to improve the capabilities of today's fighter aircraft. These advanced technologies have had two major ramifications. First, with improved aircraft maneuverability, the level of g-forces encountered by the pilot during air-to-air combat has increased to the point that his tolerance to these forces has become a major limiting factor of the aircraft maneuvering envelope. Secondly, protecting the pilot during ejection has become more difficult. Because of improved aircraft performance, operating envelopes have expanded to higher airspeeds and altitudes, increasing the severity of the environment outside the cockpit.

G-Force Tolerance The improved maneuverability of modern and future fighters has forced engineers to understand the human body's reactions to g-forces and to design seats to increase the human tolerance to them. The basic problem is to maintain the blood flow to the brain and eyes to prevent the pilot from blacking out. Primarily, active and passive are the two methods employed.

Active methods include g-suits and Anti-g Straining Manuevers (AGSM). G-suits provide external pressure to the abdomen and lower limbs, increasing the blood pressure and restricting the flow of blood to the body parts below heart level. This increased

pressure assists the heart in pumping blood to the head. AGSM refers to the pilot's tensing of his abdominal and leg muscles while breathing in short gasps. The breathing pattern increases the chest cavity pressure, and the muscle tensing increases the blood pressure. Combined, the suit and pilot actions can increase g-tolerance to approximately nine g's [4:1.3]. The AGSM requires anticipation by the crew members, however, and is quite fatiguing.

On the other hand, passive techniques require no hardware or effort by the crewmember. In one technique, the body is positioned in the seat to reduce the effort by the heart to pump blood to the head. Reducing the vertical distance between the heart's aortic valve and the head and eyes (h-value) will reduce the required blood pressure. An obvious method of applying this technique is to seat the pilot in a reclined position. However, Reference [4:5.5] showed that the pilot must recline at least 60 degrees before any significant increase in g-tolerance is obtained. At these angles however, the body is extremely susceptible to injury during an ejection. In addition, pilot visibility is severely limited when reclined to such a large angle.

Research in recent years has involved placing the pilot in a semi-prone, or leaning forward, position (see Figure 1.1). The semi-prone position has distinct advantages over the typical reclined position. Primarily, Reference [4] showed that leaning the pilot forward an angle of 35 degrees achieved the same improvement in g-tolerance as reclining the pilot backwards 65 degrees. This allows the pilot to seat in a more compact position, providing more protection in the event of ejection. In addition, this position does not impose visibility restriction on the pilot. In fact, it is easier for the pilot to look directly behind him from the semi-prone position than the reclined position [2], a distinct advantage in an air-to-air combat situation.

Windblast Protection A major danger facing a pilot upon ejection is the windblast. At speeds above 600 knots, the windblast can cause serious injuries. With the increased performance of today's aircraft, the windblast is quite severe, yet ejection seat designs have not kept pace and current seats cannot protect the pilot at the higher speeds. This situation can force a pilot during an emergency to decide whether to eject at too high a

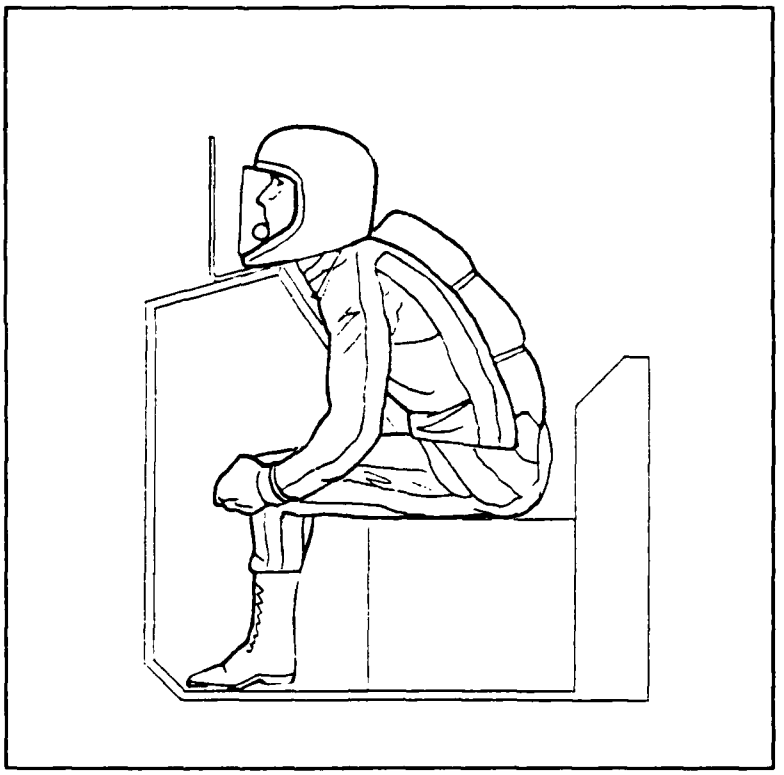

Figure 1.1. Example of Semi-Prone Seating

velocity, or to stay in a damaged and possibly out-of-control aircraft. Both options present serious risks to the pilot.

The most widely used ejection seats in U.S. aircraft, the McDonnell-Douglas Advanced Concept Ejection Seat (ACES) II and the British Martin-Baker MK series, do not shield the pilot from the windblast. The only U.S. aircraft employing windblast protection during ejection at high speeds is the F-111. This aircraft utilizes an escape capsule which completely encloses the flight crew. A capsule system was initially installed on the B-1 bomber as well, but was replaced with ACES II seats on the fourth prototype and all subsequent production aircraft. There were several reasons for the change, including in-flight instability in some flight regimes, maintainability expenses, and overly complex removal procedures for inspection [5:487]. In summary, most modern, high-performance aircraft are still equipped with ACES II and Martin-Baker ejection seats. Therefore, there

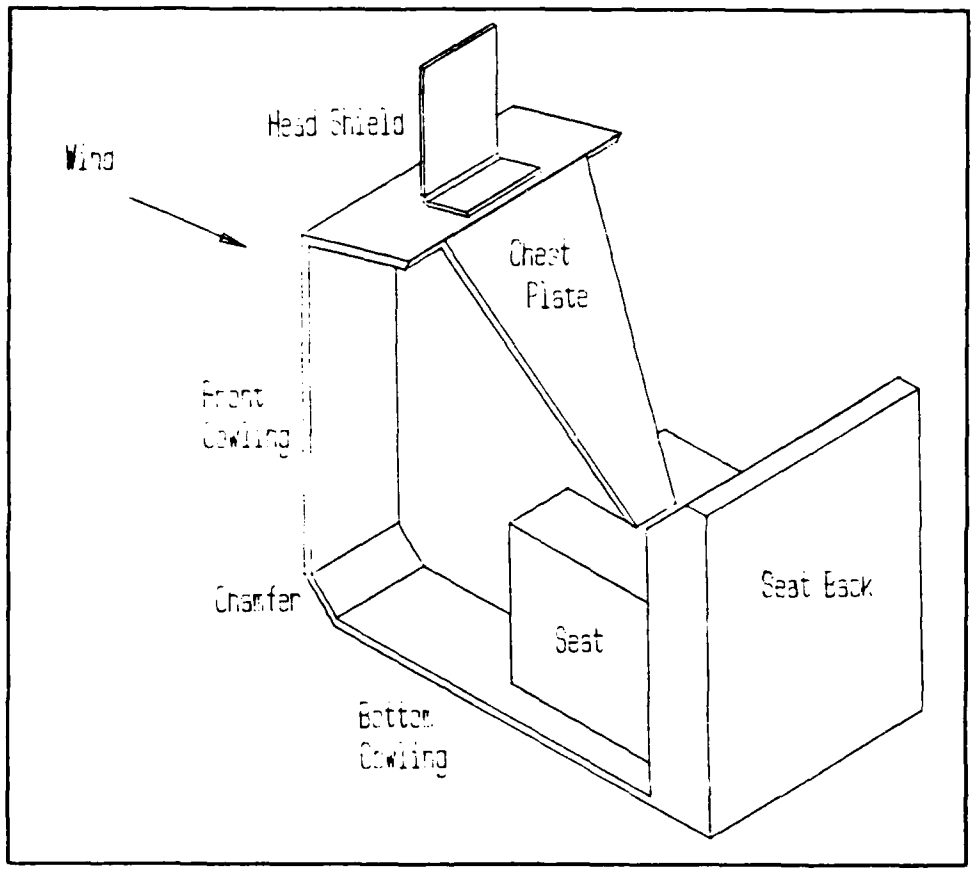

Figure 1.2. Prone Escape System (PRESS)

is a need for ejection seats capable of protecting the crew in an expanded envelope.

PRESS Design Study

In Reference [4], the authors designed an ejection system which enhances g-tolerance as well as incorporates a measure of windblast protection. Their resulting design is the Prone Escape System (PRESS) as shown in Figure 1.2.

In this seat, the crewmember can sit upright during a conventional, cruise-type flight condition, but lean forward against the chest plate at an angle of approximately 35 degrees during high-g maneuvering or an ejection sequence. In addition, once he clears the aircraft during an ejection, the pilot is provided windblast protection from a cowling and a

headshield. The study predicted that if the ideal pitch orientation could be achieved, safe ejections could be made in the PRESS at dynamic pressures, q, up to 2410 psf [4:11.7], where safe is defined as the chance for injury is 5% or less. For comparison, the ACES II is rated only up to approximately 1200 psf [1].

By designing the seat to reduce g-forces effects, the seat also inherently provides the pilot protection against ejection forces. When the spine is parallel to acceleration forces, injury due to spinal compression is most likely to occur. By rotating the spine away from vertical, the chance for injury is reduced. The design study [4] also proposed including propulsion and flight control systems for the PRESS.

Since the PRESS itself will become a flight vehicle upon ejection, it is important that it flies in a stable manner, without tumbling out of control. Thus, the design team performed a computer analysis of a simplified version of the PRESS to determine the aerodynamic characteristics and the in-flight stability for a supersonic, high altitude condition. This analysis, though not complete, showed that the overall design was a viable one. The study recommended that wind tunnel testing be performed to provide further design verification [4:7.1].

Research Objectives

This thesis is divided into two related but distinctly separate objectives. The primary objective concerns the results of wind tunnel testing to determine the baseline characteristics of the PRESS, and to determine various methods of improving aerodynamic performance. The secondary objective of the research concerns construction of a computer model and the investigation of the ability of that model to predict aerodynamic pressures about the seat.

Primary Objective As mentioned earlier, the original design study [4] included a computer analysis of the PRESS to determine the aerodynamic behavior of the seat in supersonic, high altitude flight. This analysis predicted that in supersonic flight the PRESS will stabilize in pitch with the lower cowling pointed 52 degrees above horizontal. The desired pitch angle is 35 degrees, the forward lean angle of the pilot. This pitch angle

aligns the spine perpendicular to the aerodynamic deceleration forces, minimizing the chance of injury to the pilot. The study also predicted that the seat will not tumble out of control. However, due to the nature of aerodynamics, supersonic results cannot be used to predict subsonic behavior. Thus, tests were performed in the AFIT low speed five foot wind tunnel to obtain the PRESS aerodynamic characteristics. Data of prime concern was the in-flight stability of the PRESS, specifically the orientation at which the PRESS exhibited zero aerodynamic moments.

Since early on it appeared that the PRESS would be unstable, the wind tunnel research included the testing of various shapes, sizes, and combinations of stabilizing fins to determine possible improvements in stability. Stabilizing fins are a concept which has been attempted before with some success in other ejection seat programs [7].

Secondary Objective Computer simulation is an important tool to the design engineer. With it, he can make changes to the design and quickly determine the effects of those changes. Without it, he must construct a new test model for each design and perform experiments which are costly in time and money. It is desirable, therefore, to develop a predictive computer model for the PRESS so that expensive experimental testing can be reduced. There has been little success, however, in developing cost effective analytical methods suitable to conceptual design for blunt objects at low speed. This is because the highly complex nature of a subsonic viscous fluid is numerically difficult to predict. Thus, a secondary goal of this thesis was to modify a computer code developed for ideal (inviscid) subsonic flow to predict aerodynamic pressures about the PRESS. The approach included modelling the regions of flow separation behind the seat to create an apparent body which could be analyzed using the aerodynamic paneling code.

To provide aid in modifying the computer model, water tunnel testing was conducted to provide details about the flow pattern, particularly the regions where significant flow separation is occurring.

II. Experimental Model Designs

Before any part of this thesis research could begin, experimental models had to be constructed based on the design from Reference [4]. Two such models were required, one for the wind tunnel and one for the water tunnel. The final model designs as described below were fabricated by the AFIT model shop.

Wind Tunnel Model

The following criterion were considered when designing the wind tunnel model:

- Precision required versus time and cost of construction.
  - Seat.
  - Pilot.
- Scale requirements.
  - Tunnel blockage.
  - Strain gage force limits.
- Any onboard instrumentation i.e. pressure transducer.
- Method for mounting into tunnel.
- Material.

Precision of Construction The final design of the PRESS is presented in Reference [4]. Since the design was a conceptual one, there was no effort expended on an aerodynamic refinement. Thus, the final design was presented with all flat surfaces. The decision was made to duplicate this design exactly for wind tunnel testing for several reasons. One, it was this non-aerodynamic shape that underwent a computer aerodynamic analysis. By attempting a refinement of the external shape, the eventual comparison between the results of this research and the earlier study would lose its utility. Another reason to duplicate the final design exactly was the same reason the original study did not attempt to streamline

the PRESS. To effectively improve the aerodynamics of the system, the engineer needs wind tunnel and flow visualization data. Since this thesis is the first to obtain that data, it seemed futile at best to attempt a refinement a priori. In any event, since this was a proof-of-concept experiment, any refinement seemed unnecessary. Finally, since the design is made up entirely of straight lines and flat surfaces, construction of a similar model was relatively trivial when compared to duplicating a curved, streamlined version. The only part of the model that seemed difficult to reproduce was the pilot figure. To simplify construction and increase geometric similarity, it was decided to use a "Ken" doll to represent the pilot (Ken is a registered trademark of the Mattel Toy Corporation). The doll has approximately the correct anatomical proportions and is approximately one foot tall. Thus, by assuming a six foot tall pilot, use of the doll forced the scaling of the PRESS wind tunnel model to one-sixth scale. As will be shown in the next section, this choice of scale was appropriate for testing. Thus, by using the flat-surface PRESS design and a doll for the pilot, exact geometric similarity with the final PRESS design was achieved at relatively low cost.

Scale Requirements To choose an appropriate scale for a wind tunnel model, one must consider the maximum cross sectional area of the model and the magnitudes of the expected forces. As discussed above, construction considerations dictated a one-sixth scale model. It must be shown, however, that this scale is appropriate for experimental purposes.

Tunnel Blockage A model whose maximum cross sectional area is large relative to the area of the tunnel will cause the airflow to accelerate as it passes around the model. Keeping this ratio below 7.5% [9:371] ensures that this effect is minimal and can be reliably corrected. With the model mounted at a 52 degree pitch angle (see section below on trim selection), the maximum cross sectional area occurs at 26 degrees of sideslip (nose left). With a one-sixth scale PRESS, this value is approximately 44.6 in^2. The tunnel cross sectional area is 2827 in^2. This results in a tunnel blockage of less than two percent, well within limits.

Strain Gage Force Limits The magnitudes of the forces are important because a model that is too large may produce forces that will exceed the rated maximum of the strain gage balance. However, if the model is too small, the aerodynamic forces measured by the strain gage may be hidden by the inherent electrical noise in the data collection system. Since the PRESS is a blunt, non-lifting body, it was assumed the maximum forces that the strain gage balance would experience would be in drag. Assuming a maximum drag coefficient, C_D, of 2.0, (see Chapter III) air density, ρ, of 0.0024 slugs/ft^3, and a maximum tunnel velocity of 220 ft/sec (150 mph), and using the equation

$$D = \frac{1}{2}\rho V^2 C_D S$$

the maximum drag was predicted at 35 pounds. Since the axial gage is rated at 50 pounds of force, a one-sixth scale model is within our limits.

Onboard Instrumentation To perform the computer analysis and comparison, it was necessary to construct the model with pressure ports on the impact surfaces, those surfaces exposed directly to the airflow. A 32 channel ±1 psid pressure transducer was available as part of the wind tunnel instrumentation system. The model was constructed with 51 pressure taps, any 32 of which could be read during a given test. These taps were placed along the cowling surfaces, the headshield, and the sides of the seat, directly below the pilots leg (see Figure 2.1). Those placed along the cowling were staggered in six longitudinal rows, three on each side of the centerline. The purpose of the stagger was to reduce the chances of the smooth flow being disrupted by the by the presence of one port and then immediately encountering another. The ports near the headshield recorded pressures in the vicinity of the pilot's head, and the two taps near the pilots leg indicated the flow velocity behind the cowling. These parameters are important in terms of pilot protection from the windblast.

Since the model was relatively voluminous, the transducer was placed on board the model, directly behind the front cowling, between the pilot's legs.

Tunnel Mounting As discussed in the previous chapter, Reference [4] showed that the PRESS stabilized in pitch in a 52 deg nose up attitude in a supersonic flight condition.

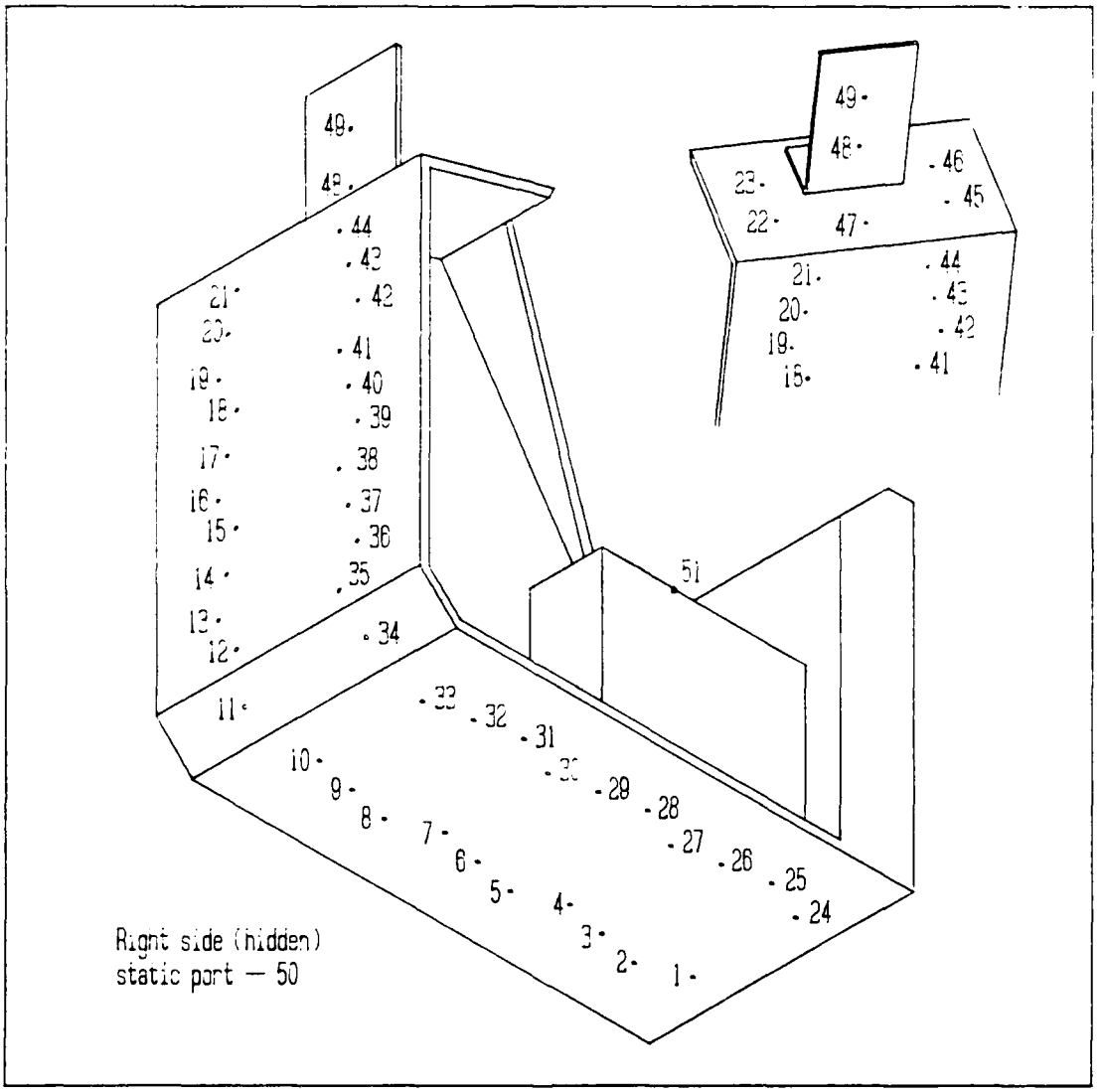

Figure 2.1. PRESS Pressure port layout

It is typical, however, that the pitching tendency of a body in subsonic flow is different than in supersonic flow. Since the PRESS is rather uniquely shaped, there is no method to predict this change. The only option was to assume that there was no change. Therefore, 52 deg was chosen as the baseline pitch angle for testing, and the model was constructed such that the strain gage balance receptacle in the rear of the PRESS model was installed at a 52 deg offset.

Materials The model shop constructed the PRESS model of wood, due to its low cost and the relative ease with which wood can be shaped.

Final Design

The resulting design is shown in Figure 2.2. The precise location of each pressure port is identified in Table 2.1. The locations are based on a standard body axis coordinate system, described in the next chapter.

Table 2.1. PRESS Pressure port layout

Port Number	x	y	z	Port Number	x	y	z
1	-6.333	0.712	0.000	15	0.000	0.712	-2.205
2	-5.757	0.962	0.000	16	0.000	0.962	-2.654
3	-5.181	0.837	0.000	17	0.000	0.837	-3.130
4	-4.605	0.712	0.000	18	0.000	0.712	-3.614
5	-4.029	0.962	0.000	19	0.000	0.962	-4.094
6	-3.453	0.837	0.000	20	0.000	0.837	-4.583
7	-2.877	0.712	0.000	21	0.000	0.712	-5.047
8	-2.301	0.962	0.000	22	-0.579	1.100	-5.575
9	-1.725	0.837	0.000	23	-1.158	1.100	-5.733
10	-1.149	0.712	0.000	47	-0.386	0.000	-5.522
11	-0.250	0.837	-0.250	48	-0.851	0.000	-6.349
12	0.000	0.712	-0.750	49	-0.851	0.000	-7.049
13	0.000	0.962	-1.220	50	-3.942	1.333	-2.455
14	0.000	0.837	-1.709				
Ports 24-46 are mirror images about y of 1-23, and 51 is an image of 50 (See Figure 2.1)							
Origin is located on PRESS centerline at intersection of lower and front cowling (extended), using standard body axis system.							

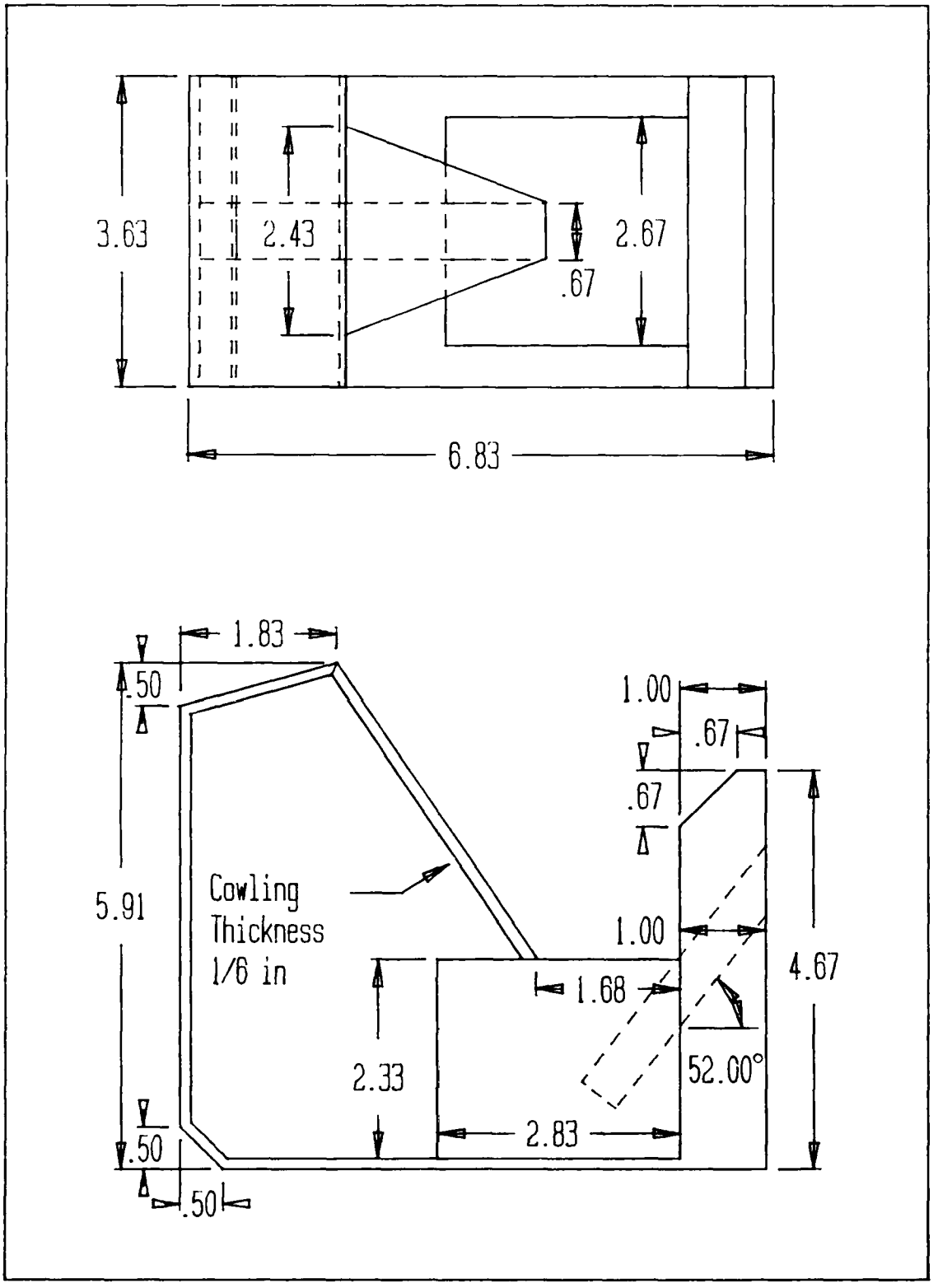

Figure 2.2. PRESS model design

Water Tunnel Model

Although the water tunnel has only a 2 × 2 ft square test section, the water tunnel model was built with the same dimensions as the wind tunnel model described above to expedite construction. This was larger than typical models, causing some constriction of the streamlines near the tunnel walls. However, since this study was more interested in flow trends rather than actual data, the larger model was satisfactory. This also allowed the water model to use the same "Ken" doll as the pilot, maintaining geometric similarity. The model was constructed of plexiglass to better withstand the environment within the water tunnel.

III. Wind Tunnel Testing

Procedures and Data Reduction

Facility Description

The Air Force Institute of Technology Department of Aeronautics and Astronautics currently maintains a low speed wind tunnel facility, located in Bldg 19, Area B, on Wright-Patterson AFB. The primary function of the wind tunnel is to support student thesis projects, although the facility is often used by the Air Force Flight Dynamics Laboratory when available. It is an open circuit, continuous flow type tunnel with a closed test section. The test section is five feet in diameter with a length of eighteen feet and a contraction ratio of 3.7 to 1. The wooden tunnel, including intake and diffuser, is located in a large building which provides a double return for the air. Tunnel air flow is induced by two 12 foot counterrotating fans driven by two sets of two 400 horsepower direct current motors. Total pressure is atmospheric, with static pressure measured by eight sets of static ports located 30 inches from the tunnel entrance and 11 feet from the test section. The tunnel is capable of a Mach number of approximately 0.26 and a Reynolds number of approximately 1.9×10^6 per foot, each parameter to be defined later in the chapter. The tunnel is currently equipped with a sting-type model support, with ranges of angle of attack from -6 to +26 degrees, and sideslip angles up to ± 6 degrees.

Instrumentation For data collection, the tunnel is equipped with:

- Digital data acquisition system, including a Z-248 computer for data reduction and presentation.
- A six component strain gage balance system.
- A three component wire balance system (not used but available if needed)
- Conventional and electrical pressure sensors.
- Conventional temperature sensors.
- A two channel hot-wire anemometer system.
- A house air supply system for studies requiring blowing.

The six components of the strain gage and their maximum ranges are:

- Two normal force ($\approx$ lift) gages of 100 lbs each.
- Two side force gages of 50 lbs each.
- One axial force ($\approx$ drag) gage of 50 lbs.
- One rolling moment gage of 40 in·lbs.

The electrical pressure system was also utilized. This system uses a 32 channel pressure transducer with a measurement range of ± 1 pound per square inch (differential).

In addition to the hardware, the computer software is currently under a complete revision. The purpose of this is threefold. First, an influx of new data collection equipment rendered the old program obsolete. Second, the department has in the past been highly dependant upon the Flight Dynamics Laboratory for technical expertise. By developing new software, the facility can be self-supporting. Third, the new program is carefully structured to cater to the tunnel's unique usage as both an educational as well as a research facility. The new code will allow the researcher to quickly perform testing and obtain data without having to develop excessive programming routines. The code is flexible enough however to allow the student to add modules and/or modify existing routines to perform specialized tasks. A functional description of this program, and improvements and corrections to the code by the author, can be found in the appendices.

Flow Angles and Coordinate System

It is important at this time to introduce the coordinate system we will use as reference for the aerodynamic forces and moments, and define the angles which determine the PRESS's orientation in the windstream.

Using standard notation, $X_B Y_B Z_B$ will refer to a coordinate system which is attached to the vehicle, where X is outward normal to the front cowling, Z is outward normal to the bottom cowling, and Y forms a dextral set by pointing to the pilots right. This is shown in Figure 3.1. Note that X and Z form the plane of symmetry. In addition, two more axis systems are typically used in stability and performance analysis [9:425]. By rotating the

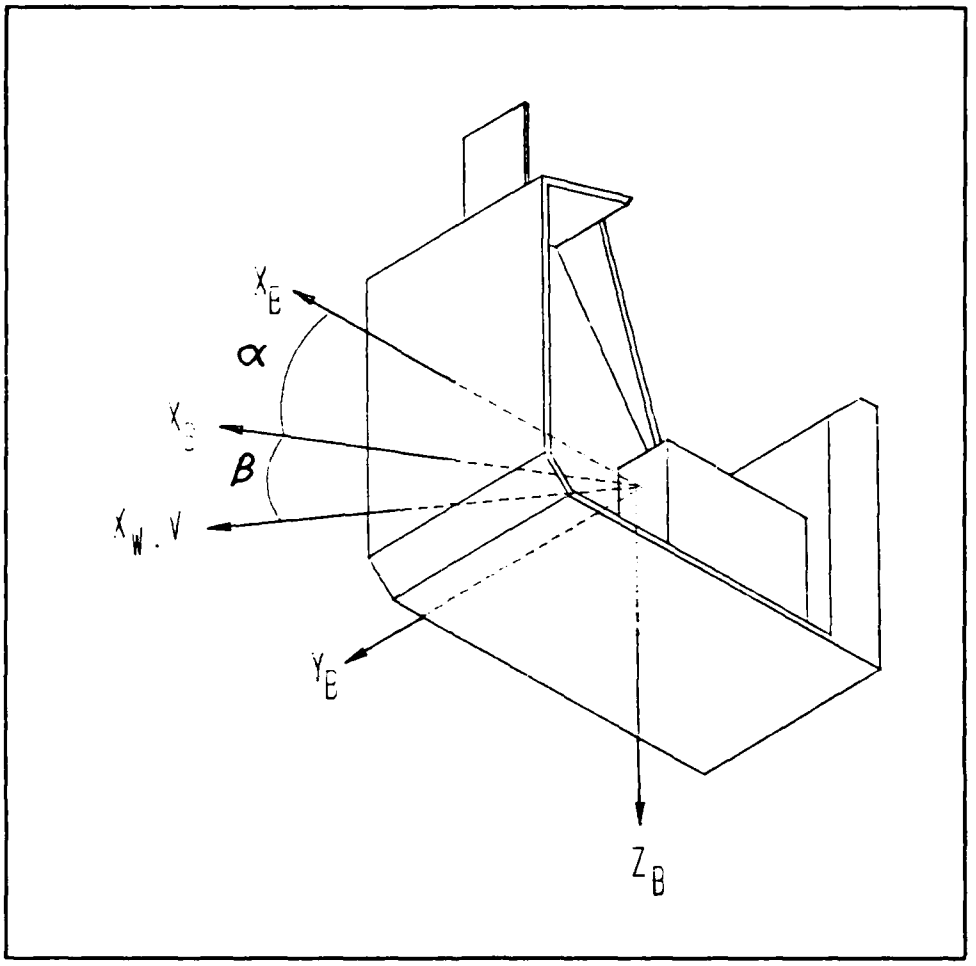

Figure 3.1. Body Axis and Flow Angles

body axis about the Y axis until the velocity vector $\vec{V}$ is in the XY plane, the stability axis system is created, identified by $X_S Y_S Z_S$. This is the standard axis system used to quantify aerodynamic forces and moments. The angle rotated is defined as the angle of attack, α, and is shown in Figure 3.1. The third commonly used axis system is the wind axis system. In this system, the axes are aligned with X pointing directing into the windstream and the other axes oriented to maintain the dextral set. This system, $X_W Y_W Z_W$, is obtained by rotating the $X_S Y_S Z_S$ system about the Z axis an angle β. This angle is called the sideslip angle and is defined as positive when the airstream is wetting the right side of the vehicle. β can also be defined as the angle between the velocity vector and the plane of symmetry

of the PRESS. This angle is shown in Figure 3.1. This thesis will present the final data in both the body system and in the stability system. The body system is important because that is the frame of reference of the passenger. The stability axis system, however, allows an easier interpretation of the seat's motion in the windstream.

The forces measured in the body frame of reference are the axial, F_X, side, F_Y, and normal, F_Z, along the positive X_B, Y_B, and Z_B axes, respectively (see Figure 3.2). The aerodynamic moments are defined as the pitching moment, M_M, rolling moment, M_l, and the yawing moment, M_N. They are defined as positive in accordance with the right hand rule about the X_B, Y_B, and Z_B axes, respectively (see Figure 3.2). Note that roll moment is identified as a lower case "L" instead of upper case. This is to avoid confusion with the lift force which will be defined next.

In addition to the forces identified earlier, two more must be included. In the stability axes, lift and drag are used in place of F_Z and F_X, respectively, which are equal in magnitude but opposite in direction to F_Z and F_X transformed into the stability reference frame. They are identified with the symbols L and D. Thus, F_X, F_Y, and F_Z denote forces in the body frame, and L and D identify stability axis forces, with side force not affected by the coordinate transformation.

Trim Attitude In any flight vehicle, there exists a flight attitude where all aerodynamic moments are zero. This point is called the trim point, and is defined by a unique combination of α and β. If a change in one of those values produces a moment which returns the vehicle to its trim position, the vehicle is statically stable. By plotting the moment as a function of the displaced angle, the slope of the curve at the trim point is a quantitative measure of the static stability of the vehicle about that axis. This technique will be used in the next chapter to analyze the stability characteristics of the PRESS.

Model Test Configurations

The primary objective of this thesis is to determine the aerodynamic coefficients for the PRESS in a low speed flight regime. In particular, the pitch angle for which there exists no pitching moments was to be established. Since early results indicated that this

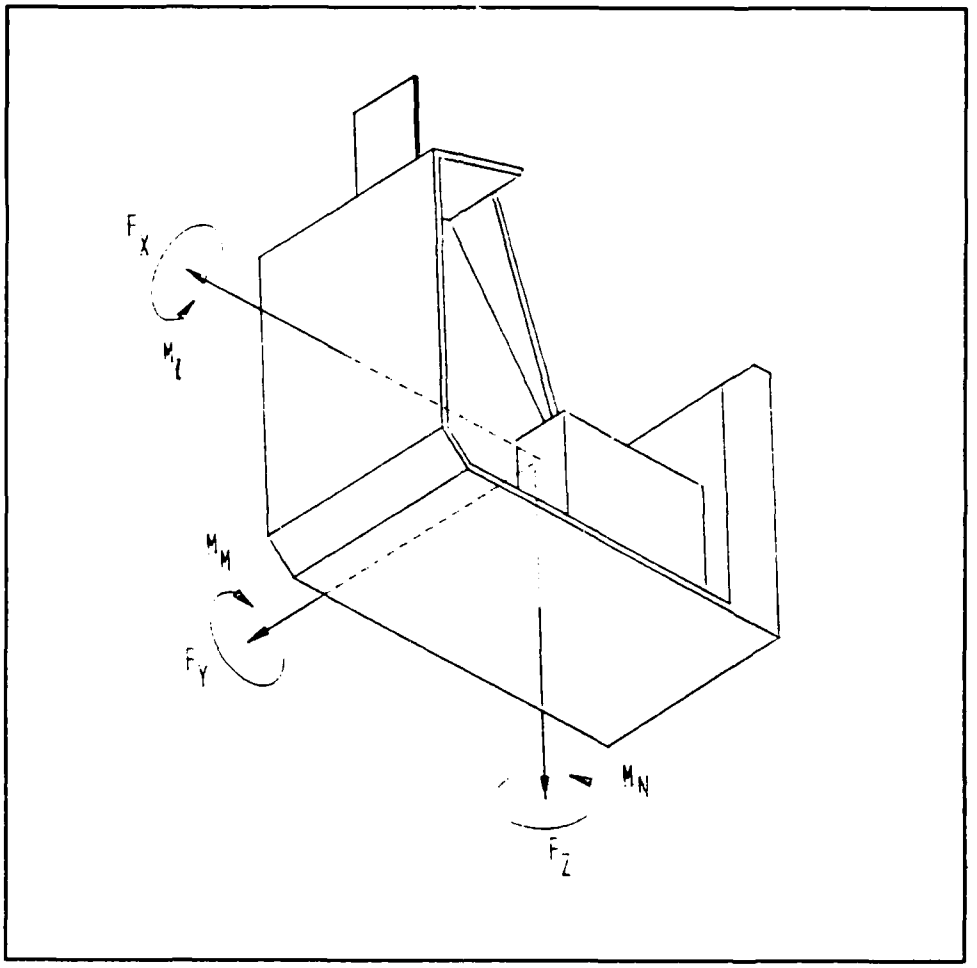

Figure 3.2. Body Axis Force and Moment Definitions

occurred at a pitch angle much higher than desired, $\alpha = 35$ deg, external fins were then tested to improve the pitch angle. Additionally, the degree of lateral stability was also determined, as well as the measured effect of stabilizing fins on the rolling and yawing moments of the PRESS. Finally, a simple pressure survey of the cowling was performed to provide comparative data for the computer analysis of Chapter VI. To obtain all of the necessary data, the PRESS model would have to be tested in a number of configurations. The configuration categories are discussed below.

Model Orientation The sting in the wind tunnel is capable of providing angles of attack from -6 degrees to $+26$ degrees. With the model constructed to provide an initial α of 52 degrees, this provided a test range of $46 \leq \alpha \leq 78$ degrees when the model was mounted upright. To be able to collect data at the ideal pitch angle of 35 degrees, the model and sting were rolled upside down, providing a test angle range of $26 \leq \alpha \leq 58$. This resulted in a total test range of $26 \leq \alpha \leq 78$. In addition, the model was tested inverted in the baseline configuration (no fins - see below) with the sting bent upwards an angle of 30 degrees. This provided a test range of $-4 \leq \alpha \leq 28$. Thus the baseline model was tested at angles of attack from -4 degrees all the way up to 78 degrees.

The sting could also provide sideslip angles of ± 6 degrees. However, the previous study [4] predicted that significant lateral effects didn't appear until β reached 12 degrees. To reach the higher sideslip angles, the model was mounted on the sting and rolled 90 degrees. Then, performing a normal α sweep actually provided a sideslip test range of $-6 \leq \beta \leq 26$ degrees.

Stability Fins To improve the stability characteristics of the PRESS, three types of aerodynamic fins were tested. Two were tails of similar design but differing size designed to decrease the pitching moment of the seat, and the other was a pair of lateral fins to improve the directional stability. To be practical devices, the fins were designed to be large enough to provide adequate forces yet small enough to fit flush on the back of the seat, the theory being that on a full scale PRESS they would unfold into the airstream as dictated by stability requirements. The details and the effects of each fin type are described below.

1. The first fin tested consisted of a simple flat plate extending from the bottom of the seat as shown in Figure 3.3. To fit the design criteria, this fin was sized to the same size as the back of the seat (3.633×4.667 inches) such that it could fold up against it. Aerodynamically, this fin was designed to provide a nose down pitching moment at positive angles of attack and lower the trim angle of attack. For this report, this fin will be referred to as the "large tail".
2. When early testing indicated that the large tail was too large, a smaller one was tested. This "small tail" was three inches in length. This tail reacts similarly to the

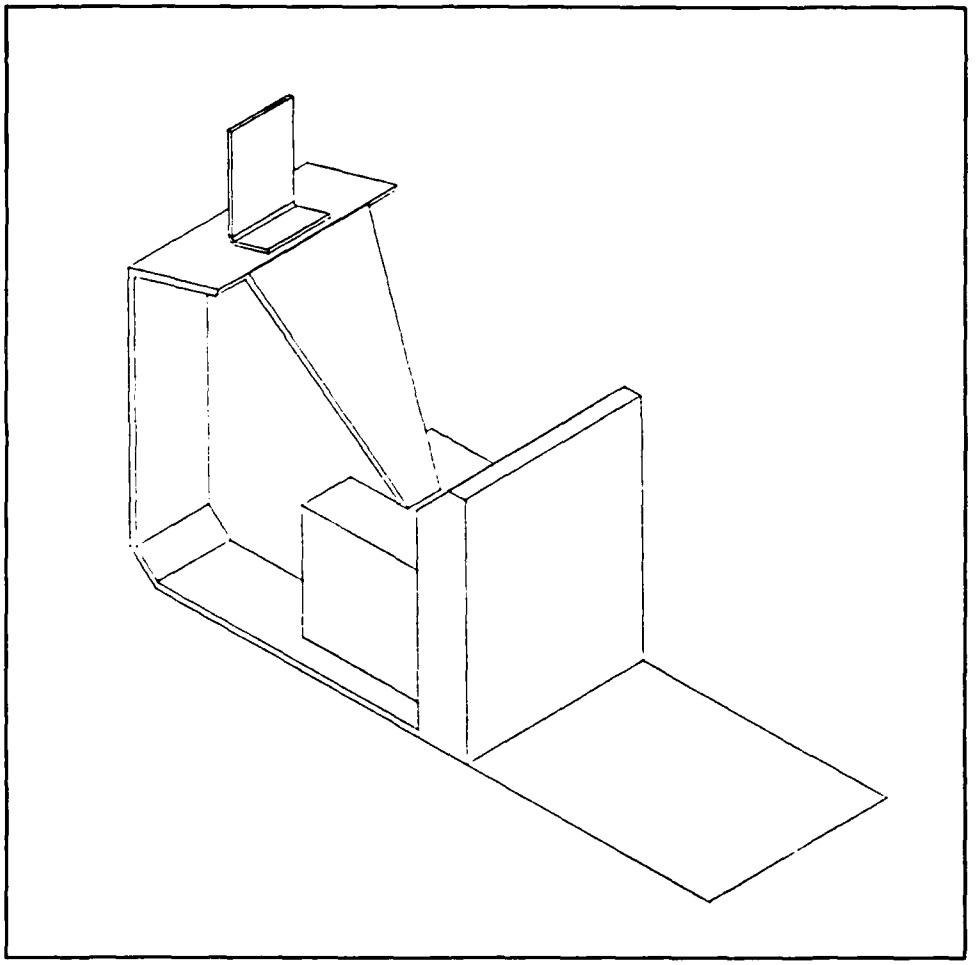

Figure 3.3. Large Tail

larger one but with less magnitude.

3. To improve the directional stability of the PRESS, yaw fins as illustrated in Figure 3.4 were constructed. These served a dual purpose. First, they projected onto the plane of symmetry a large side area behind the center of gravity. This would provide a weathercock-type stability in the same manner as the vertical tail on an aircraft. At positive angles of attack, the geometry of the fins also create a downforce aft of the CG, resulting in a nose up moment. As α increased, so would the moment, until a point when the plane of the fins coincided with the velocity vector. Thus this design

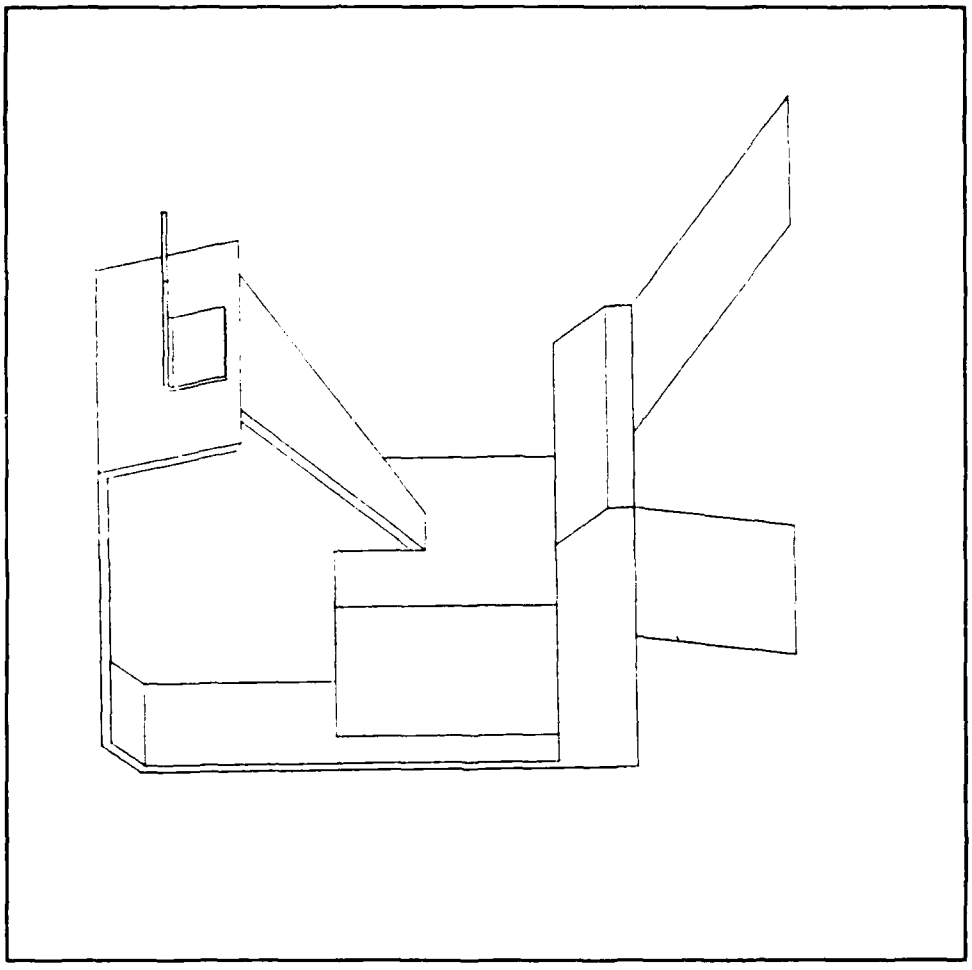

Figure 3.4. Yaw Fins

was destabilizing in pitch. This was done after preliminary test results indicated that the seat stabilized at too low an angle α. This data later turned out to be erroneous, but as will be shown in the next chapter, this was not a serious problem. These fins were also sized to be able to fold inwards and fit within the width of the seatback.

Pressure Port Layout The PRESS model was designed with 49 static pressure ports located along the cowling and headshield, and 1 on each side of the seat. However, the transducer could only operate with a maximum of 32 channels at a time. During preliminary testing, it was found that the ports were reporting symmetrical results within the

range of the statistical variation. Thus for testing, only the ports on the starboard side were used along with the centerline ports. The remaining channels were placed evenly among the port side pressure ports to provide checks on the starboard channels.

Test Procedure

For data collection, five fin configurations were tested. The baseline configuration was with no fins installed. The PRESS was then tested with the large tail, short tail, yaw fins, and finally a combination of the short tail and the yaw fins. The data collection was performed in two parts.

First, tare data was collected as described in Appendix B. This data provides the weight and CG location of the model. For accuracy, two tare runs were conducted for each configuration, and the results were averaged.

The test data was then collected as outlined in Appendix A. Initially, the tests were performed at a dynamic pressure, q, of 20 psf ($\approx$ 88 mph). However, severe model buffet at this wind speed created forces of equal magnitude of the aerodynamic forces, thus the data was extremely scattered. By increasing q to approximately 60 psf ($\approx$ 150 mph), the aerodynamic forces dominated the vibration noise, providing smoother data. The importance of velocity scaling will be discussed later in the chapter. Data points were collected every two degrees of sting angle from -6 to +26. As the sting was returned to zero, check points were conducted at 18, 12, and 0 degrees. These check points served to test repeatability and hysteresis effects. At each point, pressure data was also collected. The pressure transducer reported the difference in the local static pressure from atmospheric pressure in psi.

Data Reduction

The data reduction methodology is described in detail in Appendix A. This section will discuss the rational of the data reduction, i.e. nondimensionalization, velocity scaling, etc .... Also, model center of gravity considerations and the reduction of the pressure data will be discussed.

Velocity Scaling To perform testing that is a true simulation of a full scale model, not only geometric similarity must be achieved, but also flow similarity. Geometric similarity was discussed in Chapter II. Flow similarity is more subtle. The flow of a fluid over a surface has certain characteristics that depend on the viscosity and density of the fluid, and the velocity of the fluid relative to the surface. An example of this is the boundary layer phenomenon. As a plate moves through a fluid, a thin layer of the fluid near the surface is dragged along with it. Some distance L downstream of the plate's leading edge, however, the boundary layer will suddenly become turbulent, increasing the drag on the plate. If, however, a scaled plate is tested with length less than L, and all other condition are the same, this change in flow behavior will not be seen; the drag characteristics will be different than the full scale model. Thus, flow similarity has not been achieved. The characteristics of a flow can be described by a parameter called the Reynolds number, R_E, defined by the equation

$$R_E = \frac{V L \rho}{\mu} \tag{3.1}$$

where

V = Flow velocity

L = Some characteristic length such as wing chord

ρ = Density of fluid

μ = Absolute viscosity of fluid

By keeping R_E constant in the scaled test, one can assure flow similarity. This is because the scaled and actual governing equations are identical in nondimensional form. All flow phenomenon will therefore be appropriately scaled. To hold the Reynolds number constant when L has been reduced, however, requires an increase in velocity or density, hence the term velocity scaling. However, increasing V increases the Mach number, M, the ratio of the velocity to the local speed of sound. Improper scaling of M can distort the results more than a difference in R_E due to flow compressibility effects, so increasing V isn't the answer. Therefore, wind tunnel testing usually requires testing at lower Reynolds numbers of varying values, determining a functional relationship of the result in question to R_E, and extrapolating the data to the full scale R_E.

A flow phenomenon which can be fairly independent of R_E is flow separation, since this is often a function of geometry. As a flow follows a surface, viscous forces keep the fluid attached to the surface. If however, that surface turns away from the flow with a very small radius or a sharp edge, the fluid's momentum will overcome the viscous forces and the flow will detach from the surface.

In the case of the PRESS, it was reasoned that the many sharp edges of the seat would cause extensive flow separation, the effects of which would dominate all other viscous effects. Thus, the testing could be performed at the wind velocity that produced the best data. This meant it was not necessary to conduct a full R_E sensitivity study. Since model vibration at the lower velocity forced repeating the test program at a higher velocity (see page 3-9), a method of checking for R_E sensitivity was available. The lower and higher test velocities corresponded to Reynolds numbers of 360,000 and 600,000, respectively. Even though the data from the low velocity test was scattered from the vibrations, there was no apparent change in the data resulting from the differing R_E.

Wind Tunnel Corrections Reference [9] provides an excellent account of wind tunnel correction factors. These factors account for the presence of the walls, to make the data match freestream conditions. However, these corrections apply primarily to streamlined bodies with little or no flow separation, and the PRESS is not such a body. As a result, these boundary corrections are of questionable quality. In addition, the goal of this research was to establish trends, not hard data. Therefore, all corrections that affected data uniformly were avoided, and the only corrections that were applied were those that affected the drag force only. There were two such corrections: buoyancy and induced drag. Due to a gradual thickening of the boundary layer on the inside of the tunnel, the effective cross section continuously decreased as the flow passed the test section. Mass conservation requires a proportional increase in velocity. This in turn creates a negative pressure gradient which causes the model to "float" downstream. This is the buoyancy effect. Induced drag is that drag resulting directly from the formation of lift. The induced drag correction results when the tunnel walls attenuates the downwash present behind any lifting body, which reduces the measured induced drag.

The above corrections were applied during the reduction process. There were two more corrections made to the data after the reduction was complete.

The first was due to flow angularity in the tunnel, meaning that the air's velocity vector is not exactly parallel with the tunnel centerline. Thus, when the model was inverted in the tunnel, the angle of attack of the model was different. Since there was angle of attack overlap in the upright/inverted test runs, the data was separated by twice the flow angularity. The appropriate correction was a simple shift in the data. Testing showed a flow angularity of 0.75 degrees downward. Although this seemed a bit high, it was consistent for all data.

The final correction accounted for that data collected when the model was not at the center of the tunnel. When the model is tested throughout the normal range of angles of attack, the sting is mechanized to keep the model in the center of the tunnel. However, for those tests when higher angle of attacks are needed, the sting can be bent upwards. The design of the sting, however, then places the model above the resolvent center, nearer the top of the tunnel. This has significant effects on the streamline formation about the model, resulting in changes to the forces and moments. Although analytical corrections were considered, the most accurate correction to this effect was a vertical shift in the data, the amount and direction of which depended upon the force or moment in question.

Dimensionless Coefficients Since conditions will not be identical from one test to the next, a common data reduction procedure is to convert all data into dimensionless form. The forces and moments will be reduced to dimensionless coefficients using the equations

$$\begin{aligned} C_X &= \frac{F_X}{qS} \quad C_Y = \frac{F_Y}{qS} \quad C_Z = \frac{F_Z}{qS} \quad C_L = \frac{\text{Lift}}{qS} \\ C_D &= \frac{\text{Drag}}{qS} \quad C_M = \frac{M_M}{qSL} \quad C_l = \frac{M_l}{qSL} \quad C_N = \frac{M_N}{qSL} \end{aligned} \tag{3.2}$$

where

S = Reference area

L = Reference length

To be consistent with the original study [4] and standard ejection seat analysis techniques, the reference values will be defined as follows. The reference area, S, is defined

as the projected frontal area at zero degrees angle of attack and sideslip. The hydraulic diameter is defined here as the diameter of a circle whose area is equal to S, and is used as the reference length, L. These values are $S = 0.164$ ft^2 and $L = 0.457$ ft.

The pressure data will be transformed into a dimensionless coefficient of pressure using the equation

$$C_p = \frac{\Delta p}{q} - 1 \tag{3.3}$$

where

Δp = Pressure difference from atmospheric, psf

In incompressible flow ($M < .3$), Eq 3.3 becomes

$$C_p = 1 - \frac{V^2}{V_\infty^2} \tag{3.4}$$

where

V = Local velocity

V_∞ = Freestream velocity

Using this definition, freestream flow has a C_p of zero and the C_p at a stagnation point (flow brought completely to rest) is one.

Center of Gravity Considerations The original study [4] conducted their analysis with three different center of gravity (CG) locations. These locations corresponded with the 5th, 50th, and 95th percentile pilots. Since each pilot was a different size, each placed the CG of the overall system at slightly varying locations. The 50th percentile pilot data was a rough average of the overall results, therefore the CG location was chosen to correspond to this case. The moments measured by the strain gage balance during testing, however, were referenced to the Balance Moment Center (BMC). Therefore, all moments were transferred to the 50th percentile CG for analysis.

IV. Wind Tunnel Test Results

The primary objective of this research was to obtain the low speed aerodynamic characteristics of the PRESS through wind tunnel testing. The previous chapter described the test facilities and the methodology of the wind tunnel testing. This chapter will present the results of that testing. These results can be divided into four categories: force and moment data, pressure data, stability augmentation effectiveness, and center of gravity considerations. Each of these will be presented and discussed individually. All results will be presented in accordance with the nondimensional coefficients defined on page 3-12.

Force and Moment Data

The force data will be presented in two coordinate systems. First, the data will be presented in body coordinates (see page 3-2). Data presented in this form is important to bio-engineers because the force directions are always constant relative to the pilot. In this way, the forces exerted on the pilot are immediately apparent. In addition, the data will be presented in a stability axis frame of reference as described on page 3-3. This frame of reference is important because it is the standard coordinate system used for stability and vehicle performance analysis. Aerodynamic drag, for example, is a stability axis force and will determine the deceleration of the PRESS in the freestream. The results will be further divided into longitudinal and lateral components. The longitudinal data refers to forces and moments which occur within the plane of symmetry, such as lift, drag, and pitching moments. The lateral forces and moments are those which will move the plane of symmetry, i.e. side forces and rolling moments.

Longitudinal Forces and Moments The longitudinal aerodynamic data can be found in Figures 4.1 through 4.5.

Normal and Axial Forces From a flight mechanics point of view, the normal and axial force plots (Figures 4.1 and 4.2) are not very informative in themselves, but they clearly identify the forces that the pilot will experience in ejected flight. Reference [7] related an attempt to place a stabilizing fin on an ACES II style open ejection seat system.

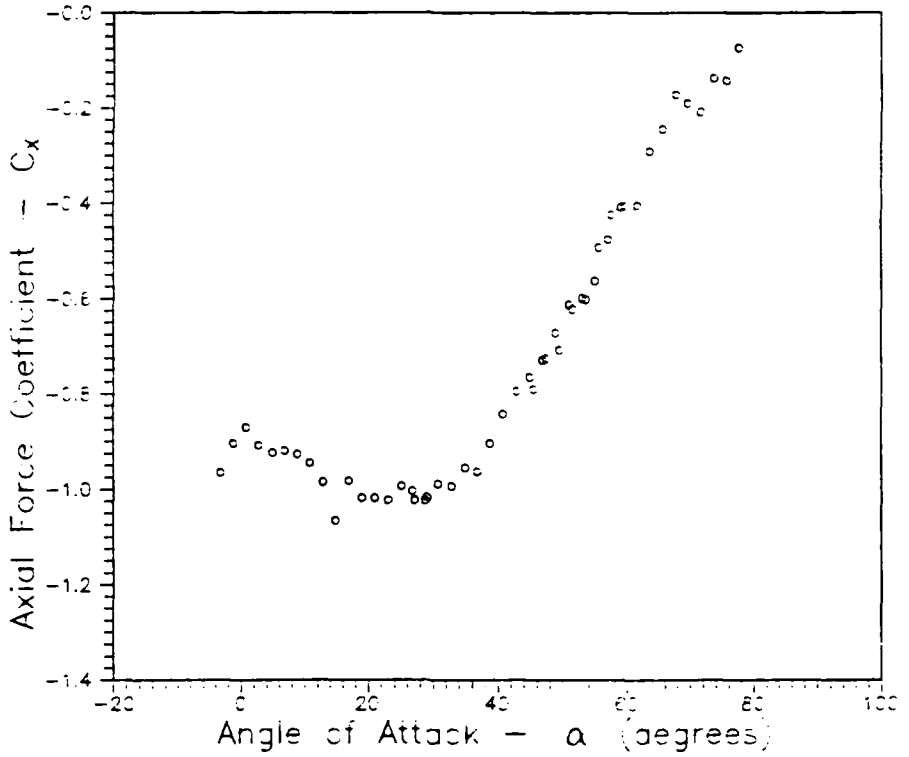

Figure 4.1. PRESS Axial Force as a Function of Angle of Attack

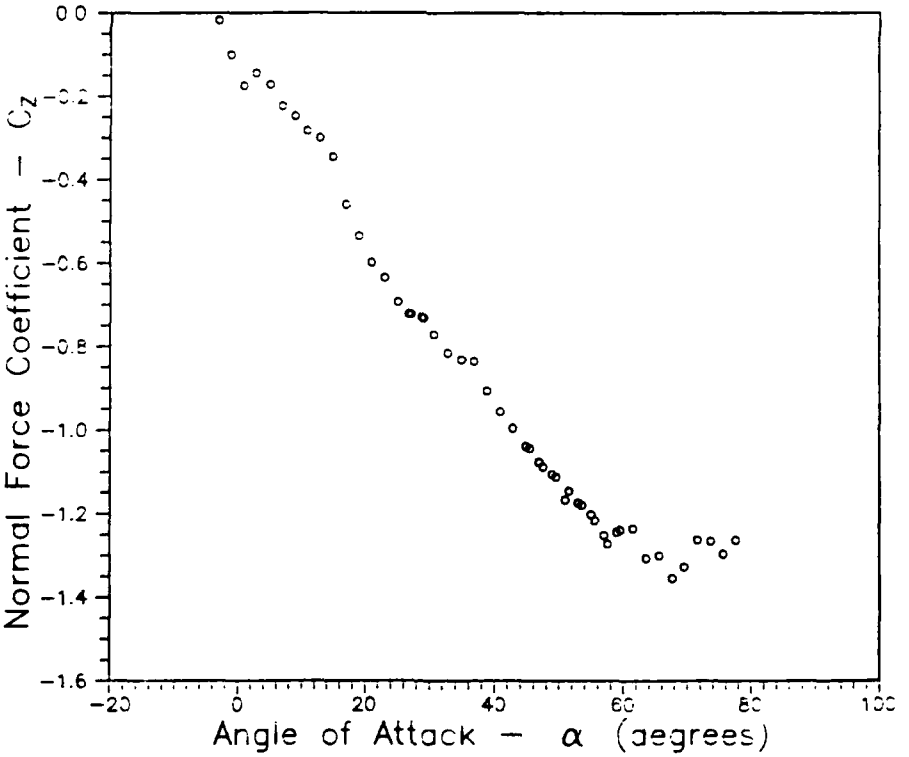

Figure 4.2. PRESS Normal Force as a Function of Angle of Attack

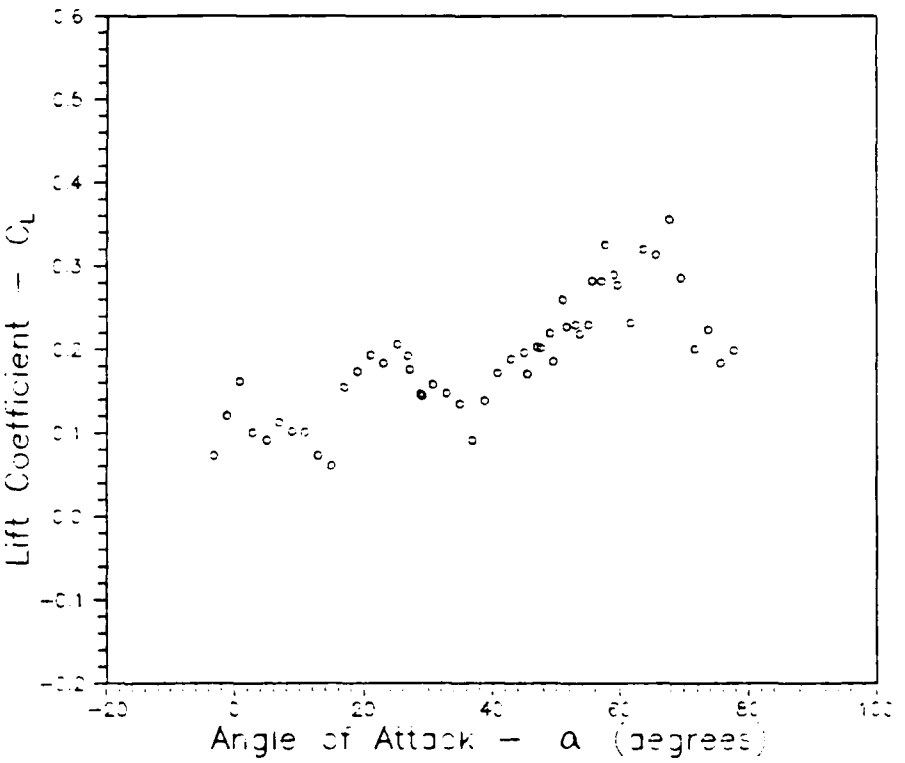

Figure 4.3. PRESS Lift as a Function of Angle of Attack

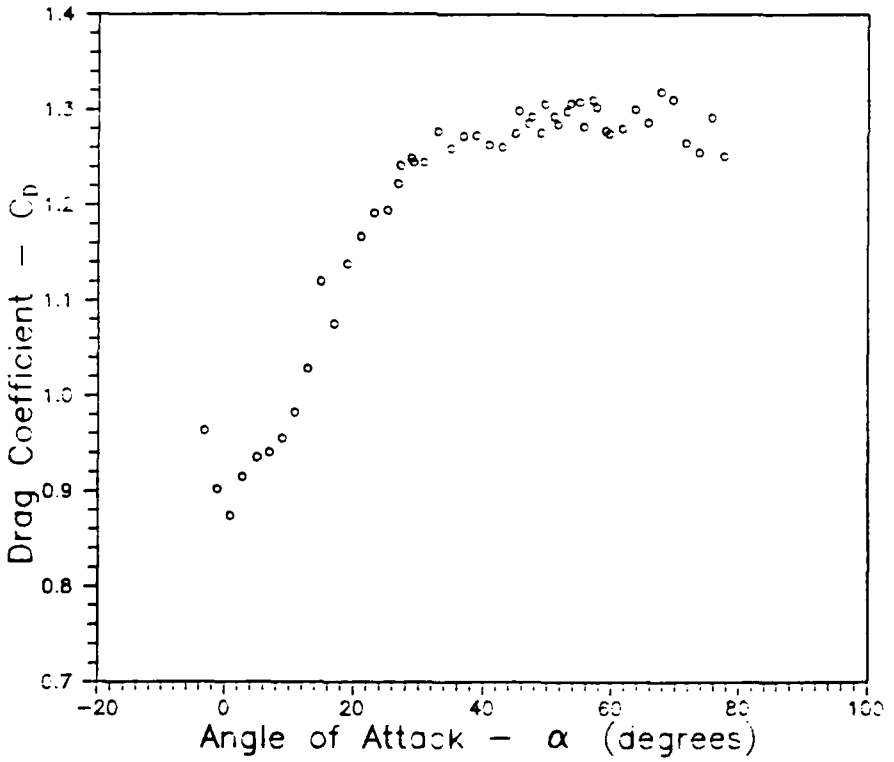

Figure 4.4. PRESS Drag as a Function of Angle of Attack

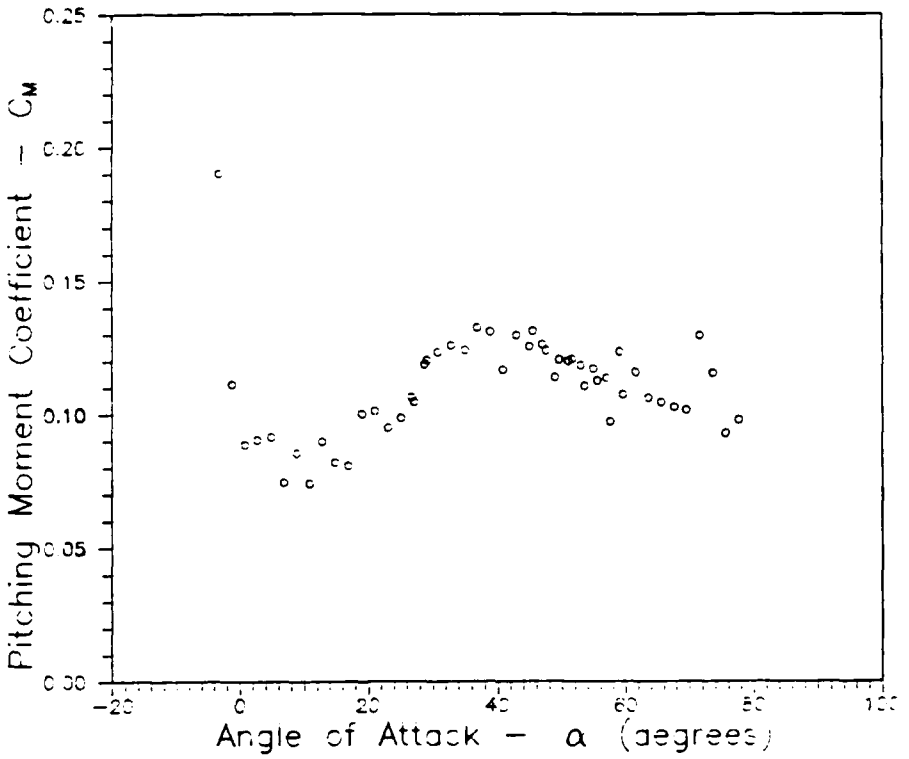

Figure 4.5. PRESS Pitching Moment as a Function of Angle of Attack

The fins stabilized the seat as intended, but they also produced enough additional normal forces that, combined with the catapult rocket, the resulting normal acceleration exceeded safety limits.

Assuming the vehicle will trim at the desired 35 degree angle of attack, and will not exceed that value, the maximum normal force the pilot will feel occurs at the trim point and is $C_Z = -0.82$ (see Figure 4.2). Using Equation 3.2, we can determine the maximum normal force to be

$$\begin{aligned} F_Z &= qSC_Z \qquad (4.1) \\ &= (57)(.164 \cdot 6^2)(-0.82) \\ &\approx -276 \text{ lbs} \end{aligned}$$

Knowing the mass, m, of the PRESS to be 15.481 slugs [4:E.42], we can find the maximum

normal acceleration, a_z, using the equation

$$\begin{aligned} a &= F_Z/m \qquad (4.2) \\ &= -276 \text{ lbs}/15.481 \text{ slugs} \\ &= -17.8 \text{ ft/sec}^2 \\ &= -0.55 \text{ g} \end{aligned}$$

Thus, the pilot will feel .55 g's upwards in addition to any accelerations caused by the catapult rocket. In a similar manner, the maximum axial force occurs at approximately 24 degrees α and is $C_X = -1.03$. Using Equations 4.1, we find that the maximum axial force is approximately 347 lbs rearward, and the resulting axial deceleration is 0.70 g's.

Lift and Drag Lift is a rather unimportant parameter in ejection seat analysis, since one is primarily interested in stability rather then performance. The one value of interest is the acceleration imparted to the seat away from the parent aircraft by the lift force. From Figure 4.3 we see that the C_L at the moment of ejection when the angle of attack is zero degrees is approximately 0.13. Using the same procedure as before, we can approximate the lift force on the full scale model at 43.7 lbs and an acceleration away from the parent aircraft of 0.09 g's. Since the catapult rocket will provide acceleration on the order of 7 g's [4:10.31], the lift force is insignificant, but in the right direction.

The drag experienceed by the PRESS in ejected flight is very important because it determines the deceleration rate. Again, using the methodology above, we obtain the drag coefficient from Figure 4.4 at the trim condition, $C_D = 1.27$, and from Eq (4.1) we see that the braking force at the test velocity is 427 lbs. This results in a deceleration of 0.86 g's.

Pitching Moment Of all the parameters measured in the test program, the most important was the pitching moment. As discussed in the Introduction, maximum aircrew protection from deceleration forces occurs when the PRESS has a trim angle of 35 degrees. Thus it was important to determine the actual angle at which zero moments occur, and if it was away from the ideal, determine methods of correcting it.

Initial testing of the PRESS in the baseline configuration did not find a trim point within the range of tested angles of attack, $-4 \leq \alpha \leq 78$ (see Figure 4.5). The PRESS exhibited a positive pitching moment at all angles tested.

Lateral Forces and Moments The lateral aerodynamic data can be found in Figures 4.6 through 4.8. Since side force is not affected by a coordinate transformation about the pitch axis, it is the same in either body or stability axis systems. In addition, the roll and yawing moments are of little interest in body coordinates, unless they are large enough to create physical problems for the pilot, so they too will be presented in the stability axis system only.

In theory, all lateral data for the PRESS should be odd functions in β, since the PRESS XZ plane is one of symmetry. However, the model was actually asymmetrical due to the presence of the pressure tube, and the fact that the pilots right leg was partially removed to accomodate the tubing, therefore the data is somewhat skewed. However, the effects are small, and the overall trends are still clearly evident.

Side Force Side forces experienced by the PRESS are relatively unimportant, but are included for completeness.

Rolling Moment As predicted in Reference [4], the PRESS exhibits a negative rolling moment when subjected to a positive sideslip (see Figure 4.7). For aircraft this is commonly called positive lateral stability [10:261]. To understand why this is positive stability, imagine the following sequence of events. As the PRESS is flying through the air, some random force rolls it to the right. This tilts the lift vector to the right, resulting in a positive sideslip. This positive sideslip then causes a negative rolling moment, which restores the seat to upright flight. However, as discussed above, the lift forces are relatively weak, resulting small sideslip angles. Fortunately, the magnitudes of the rolling moment coefficients are much larger than the study predicted for the supersonic case, which will overcome the small β's and help to stabilize the seat.

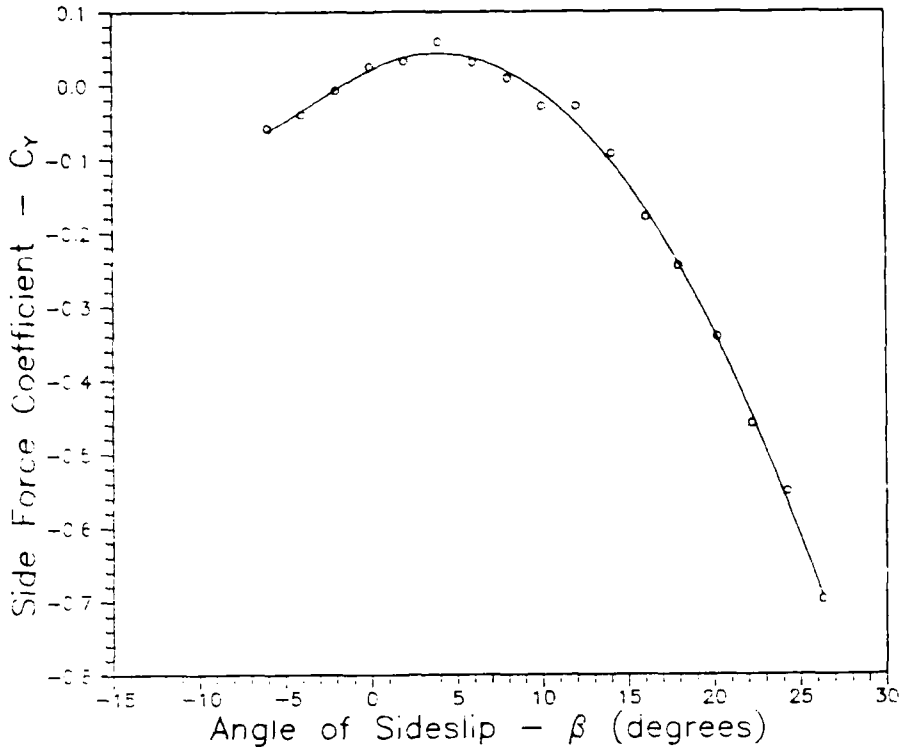

Figure 4.6. PRESS Side Force as a Function of Sideslip

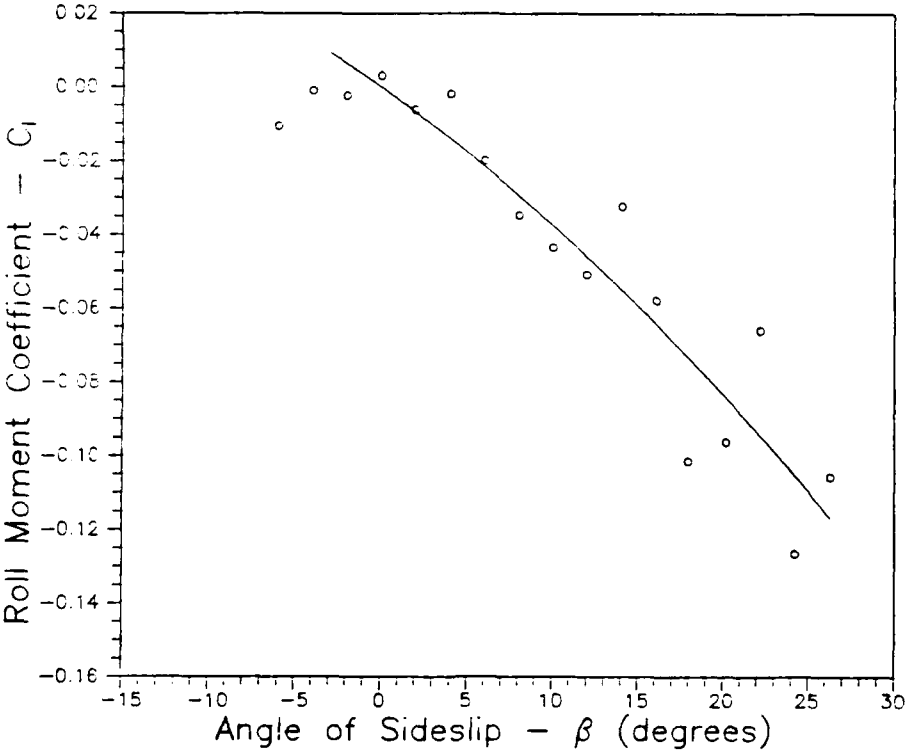

Figure 4.7. PRESS Rolling Moment as a Function of Sideslip

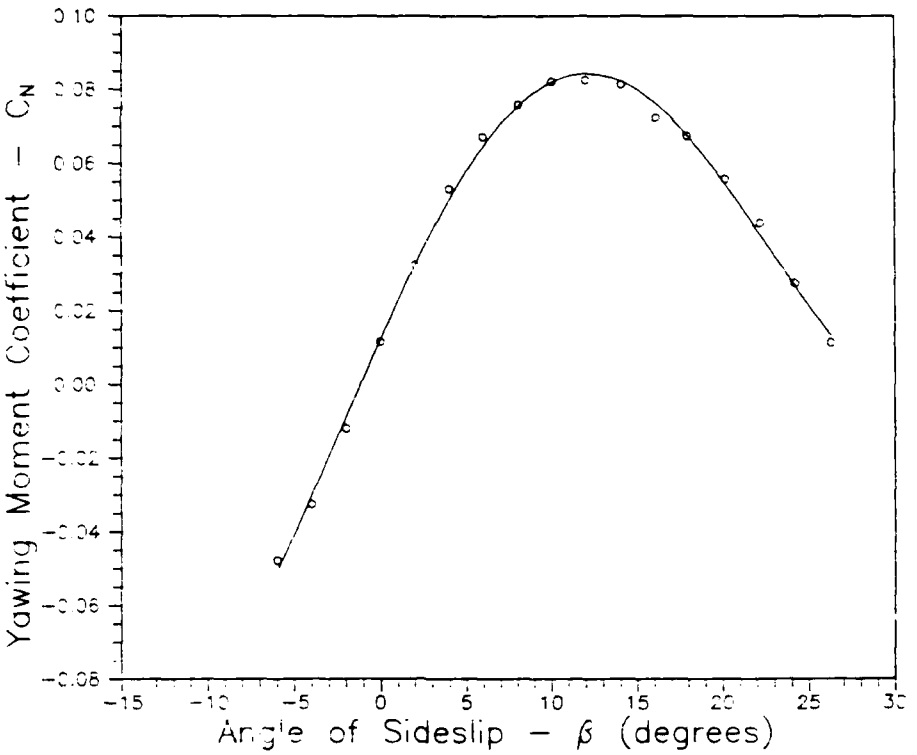

Figure 4.8. PRESS Yawing Moment as a Function of Sideslip

Yawing Moment The yawing moment of the PRESS can be seen in Figure 4.8. This plot shows that for positive sideslip (nose left), there is a positive yawing moment (nose right). Thus the PRESS is directionally stable. However, should β exceed approximately 30 degrees, Figure 4.8 would indicate that the PRESS becomes directionally unstable. This would make sense from a geometrical perspective, since high sideslip angles would expose the center support panel between the pilot's legs to the freestream. This results in a large side area near the front of the PRESS, dramatically shifting the center of pressure, the point where the aerodynamic forces appear to act, forward of the PRESS's center of gravity.

Pressure Data

The purpose of recording surface pressures on the wind tunnel model was to provide a method of comparing experimental data to the analytical study performed in Chapter VI. However, since the wind tunnel balance measures net forces and moments, the pressure data provides information that the balance cannot, namely, forces and flow velocities at specific points on the model. The pressure ports on the model can be separated into three

regions: the impact surfaces, the upper cowling near the headshield and the pilots head, and behind the cowling near the pilot's torso and legs. Representative ports from each region are plotted as functions af angle of attack in Figures 4.9 through 4.11.

Beginning from the bottom rear of the cowling and proceeding forward and up the front cowling, Figure 4.9 shows that each port on the cowling measures its maximum pressure at a lower angle of attack than the preceeding one. This should come as no surprise since maximum pressures occurs when a surface is normal to the freestream flow. One should note than none of the ports reach unity. At zero sideslip, the stagnation streamline should lie in the plane of symmetry. Since the ports are not in that plane, one would not expect stagnation to occur.

A high angles of atack, the upper cowling is positioned such that the trailing edge is below the leading edge. Therefore, one would expect the flow to separate off the top edge of the front cowling. This will be shown to be true in Chapter V. This flow separation near the headshield is clearly evident in Figure 4.10. All five ports indicate similar values and trends at the higher angles of attack, regardless of position or orientation. Note in this region that the pressure coefficient is negative, meaning that the local flow is higher than the wind velocity. This would indicate that there is significant swirling occuring in this region. As the angle of attack is decreased, however, first the higher port (49) and then the lower port (48) on the headshield are no longer shielded from freestream flow by the front cowling. Since they are no longer enveloped within the separated flow region, they begin to display characteristics similar to the cowling ports in Figure 4.9.

Finally, we see from Figure 4.11 that the pressure measured at port 50 ranges from -0.40 to -0.75 throughout the tested angles of attack. Again, the negative values indicate that the velocity at the port location is higher than the freestream. From Eq (3.4) we can determine that the flow velocity is 20% faster at the trimmed pitch angle. This type of information is important to ejection seat engineers wishing to protect the passenger from flailing injuries.

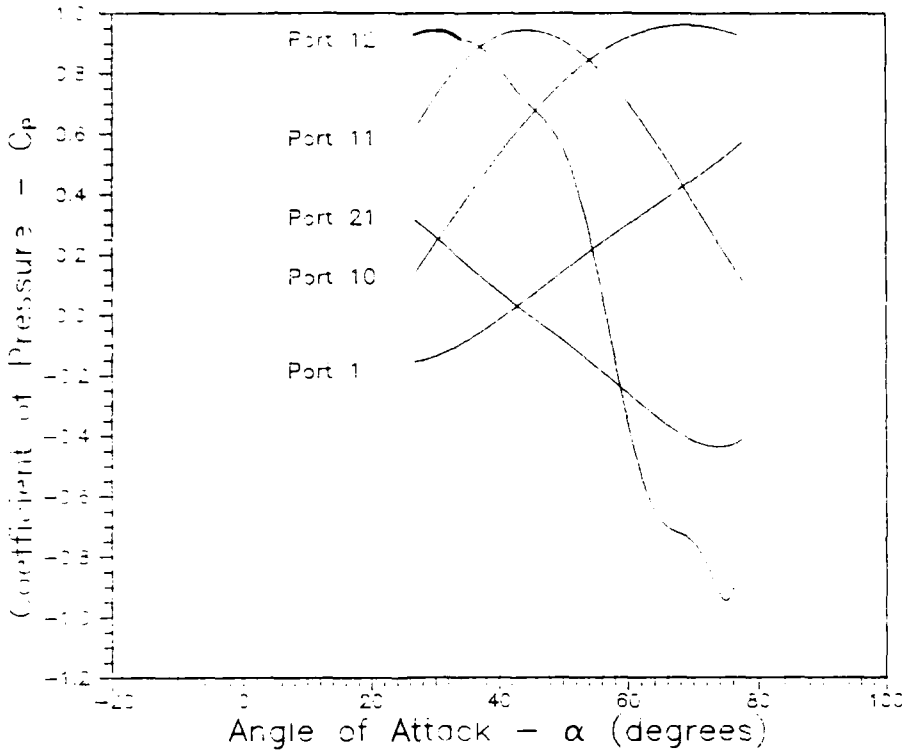

Figure 4.9. Cowling Pressures as a Function of Angle of Attack

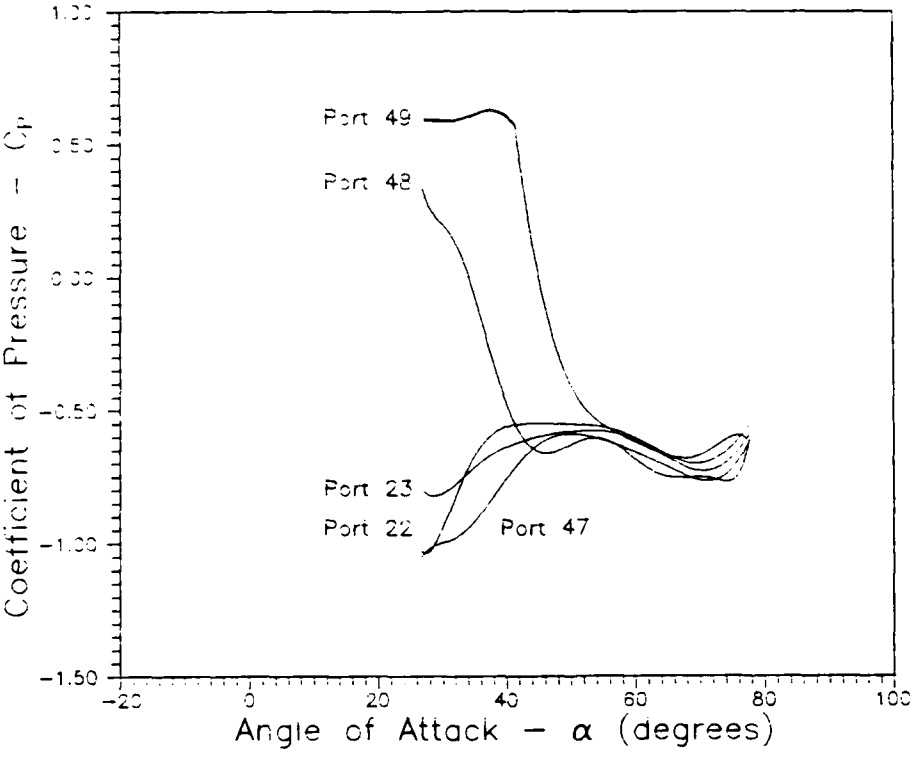

Figure 4.10. Upper Cowling Pressures as a Function of Angle of Attack

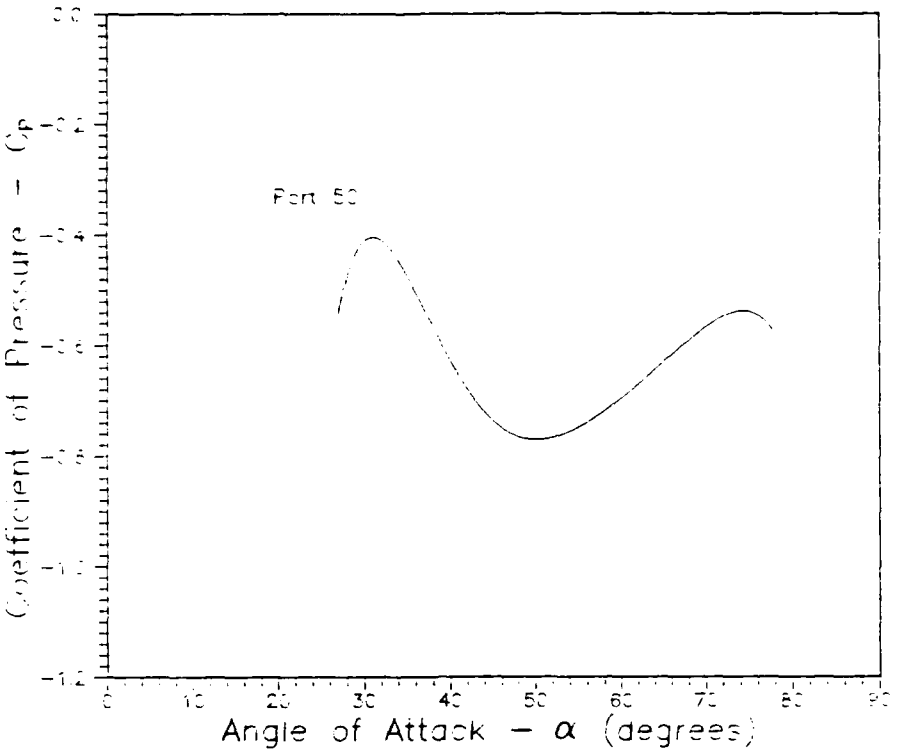

Figure 4.11. Seat Pan Pressure as a Function of Angle of Attack

Stability Augmentation Effectiveness

The lack of a pitch trim point was a problem that was detected early in the test program. Therefore, testing was performed with the large and small tails to determine their effectivness in changing the pitch trim angle. In addition, the yaw fins were tested to improve the directional stability, and to determine their effect on the lateral stability of the PRESS. The tails and yaw fins are described starting on page 3-6. The effects of each device are compared to the baseline data in Figures 4.12 through 4.19.

Force Effects The purpose of these external devices was to modify the moment characteristics of the PRESS. Since moments are created by applying forces away from the CG, the force coefficients are effected as well. These forces act normal to the surfaces of the fins. Since the yaw fins increased the frontal area but not the top projected area, one would expect the axial force to be increased significantly, but very little change in the normal force should be noted. Conversely, the area of the tails contribute only to the top projection, thus only normal force should be effected. Both of theses can be seen in Figures 4.12 and 4.13. It should be apparent that lift and drag are effected from both

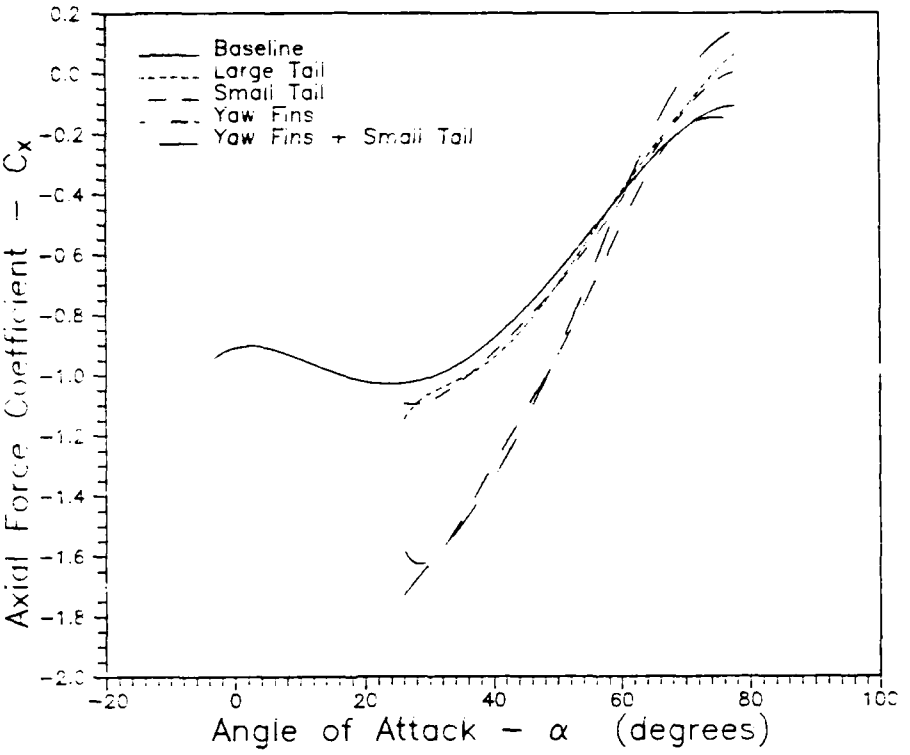

Figure 4.12. Effect of Stability Augmentation Devices on Axial Force

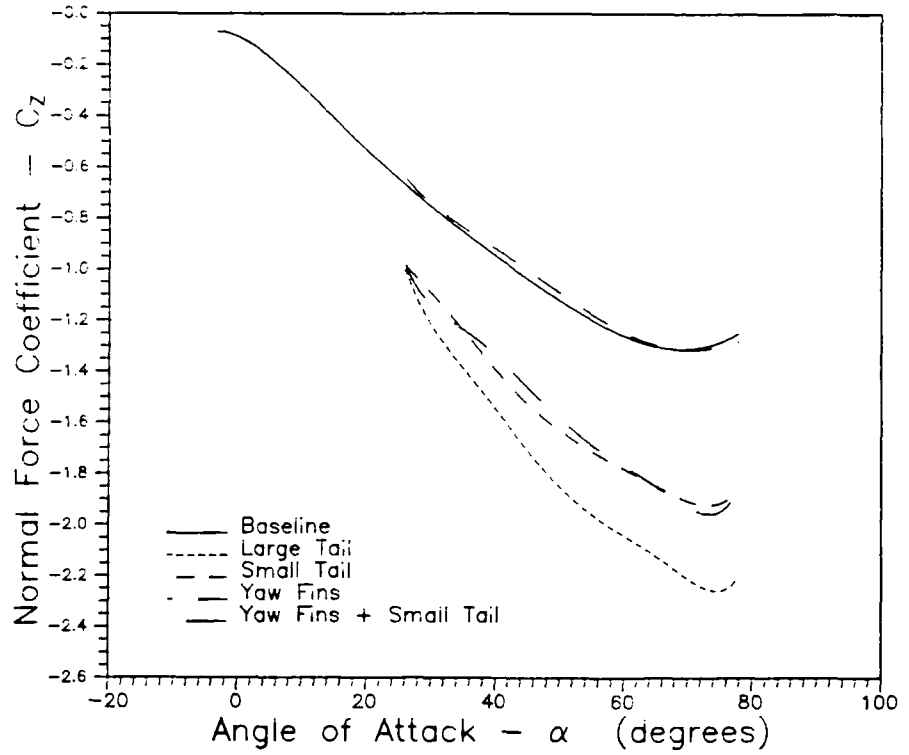

Figure 4.13. Effect of Stability Augmentation Devices on Normal Force

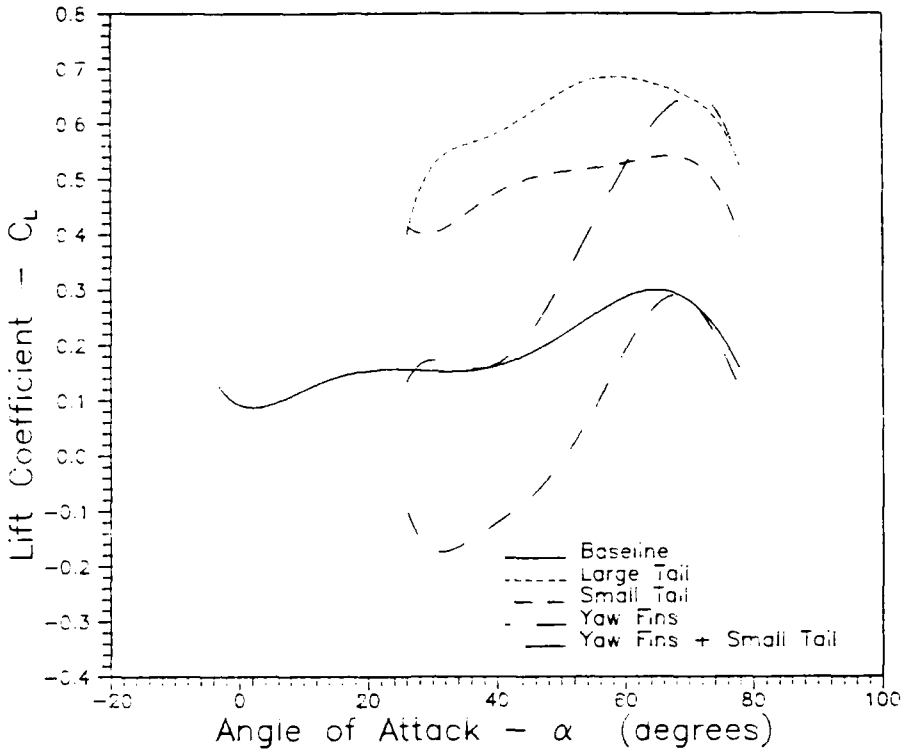

Figure 4.14. Effect of Stability Augmentation Devices on Lift

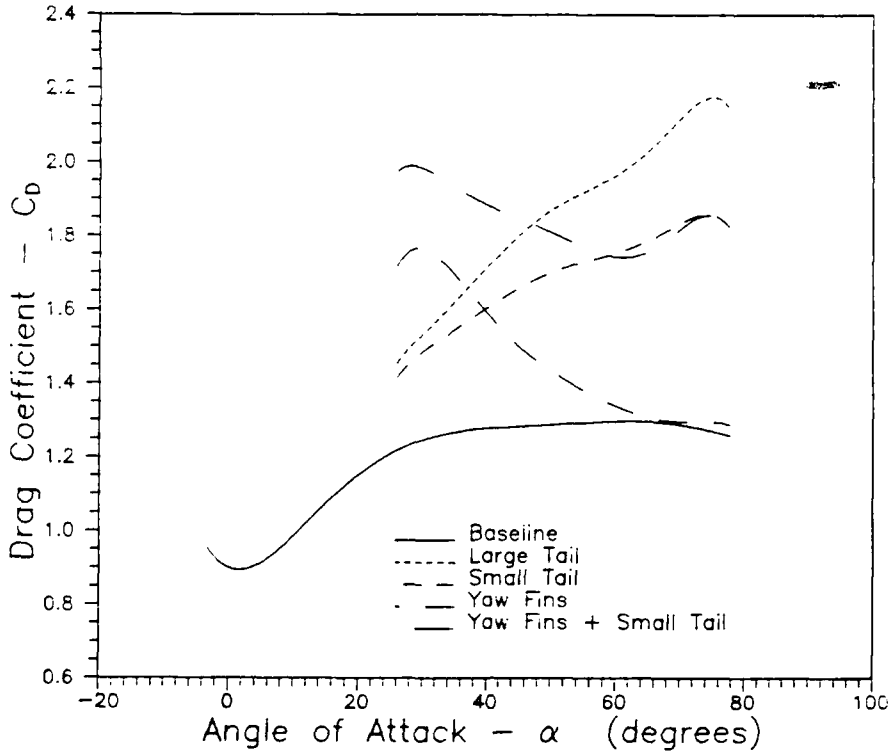

Figure 4.15. Effect of Stability Augmentation Devices on Drag

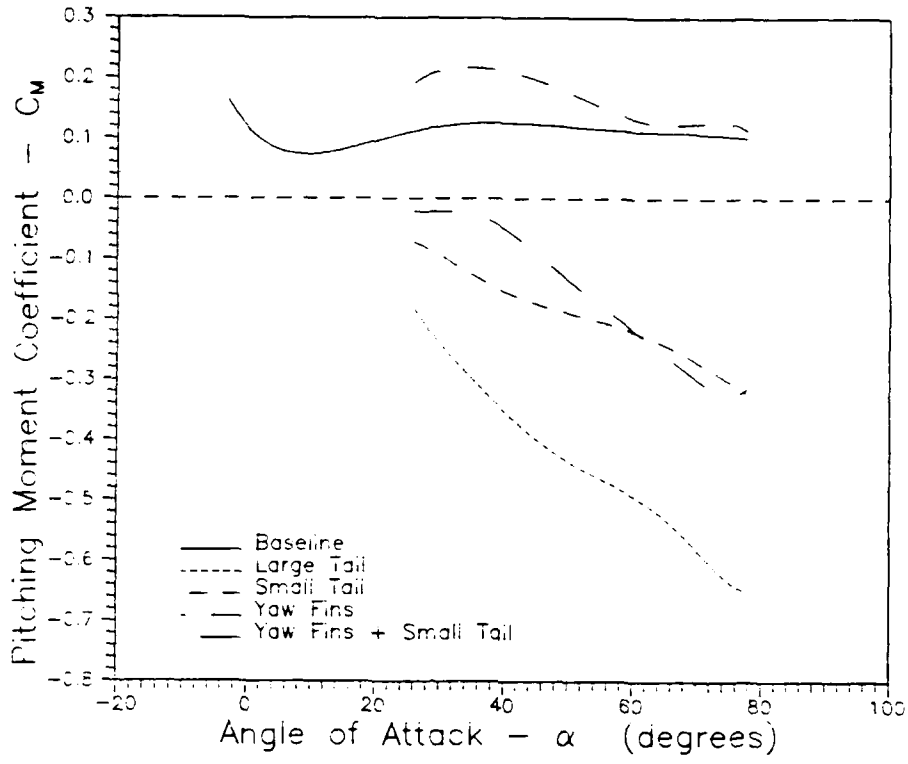

Figure 4.16. Effect of Stability Augmentation Devices on Pitching Moment

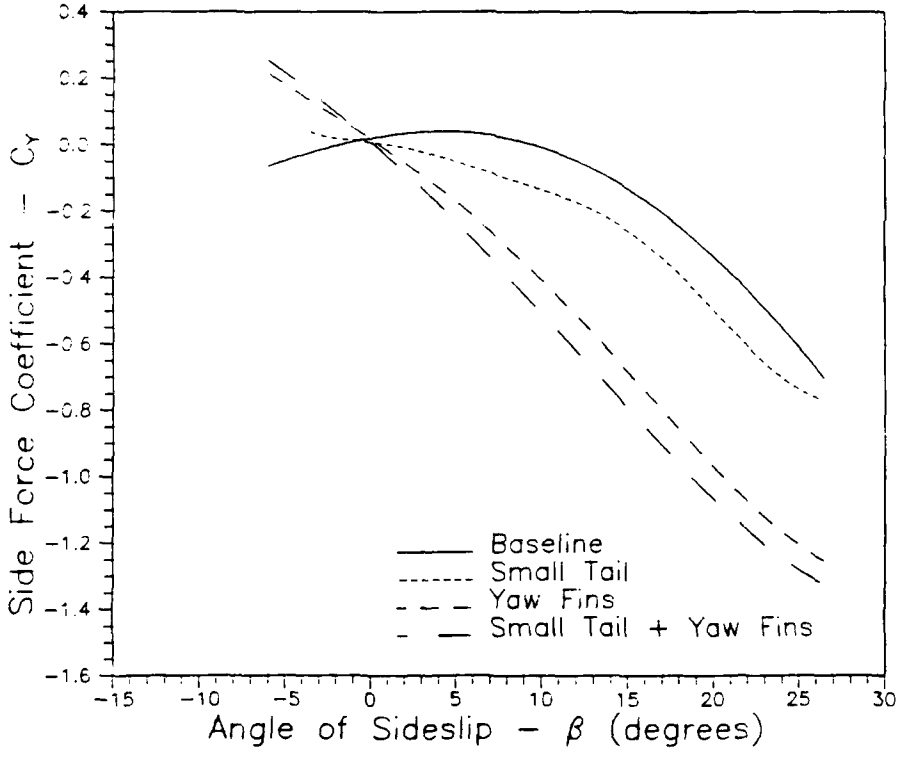

Figure 4.17. Effect of Stability Augmentation Devices on Side Force

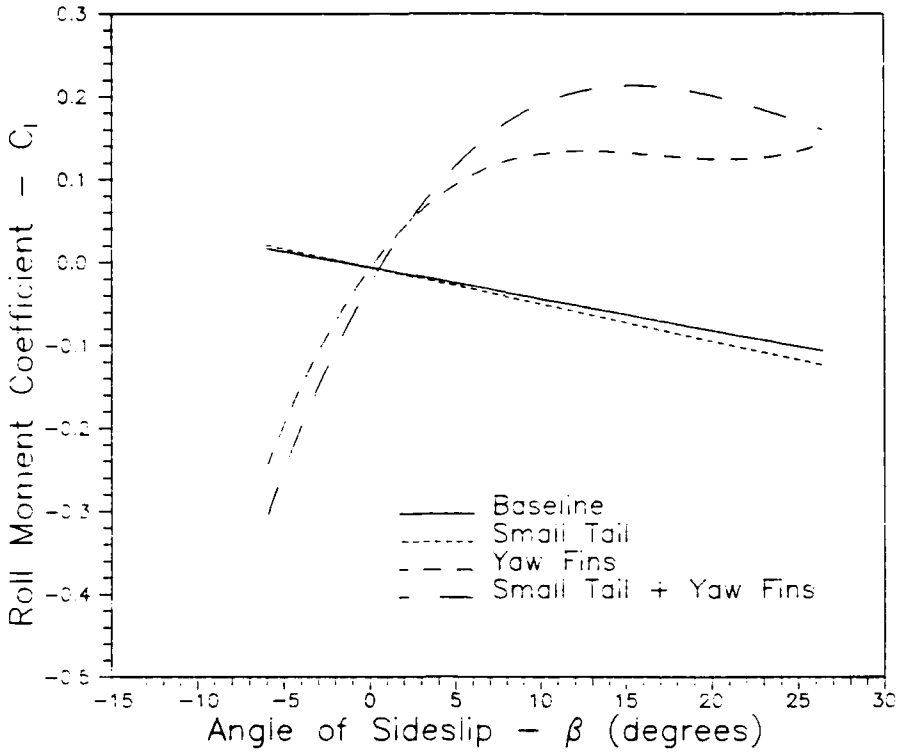

Figure 4.18. Effect of Stability Augmentation Devices on Rolling Moment

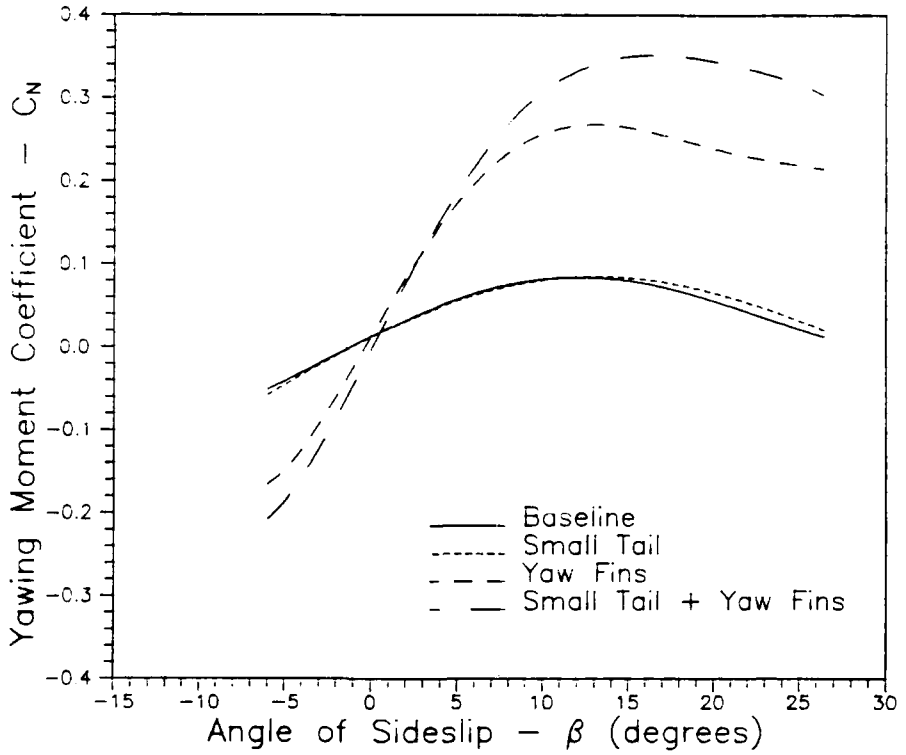

Figure 4.19. Effect of Stability Augmentation Devices on Yawing Moment

types of fins from the coordinate transformation involved. An example of this is the effect of the tails on the drag force. At zero α, the tail should have no effect on drag since the area projects in the lift direction. However, as the angle of attack increases, the tails present some frontal area, increasing the drag above that for the baseline condition (see Figure 4.15). Finally, one can see the effect of the small tail and the yaw fins on the side force component in Figure 4.17.

Moment Effects As discussed earlier, the pitching moment of the PRESS's baseline configuration was always positive throughout the entire test range. This is a problem which must be fixed if the PRESS is to be a practical design. As a first attempt to correct this deficiency, the large tail was tested. As shown in Figure 4.16, this tail was too effective, causing severe negative moments and too low a pitch trim angle of attack. The model was then retested with the short tail. The figure shows a positive increase in the pitching moment as compared to the large tail's effect, but it was still too negative. The trend, however, would seem to indicate that the PRESS cannot be trimmed with tail alone. The tails do indeed change the magnitude and the slope of the pitching moment, but both curves appear to intersect the zero moment axis at nearly the same angle of attack, ($\approx$ 18 degrees). By installing an even shorter tail, one might achieve the correct trim angle, but the curve will be so flat that neutral stability will result (see page 4-17).

The yaw fins were designed to provide an increase in the directional stability of the PRESS, but they also were intended to create a positive pitching moment. This design resulted from analyzing the data before the data reduction program was properly debugged. The data indicated that a positive moment was needed, which later proved erroneous. As it turned out, however, combining the yaw fins with the short tail provided almost the exact moment needed to trim the PRESS at 35 degrees (see Figure 4.16).

For the lateral moments, the yaw fins multiplied the yaw restoring moment by a factor of over three, and combined with the short tail, a factor of four (see Figure 4.19). However, in Figure 4.18 one can see that the fins caused the rolling moments to reverse their sign, causing lateral instability.

Center of Gravity Considerations

As a vehicle flies through the air, the total aerodynamic force on that vehicle can be resolved into a single resultant vector, $\vec{R}$, acting through a point known as the center of pressure, CP. If that vehicle is in trimmed flight, the center of gravity must lie along the resultant's line of action, otherwise a moment would exist. For stability, however, the CG is restricted to that region of the line such that $\vec{R}$ is pointing away from the CG. In this way, angular displacements of the vehicle will create restoring moments. The vehicle is considered neutrally stable if the CP and the CG are coincident, because an angular displacement will not create an aerodynamic moment. However, determining the center of pressure for blunt objects is difficult because the location of the CP is typically very sensitive to angle of attack.

Earlier we noted that the baseline PRESS configuration did not exhibit a trim point at any tested angle of attack (see page 4-6). This indicates that $\vec{R}$ is always located above the CG. In addition, it appeared that although external tails pushed the trim point to within the test range, they alone could not trim the PRESS at the desired angle. However, by shifting the CG to a point along $\vec{R}$, we should be able to trim the model at any angle we desire.

To determine the CG shift required to trim the PRESS at $\alpha = 35$ degrees, we must first find the center of pressure at this angle. Using Figure 4.20 as a guide, we can write the moment at point P as

$$C_{M_P} = C_{M_{CG}} + \frac{x}{L}C_Z - \frac{z}{L}C_X \tag{4.3}$$

where the distances x and z have been nondimensionalized by the reference length, L. Since we want the PRESS to be in trim when the CG is at point P, we will set $C_{M_P} = 0$. Solving Eq (4.3) for z yields

$$z = \frac{L}{C_X}C_{M_{CG}} + \frac{C_Z}{C_X}x \tag{4.4}$$

Since we have chosen to trim the PRESS at 35 degrees, will substitute into Eq (4.4) the coefficients measured at that angle, and use the reference length for the full scale seat ($L \times 6$).

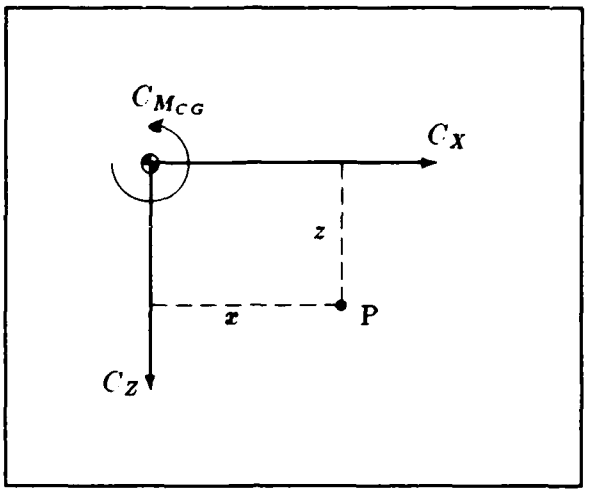

Figure 4.20. Center of Gravity Forces and Moments

The coefficients for the baseline PRESS at 35 degrees angle of attack are

$$\begin{aligned} C_X &= -0.955 \\ C_Z &= -0.831 \\ C_{M_{CG}} &= 0.124 \end{aligned}$$

Substituting these values into Eq (4.4) yields

$$z = -0.356 \text{ ft} + 0.8706x \tag{4.5}$$

This equation represents the locus of CG locations that will stabilize the PRESS at 35 degrees angle of attack, and therefore also represents the line of action of $\vec{R}$. This line is overlayed on a sideview of the seat in Figure 4.21, illustrating the possible CG travel. To determine the CP, we then find the point on the line such that

$$\frac{\Delta C_M}{\Delta \alpha} = 0 \tag{4.6}$$

Four points along that line were considered as possible CG locations. Transforming the baseline C_l data using Eq (4.3), the resulting pitching moment curves for each of these CG locations are shown in Figure 4.22. Using the definition of neutral stability, Eq (4.6), one can see that the PRESS is neutrally stable when the CG is located at point B, whose

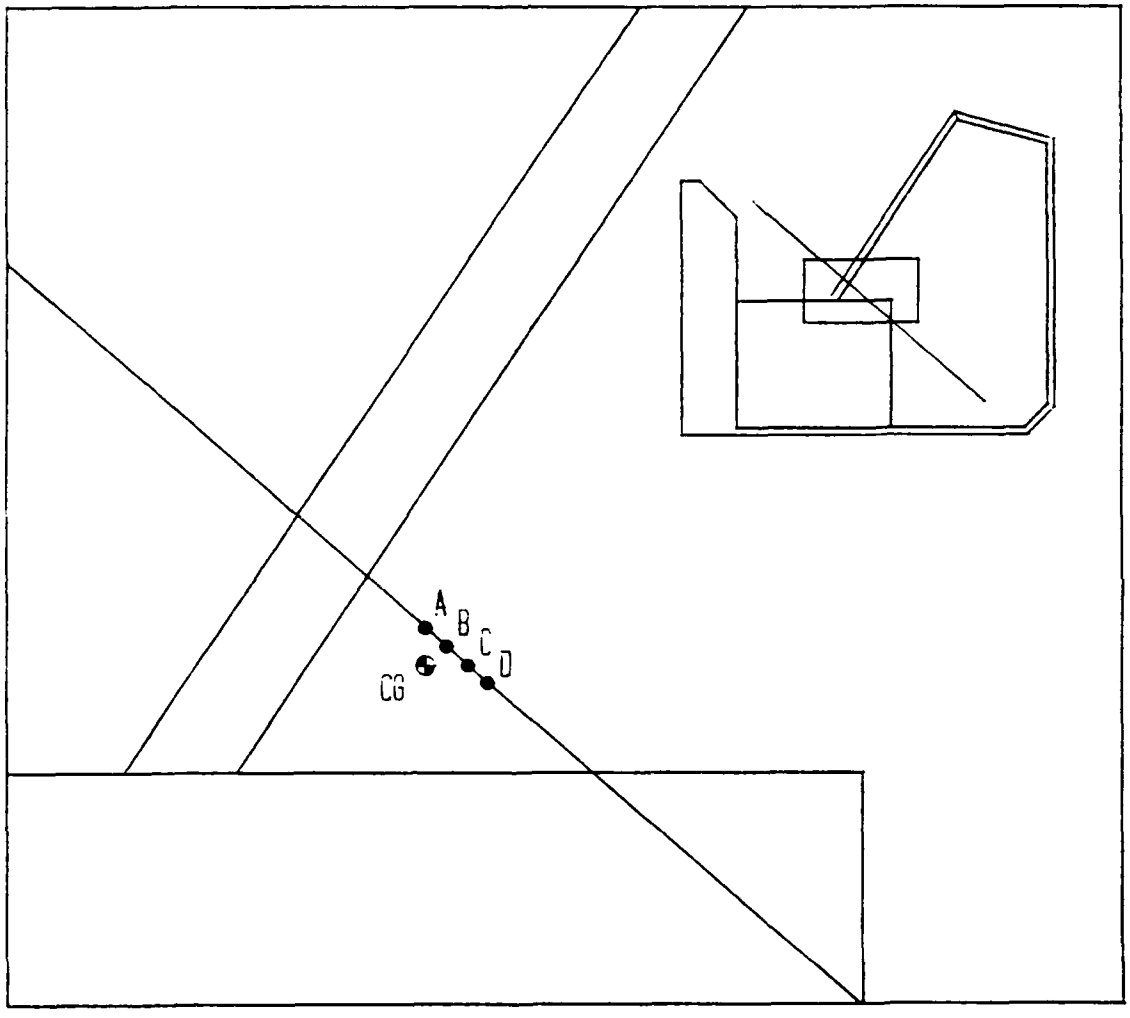

Figure 4.21. CG Locations to Trim PRESS at 35 Degrees

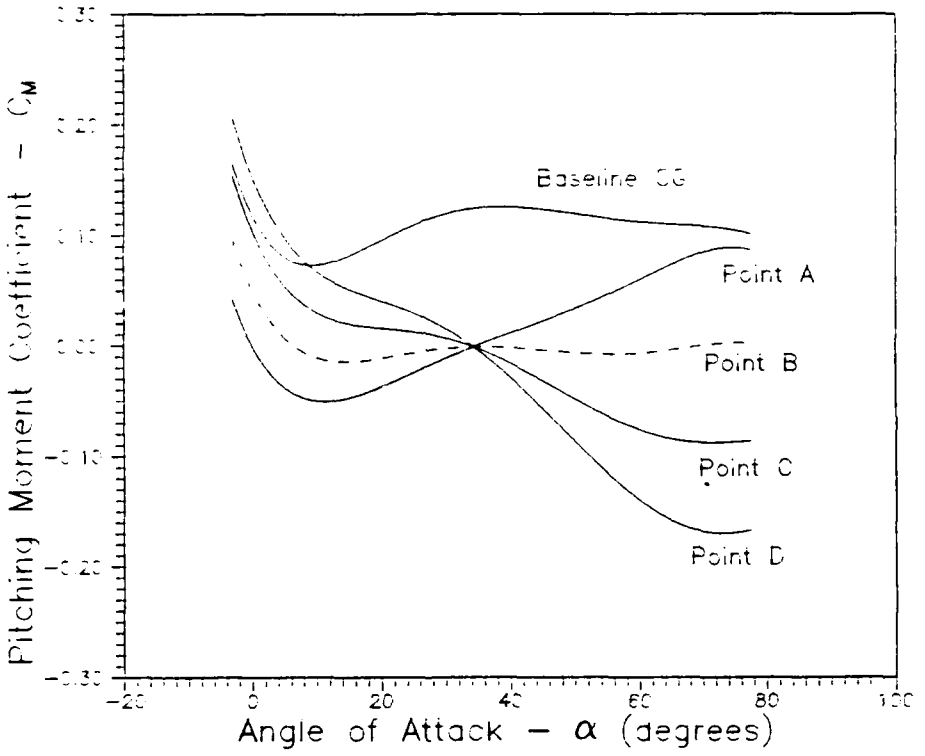

Figure 4.22. Effect of VaryingCG Locations on Pitch Stability (Baseline)

pitching moment curve is shown in Figure 4.22 as a dashed line. Shifting the CG to points C and D will stabilize the seat, while shifting to point A will cause the seat to become unstable. Therefore, the center of pressure must be located at point B. The coordinates of point B relative to the CG as defined by Figure 4.20 are

$$x = 0.20 \text{ ft}$$
$$z = -0.18 \text{ ft}$$

This point represents the smallest possible CG shift for stable, trimmed flight at 35 degrees angle of attack, a total shift of 3.24 inches.

A similar analysis was performed for the PRESS with the short tail installed because physical requirements may not allow a forward shift of the CG. The coefficients at 35 degrees α for this case are

$$C_X = -0.995$$
$$C_Z = -1.247$$
$$C_{M_{CG}} = -0.133$$

The CG locus and selected points are illustrated in Figure 4.23, and the resulting pitching moment curves for each points can be seen in Figure 4.24. We can see from these figures that the PRESS center of pressure with the short tail is located at point E, whose coordinates relative to the original CG are

$$x = -0.40 \text{ ft}$$
$$z = -0.44 \text{ ft}$$

This represents a CG shift of 7.14 inches. Again, the C_l curve for this CG location is shown in Figure 4.24 as a dashed line. The minimum required CG shift to trim and stabilize the modified PRESS at 35 degrees, however, is 1.5 inches, the closest approach of the line to the original CG location.

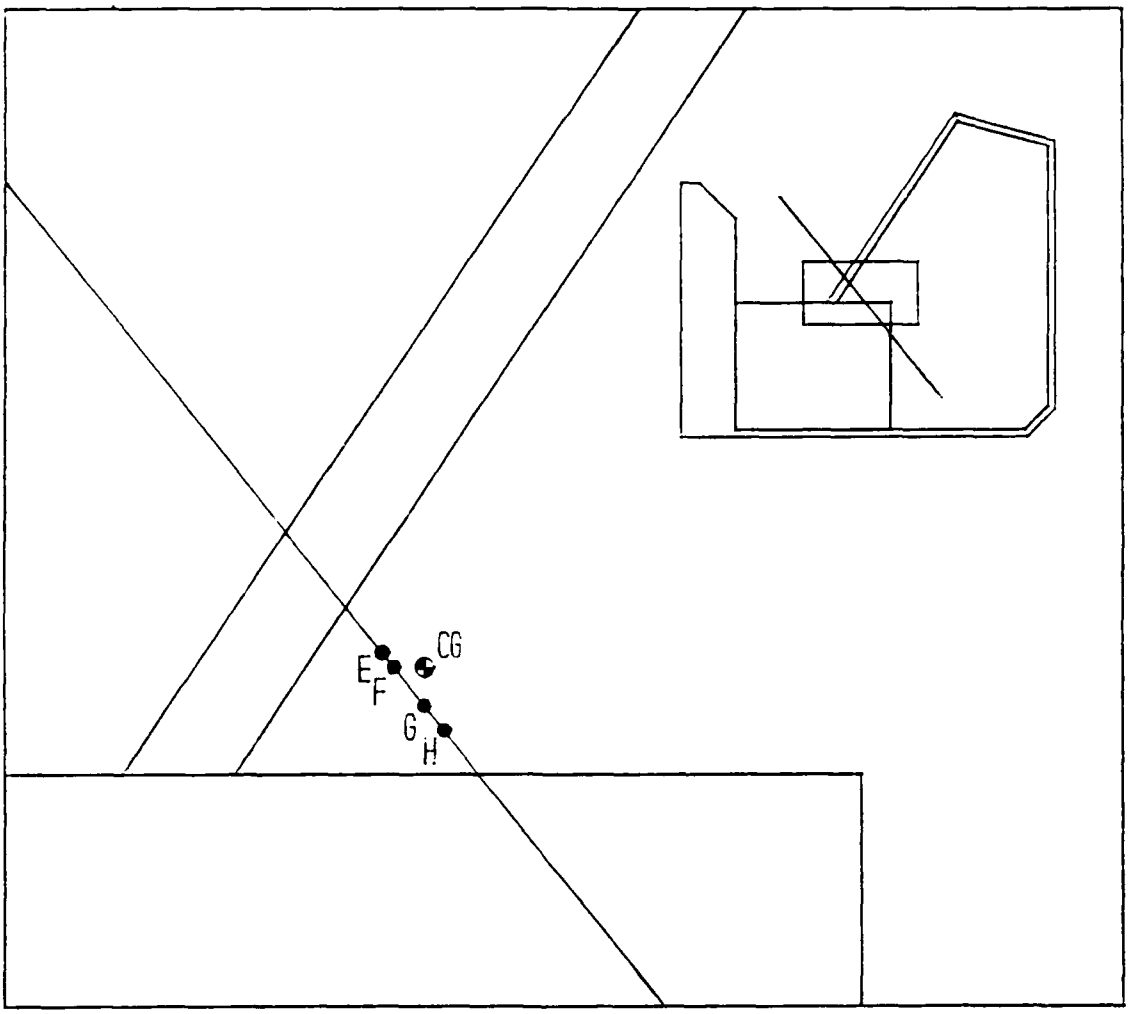

Figure 4.23. CG Locations to Trim PRESS at 35 Degrees with Short Tail

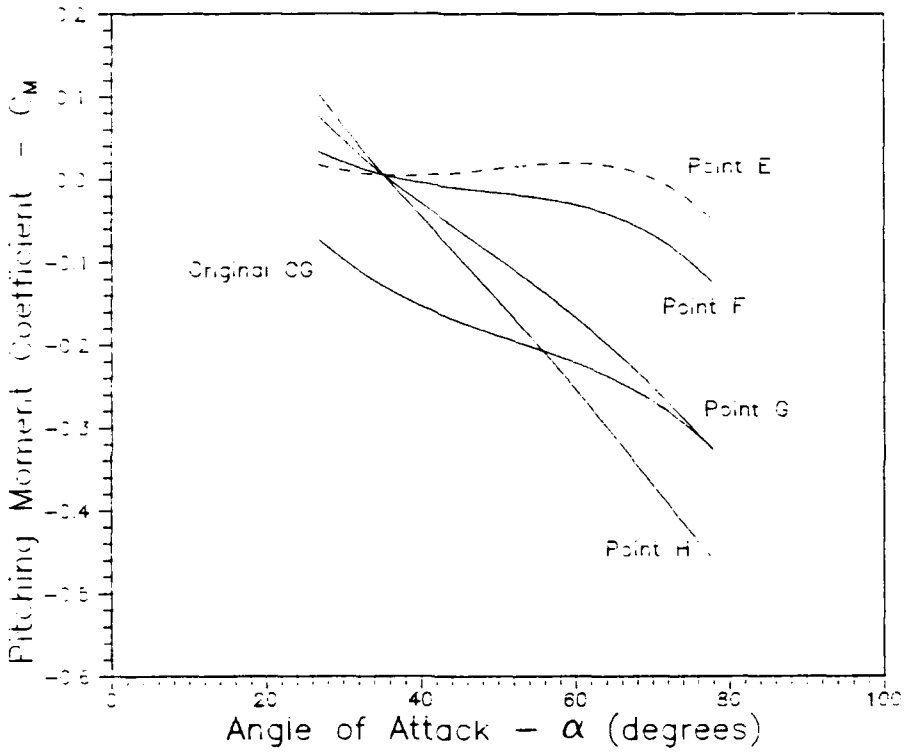

Figure 4.24. Effect of Varying CG Locations on Pitch Stability (Short Tail)

V. Water Tunnel

Flow Visualization

To construct a reasonable apparent body as described in Chapter VI, some type of flow visualization technique was required. The most efficient method in terms of time, cost, and availability was to use the Flight Dynamics Laboratory two-foot water tunnel. This chapter will describe the facilities and test procedures, and will present some qualitative results.

Facility Description

The Two-Foot Hydrodynamic Test Facility is located in Bldg 25a, Area B, at Wright-Patterson AFB, and is operated by the Aeromechanics Division of the Flight Dynamics Laboratory. The primary purpose of the water tunnel is to use inexpensive models and colored dyes to provide a qualitative simulation of the flow pattern produced by a flight vehicle at virtually any flight condition.

This facility is a closed circuit vertical water tunnel with a maximum test section velocity of 0.85 feet per second, with the optimum for flow visualization (using dye injection) being 0.25 feet per second. The test section has a 2'×2' cross section and a length of 4 feet. The test section is constructed of two inch plexiglass on two adjacent sides for viewing and a slide away door to permit quick access to the model. The tunnel design includes a 7,000 gallon reservoir above the test section, and sufficient pumping capability to test continuously at 0.85 feet per second. A dye injection system for flow visualization is available. Colored dye can be injected into the flow either from the model, if equipped with dye ports, or from a rake located upstream from the model.

Test Configurations

To be able to observe the entire flow field about the PRESS, four different dye injection sources were utilized. The various techniques were combined as needed to provide flow information in the region of interest. In some cases, the use of one dye source did not

permit the use of another due to a local disruption of the flow pattern. The various dye sources are illustrated in Figure 5.1 and described below:

1. A dye rake injected red dye into the freestream approximately three inches upstream of the model. The rake could be positioned such that the dye followed the flow streamlines all the way past the model. It could also be adjusted during a test to other positions. The rake is shown in Figure 5.1(a).

2. Dye ports mounted on the sides of the cowling discharged blue dye laterally from the model. The flow in this region was suspected to be separated and highly turbulent. The dye ejected into this region would therefore mix rapidly and form a cloud rather than streamlines, and would completely fill the separated region. The difference in color provided visual contrast between the separated flow and the laminar freestream flow. These ports are shown in Figure 5.1(b).

3. External tubes were mounted longitudinally along the lower surface of the model, discharging blue dye over the front surface as shown in Figure 5.1(c). The dye flowed down the model's front surface and indicated the flow separation at the corner near the head shield. This proved less than successful because the dye had to flow the length of the front surface before it reached the region of interest. At the lower angles of attack when that surface was relatively normal to the freestream flow, the flow direction near the surface was primarily lateral and the dye left the seat on the side before it reached the corner. In addition, the presence of the dye tubes running longitudinally along the bottom of the model severely affected the flow in that region. Thus, flow visualization was limited to the upper surface. This method was improved for the next set of ports.

4. External tubes were mounted in as indicated in Figure 5.1(d) to indicate the separated flow behind the seatback. With the placement of the dye tubes behind the seat and out of the primary flow, there was no disruption of the flow pattern elsewhere. In addition, the dye was discharged at the point where the anticipated flow separation would occur, eliminating the lateral flow problem.

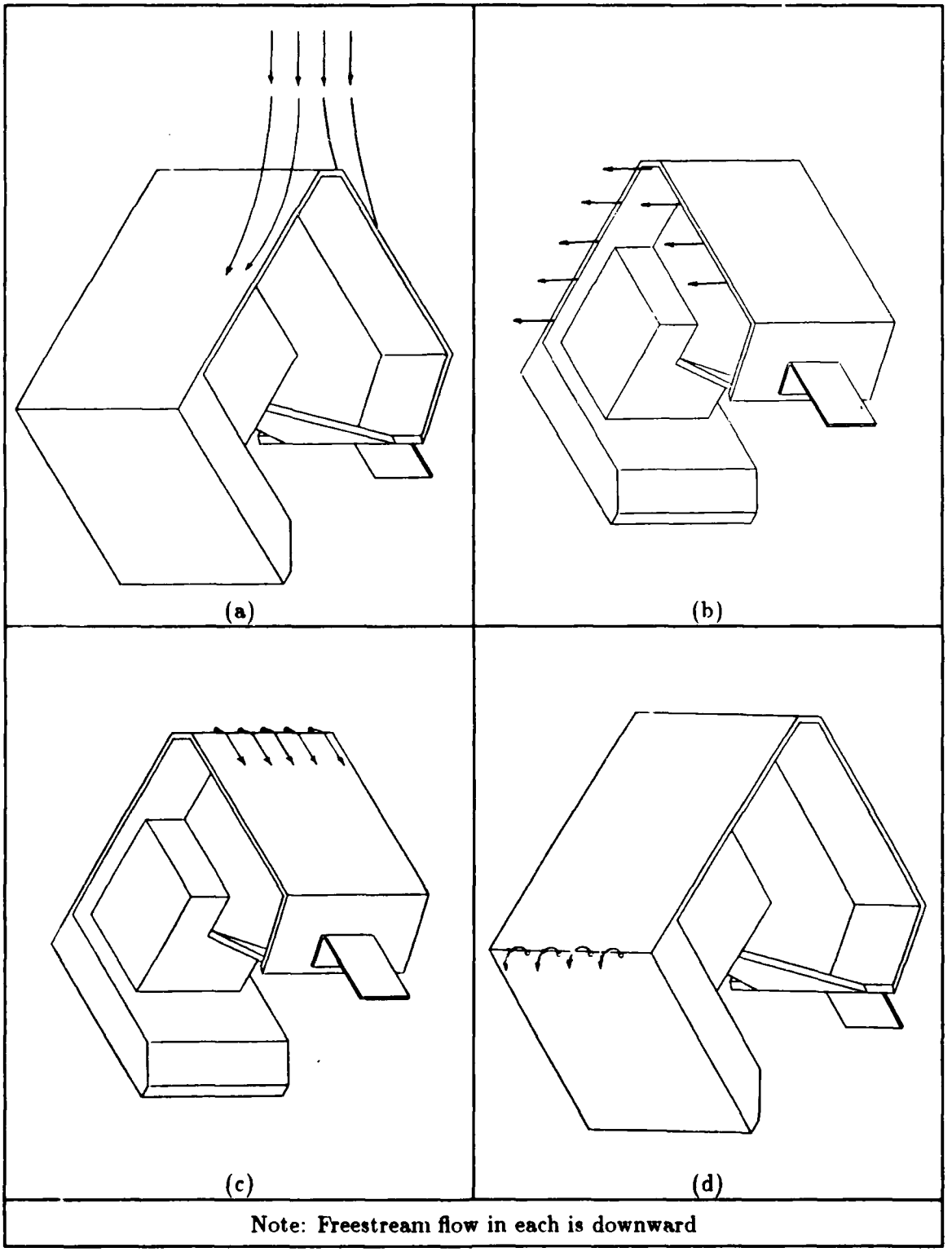

Figure 5.1. Dye Source Locations

Data Collection

The two foot water tunnel is not currently equipped with data collection equipment, since it is primarily a flow visualization facility. However, qualitative data can be obtained using still and video photography. Two still cameras were positioned at right angles to each other to provide two dimensional imaging of the flow pattern. Also, two video cameras were also orthogonally placed, with the two images recorded side by side in a split-frame format for comparison.

Test Procedure

The primary data sought in the water tunnel was the flow pattern about the PRESS when positioned at the predicted trim angle of attack of 52 degrees and no sideslip. This was the condition for which the computer model in Chapter VI would be constructed. Additional data included obtaining flow visualization at various angles of attack about the trim angle. With the remaining time available, partial flow data was collected with the PRESS at β's of 8 and 14 degrees for database purposes.

The test procedure was to place the model at an initial angle of attack of 40 degrees and the appropriate β for that test, and the water flow was set at 0.25 feet/sec. This velocity corresponds to a R_E of 11400, although this is relatively unimportant in light of the discussion in Chapter IV. The angle of attack, α, was then increased in six degree increments to a maximum of 70 degrees. Photographic data was collected at each increment.

Results

A sampling of the water tunnel results are illustrated in Figures 5.2 and 5.3. The major findings of the water tunnel testing can be divided into two parts: flow separation and vorticity. Flow separation will occur at surface discontinuities such as corners and its location is virtually independent of the model's angle of attack for the range of α's tested. Vortical flow occurs off the edges of the cowling laterally and is a strong function of α as discussed later.

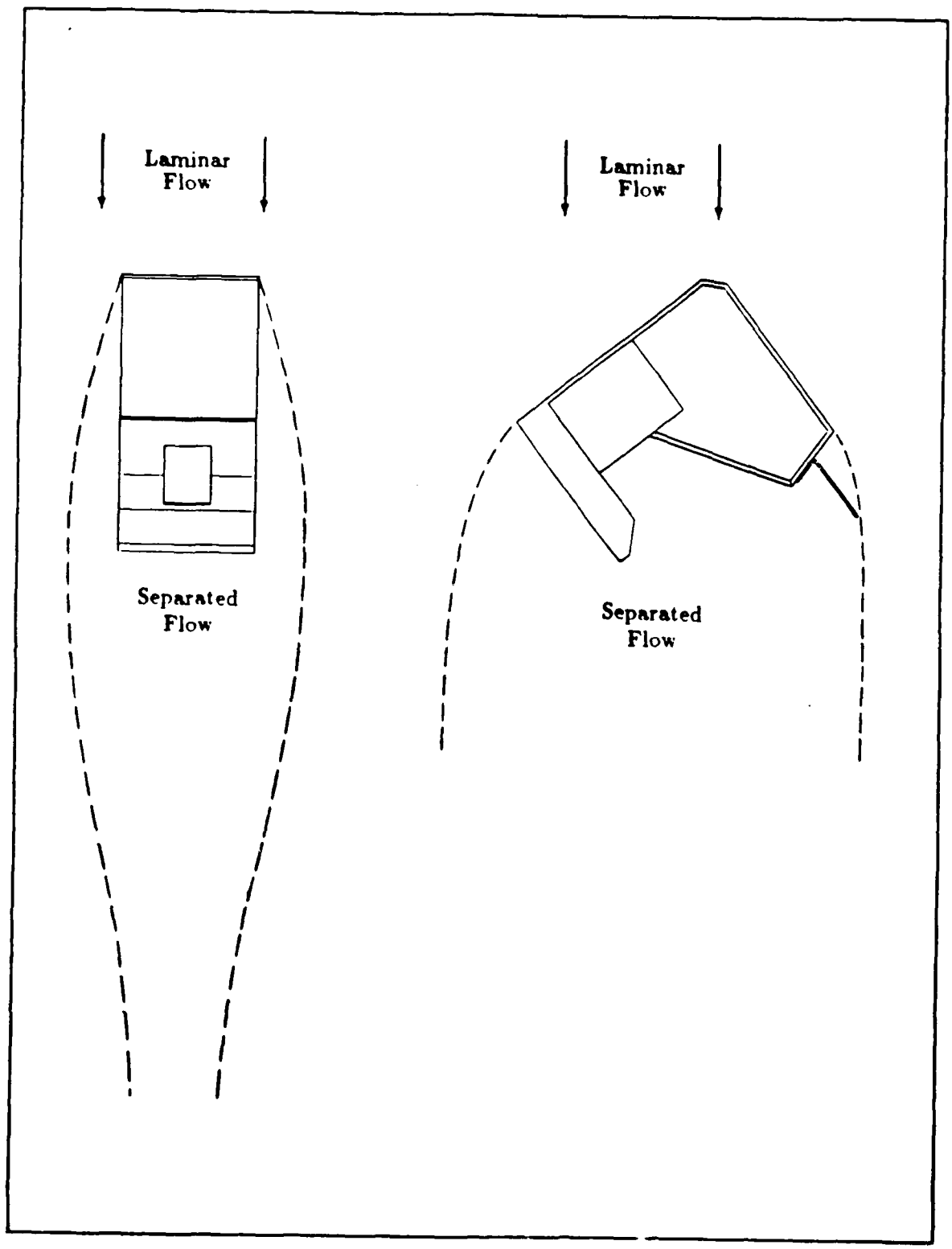

Figure 5.2. PRESS Flow field, α = 52 deg (Shear layer shown as dashed line)

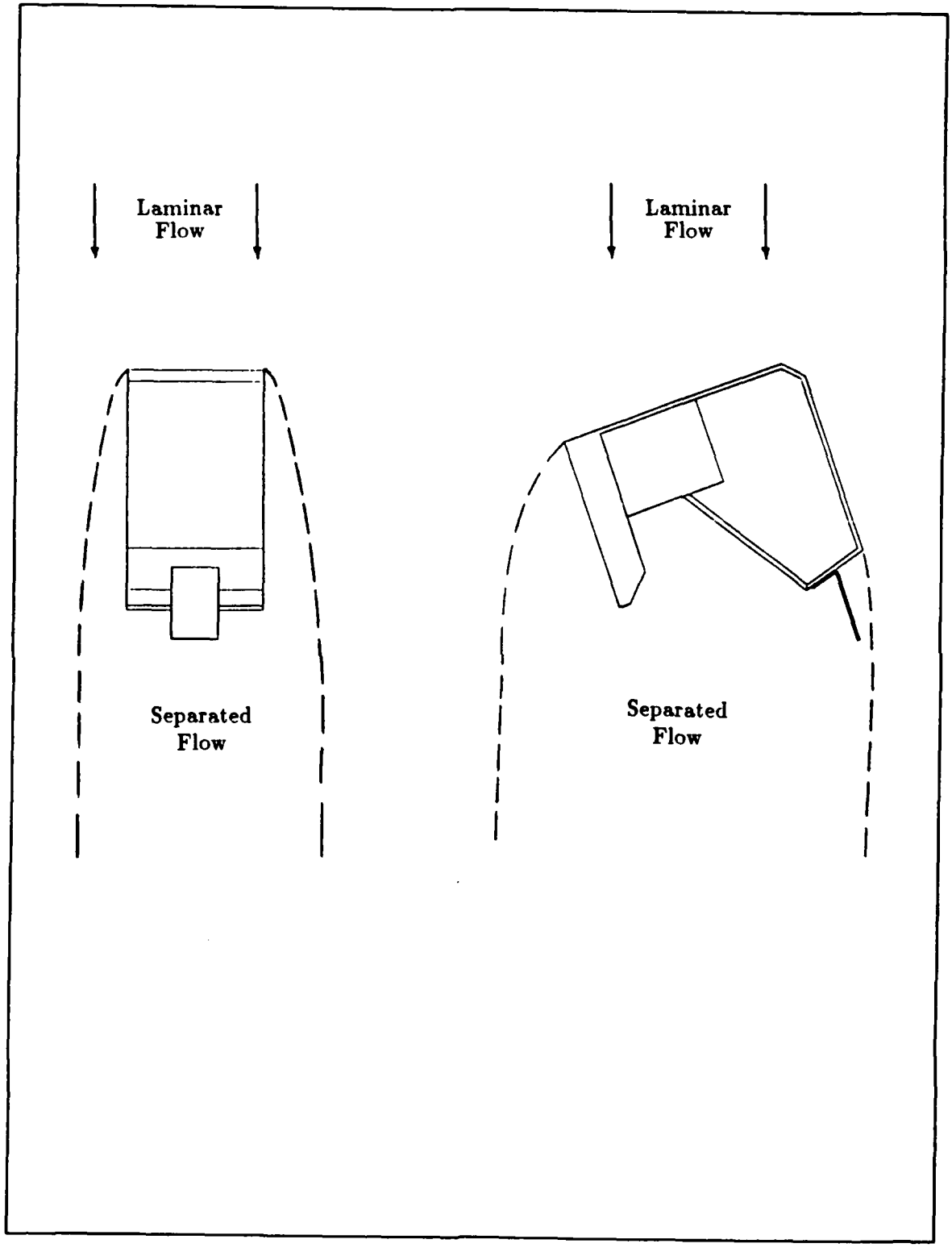

Figure 5.3. PRESS Flow field, α = 70 deg (Shear layer shown as dashed line)

Flow Separation The predominant flow characteristic present about the PRESS is the extensive flow separation. As expected, the separation "bubble" occurs in three regions: off the bottom rear of the seat, off the sides of the cowling, and over the top in the region of the headshield. The turbulence in these separated regions creates a large portion of the aerodynamic drag on the PRESS. Drag is a concern in ejection seats because excessive drag can cause large deceleration forces which may exceed the physical limits of the passenger.

The flow separation occurring in the longitudinal plane, i.e. top and bottom, behaved predictably. The region of separation begins at the sharp edge and expands into the flow in a direction roughly parallel to the surface from which it just separated. This shear layer, the demarcation line between separated flow and the laminar freestream flow, then turns with the freestream flow to become parallel with the freestream within approximately one body length. The position of the shear layer then remains constant as it travels downstream.

Vortical Flow Unlike the longitudinal flow separation, the flow separating from the sides of the PRESS behaves in an unexpected manner. When the PRESS is at extremely large angles of attack it presents the bottom surface of the seat nearly perpendicular to the oncoming flow. At this condition, the flow shear layer behaves as described in the previous section. However, when the PRESS is at the angles near the trim condition, the chamfered "nose" of the seat is pointed into the flow. In this position, the region of flow separation is much smaller, i.e. the shear layer stays much closer to the sides of the PRESS as it progresses downstream than it does at the higher α's. In addition, as the flow continues past the model, the shear layers created on opposite sides curve back towards each other, reaching a minimum separation distance of approximately two thirds of the PRESS's width. This minimum separation is reached at approximately three body lengths downstream from the nose of the PRESS.

This phenomenon can possibly be explained by deducing from the PRESS geometry that vortices are created as the flow separates off the sides of the cowling. These vortices are illustrated in Figure 5.4. The vortices are created by the angles formed by the cowling relative to the flow direction. As the flow separates laterally, the energy created by each vortex keeps the flow near its core rather than allowing it to propagate into the freestream.

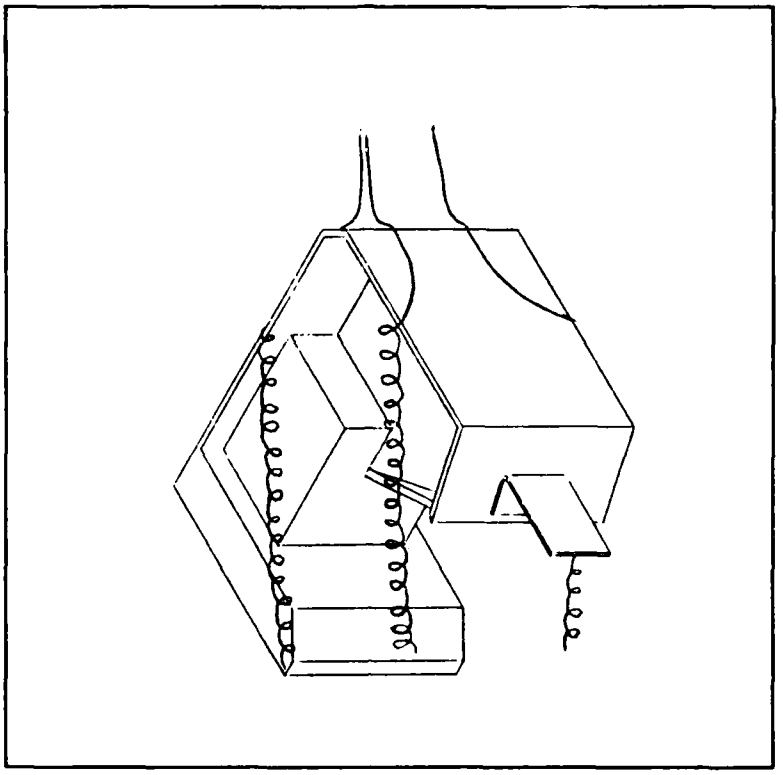

Figure 5.4. Lateral Separation Vorticity

As the flow passes beyond the model, the mutual induction of the vortices draw the lateral shear layers towards each other. Recalling the discussing on page 2-7 concerning the constriction of the streamlines due to an oversized model, it must be noted that this attraction of the shear layers towards one another might be a result of the wall's presence. However, one would expect the same result for all α's if this were true, and that is not the case.

VI. Computer Analysis

As discussed in the Introduction, the purpose of computer simulation was to investigate a cost-effective alternative to physical modelling. Constructing an experimental model costs both time and money, and significant changes to the design can render a previous model obsolete. On the other hand, a properly constructed computer model can be easily reconfigured to meet the new design needs. Thus, a logical step early in the aerodynamic analysis of the PRESS was to develop such an analytical model. In the original design study, a computer analysis was performed for the PRESS for a supersonic flight condition [4:7.5]. The simulation technique that they employed was relatively simple to implement. However, low speed analytical methods are much more complex, since the governing equations for a subsonic, viscous fluid are elliptic. In particular, if the vehicle in question is blunt, i.e. not streamlined, extremely elaborate programs are required to get reliable results. As a result of the time and cost required to perform a design trade study using such elaborate coding, such methods are not efficient for preliminary design considerations, particularly student projects. Thus, it was a secondary goal of this thesis to utilize a subsonic paneling code, generally considered highly inaccurate for blunt objects, to determine the aerodynamic pressure distribution on the cowling. In order to use this code, a computer model of the PRESS was modified to include the regions of flow separation. The combination of the physical seat and wake regions is called an apparent body.

Modified Newtonian Method

The aerodynamic code used by the PRESS design team was the MARK IV Supersonic-Hypersonic Arbitrary-Body Program [4:A.1]. This program utilizes the Modified Newtonian Method to calculate the pressure coefficients about the flight vehicle. This method

determines the C_p for a given surface using the equation

$$C_p = K \sin^2(\delta) \tag{6.1}$$

where

K = Modified Newtonian coefficient, unique for each shape, velocity

δ = Angle of freestream flow vector relative to surface plane

To use the MARK IV code, the external shape of the test item is modeled as a system of flat panels. The program then uses Eq (6.1) and the problem geometry of each panel to obtain a local C_p. The individual panels and their respective pressure coefficients and locations are then appropriately manipulated to obtain aerodynamic force and moment coefficients.

The trick to using Eq (6.1) is determining the correct value of K. As the method was originally developed, K was a direct function of Mach number and valid only for bodies at high supersonic and hypersonic velocities [11]. For a sphere, K asymptotically approaches a maximum value of 1.833, approximately reached at $M = 5$. Because of this asymptotic nature, the Modified Newtonian was developed for hypersonic speeds ($M \geq 5$) where K is held constant at 1.833.

Ejection seat designers soon discovered, however, that by modifying K, Eq (6.1) provided reasonably good correlation with experimental data, even at low supersonic speeds. Reference [11] produced evidence that aerodynamic data for ejections seats have been accurately predicted for velocities as low as Mach 0.6. However, these studies required experimental data to establish K. In a similar manner, by comparing computer analysis to experimental results, Chiang [3] determined that the optimum K for an ACES II ejection seat at Mach 1.2 and 20,000 feet was 1.4. For lack of a better method, Reference [4] made the assumption that the PRESS was sufficiently similar to the ACES II in shape and used the same value for K. Thus, their analysis was limited to the same flight conditions. Since no K was available for subsonic velocities, this technique could not be applied for the low speed case.

Subsonic Aerodynamic Paneling Techniques

Aerodynamic paneling codes operate on the general principle that any arbitrary body being modeled can be approximated with smooth panels. These panels are typically flat for numerical simplicity, although not necessarily required to be so. Solutions to the flow's governing equations are found for control points within the interior of each panel. Because of the nature of these governing equations, the solution for a given panel may be independent of the other panels (supersonic), or they may be interrelated, requiring a simultaneous solution for all the panels (subsonic). The Modified Newtonian Method described above is an example of a supersonic paneling code, with the solution for each panel dependent only upon its orientation to the freestream.

Subsonic paneling codes are much more complex, however. They are based on potential theory, a good discussion of which can be found in Reference [8]. The major feature of this theory is that fluids are mathematically described as having no viscosity, and phenomena such as flow separation, turbulence, and aerodynamic drag cannot be predicted. Potential flow based paneling codes are very easy to use, however, and on streamlined vehicles where viscous effects are insignificant, they are very accurate.

Problems occur, however, when paneling codes are used to analyze blunt objects. Recalling our discussion on page 3-11, flow separation can occur at edges, when the flow is forced to turn too sharply. The result of sharp corners in potential theory is numerical singularities, because instantaneous changes in flow direction require infinite velocities. Since the control points by definition are in the interior of smooth panels, and cannot lie on such an edge, there are always finite solutions. Computationally, however, these singularities will cause velocity spikes at those control points near the edges, and depending on the angle made by the corner, their effects can propagate significantly into otherwise well behaved flow. As a result, paneling codes have not been used in the past to analyze blunt objects. Reference [6] cited a recent attempt to use QUADPAN© [12], a paneling code developed by the Lockheed Corporation, on an escape capsule. The initial results were so inaccurate that it was immediately abandoned.

In light of the above discussion, use of a paneling code for the PRESS, whose flow

field is dominated by separation, required a different approach to the construction of the computer model.

Apparent Body Analysis

Although the flow within the regions of separation is extremely turbulent, the flow outside of those regions is very smooth and can be approximated with potential theory quite accurately. Therefore, it was hypothesized that if one modeled all separated flow regions as part of the seat, then a potential paneling code should be able to accurately predict the laminar flow solution. This computer model is known as an apparent body. However, to do this, it was necessary to either predict or determine experimentally the location of the separated flow regions. Since the unique shape of the PRESS prevented the use of any known flow solutions for predictive purposes, some sort of flow visualization was required. For this reason, the water tunnel testing of Chapter V was performed to identify the shear layer marking the intersection of the laminar and turbulent flow regions.

Using the flow visualization data for the PRESS at 52 degrees angle of attack and zero sideslip (see Figure 5.2), a three dimensional body was constructed, illustrated in Figure 6.1. The front and bottom cowling and the connecting chamfer section form the front portion of the body. These surfaces will be referred to as the impact surfaces, since they are in direct contact with freestream. The remaining surfaces of the seat were enclosed within the separation envelope. The rest of the apparent body shape represents the demarcation between the separated flow in the interior, and the laminar, potential flow around the exterior. Since the turbulent flow region appeared to stabilize in shape and continue downstream with a constant cross section, this portion was constructed ten body lengths long and capped with a surface normal to the freestream. It was reasoned that by being that far downstream, the 90 degree edge would have little effect on the results near the seat itself. In addition, at the junction of the envelope and the seat cowlings, there were still some slight edges present. This was unavoidable with the geometry software available, and the results will be clearly evident.

To perform the analysis, QUADPAN was chosen for its ease of use and student

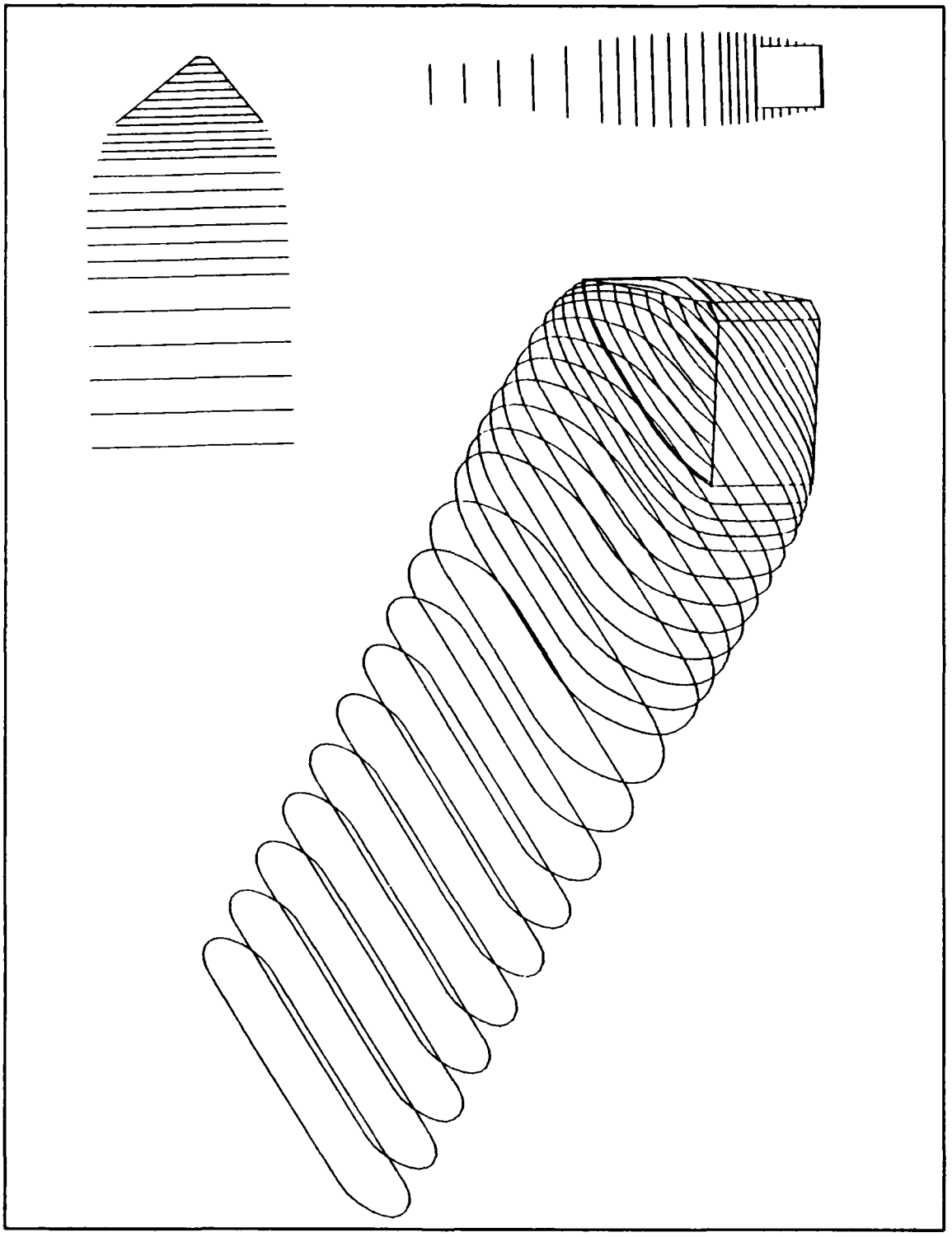

Figure 6.1. PRESS Apparent Body Computer Model

availability. Arrangements were made with the Aircraft Dynamics Branch of the 4950 Test Wing to utilize their Computational Aerodynamic Workstation (CAW). This facility features QUADPAN on a DEC MicroVax III minicomputer. In addition, the CAW incudes a digitizing pad and associated software, and a graphics system to display the geometry and results.

QUADPAN Results

QUADPAN outputs data of two types. First, it determines the pressure coefficient at the control point of each panel. Next, the code uses those C_p's and the area and orientation of each panel to determine forces and moments of the vehicle.

Pressure Data The overall pressure distribution on the impact surfaces is shown in coefficient form in Figure 6.2. Recalling that decreasing C_p indicates increasing local velocity, the large gradients near the sides clearly show the effects of the edges on the apparent body. These gradients are a result of the velocity spikes discussed earlier (see page 6-3). However, as will be shown in the next section, the edge effects were not a significant problem.

Comparison to Wind Tunnel Results Recalling from the discussion on page 2-3 and Figure 2.1, the cowling pressure taps were staggered in six rows to avoid flow interference. These rows were located at 0.712, 0.837, and 0.962 inches from the centerline, and will be referred to as the inner, center, and outer row, respectively. Due to symmetry, only the starboard ports will be considered. If we take the contour plots in Figure 6.2 and cut slices at the appropriate distance, we can plot the pressure coefficient distribution for that station. If we then overlay on those plots the experimental data, a comparison can be made between the QUADPAN and wind tunnel results. These comparisons can be seen in Figures 6.3 through 6.5. One can see that there is a very close correlation between the experimental data and the values predicted by QUADPAN for the impact surfaces.

In Figure 6.3 we see that the predicted pressures are consistently higher than the experimental pressure ports for the front cowling with three exceptions (ports 12, 20,

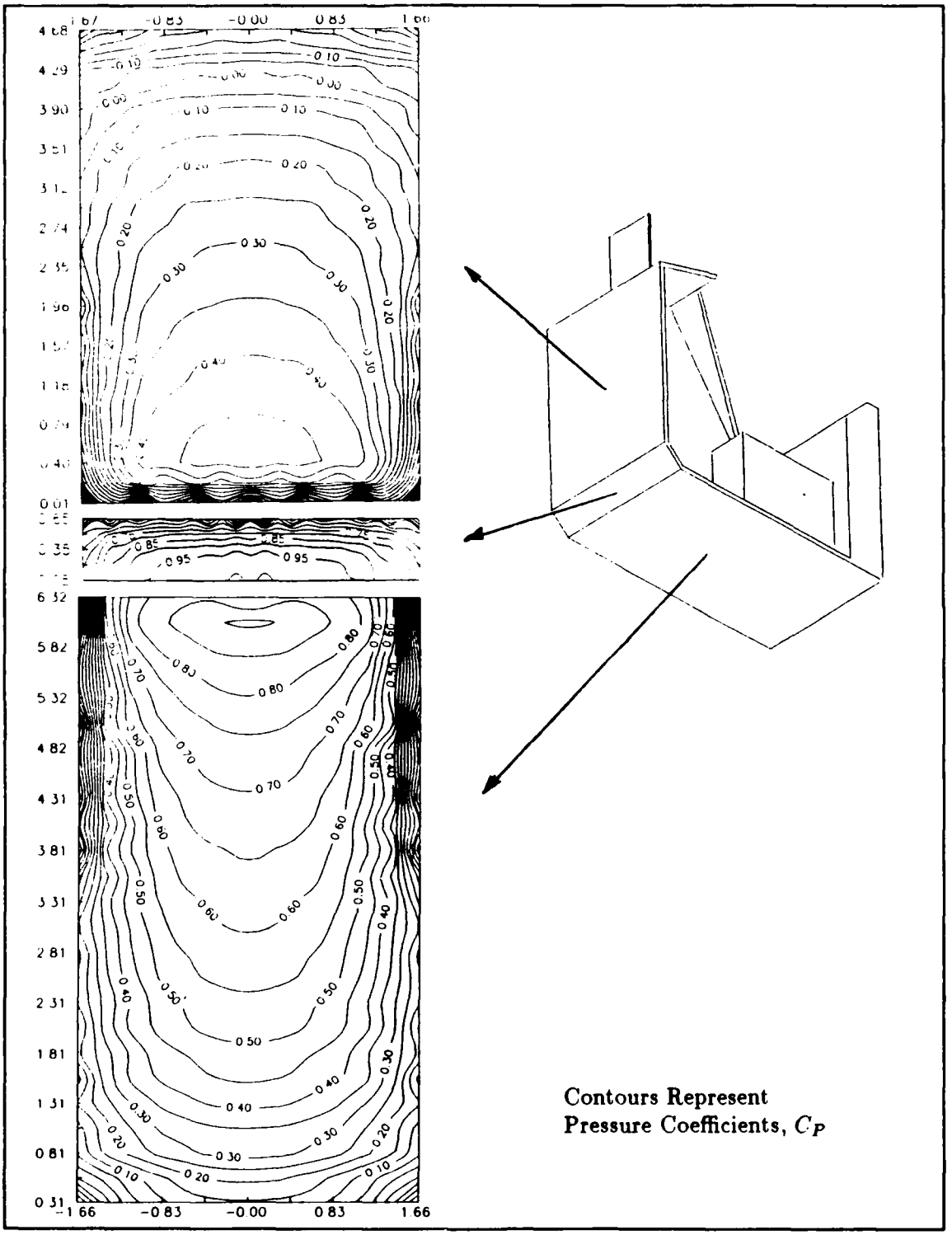

Figure 6.2. QUADPAN Pressure Output for Impact Surfaces

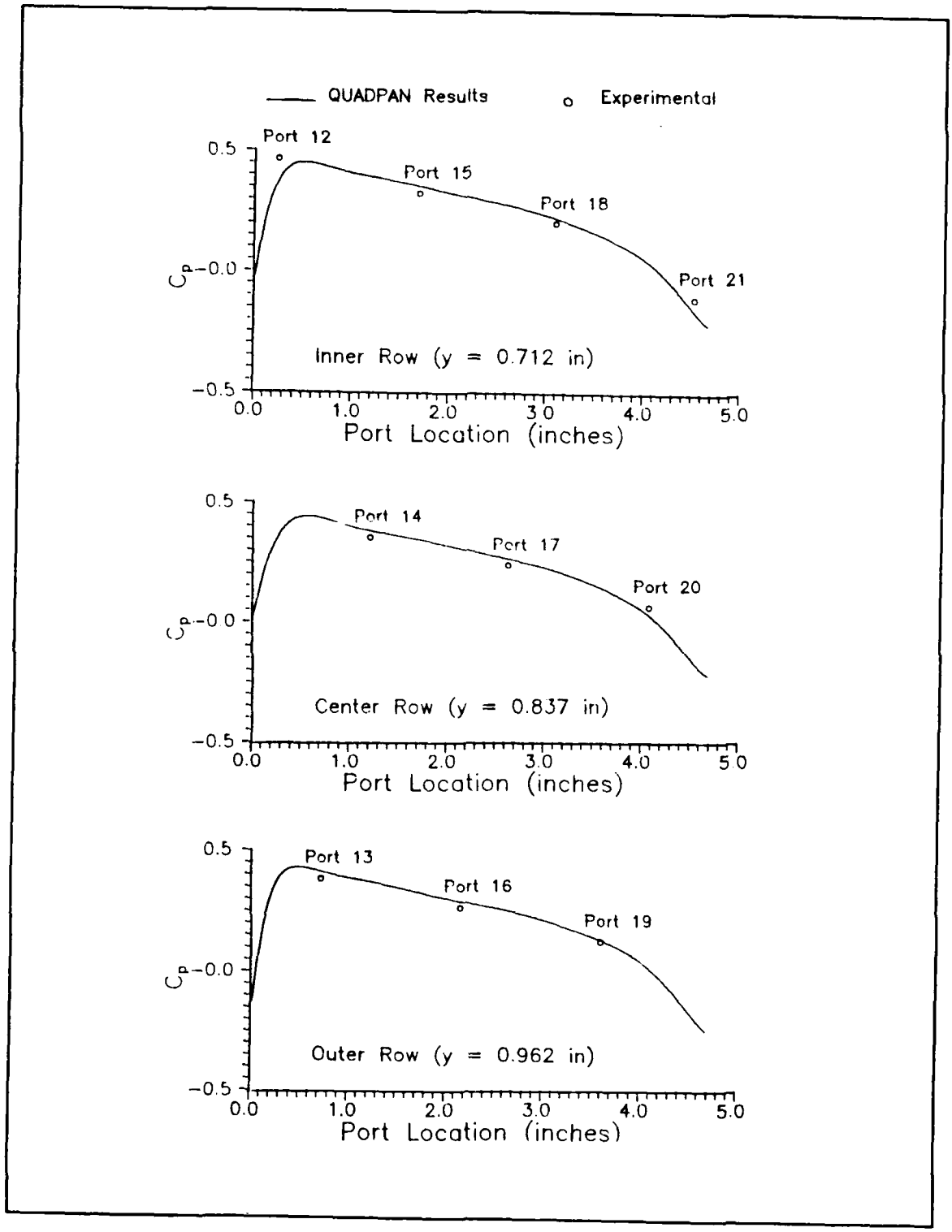

Figure 6.3. QUADPAN/Wind Tunnel Comparison of C_p for Front Cowling

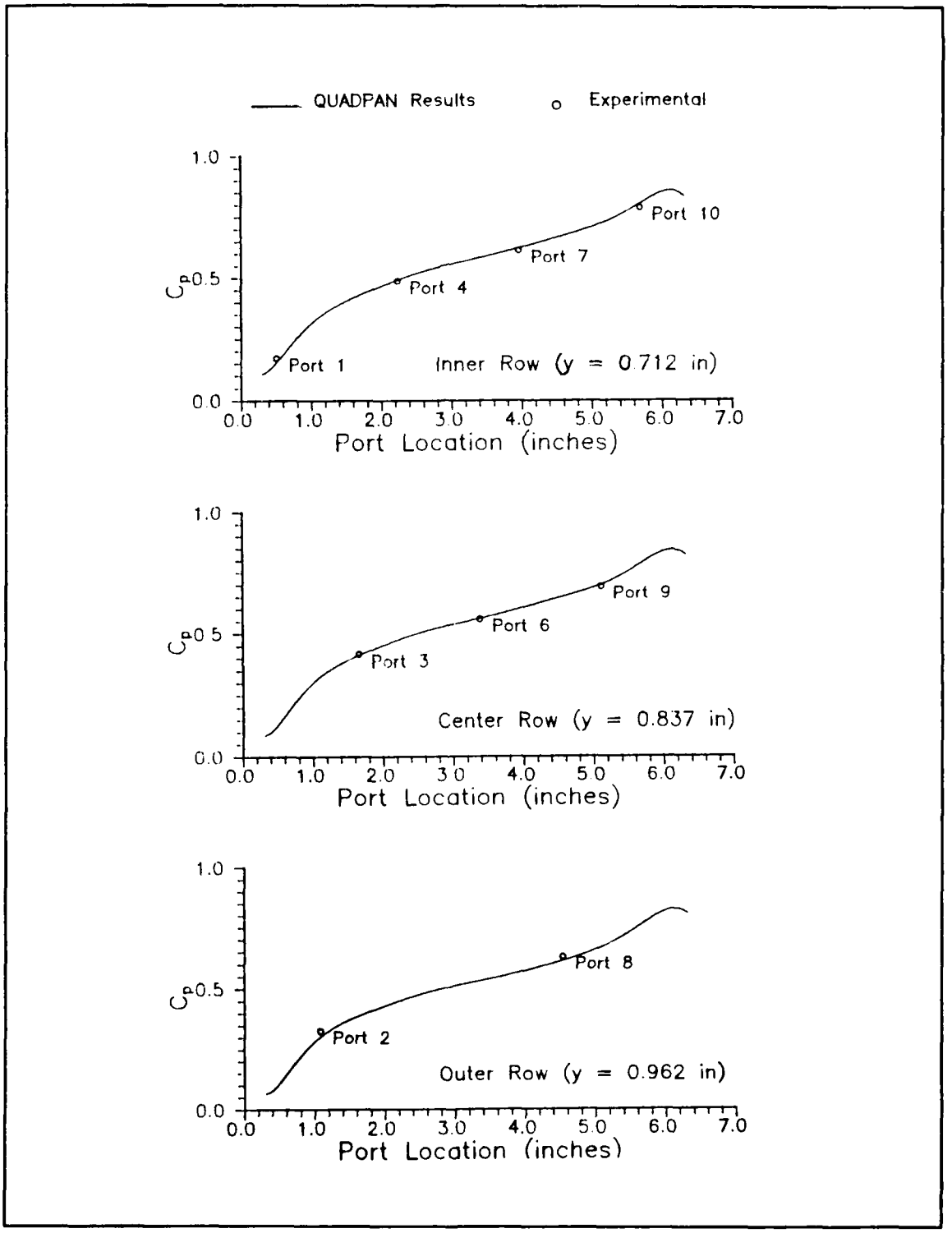

Figure 6.4. QUADPAN/Wind Tunnel Comparison of C_p for Bottom Cowling

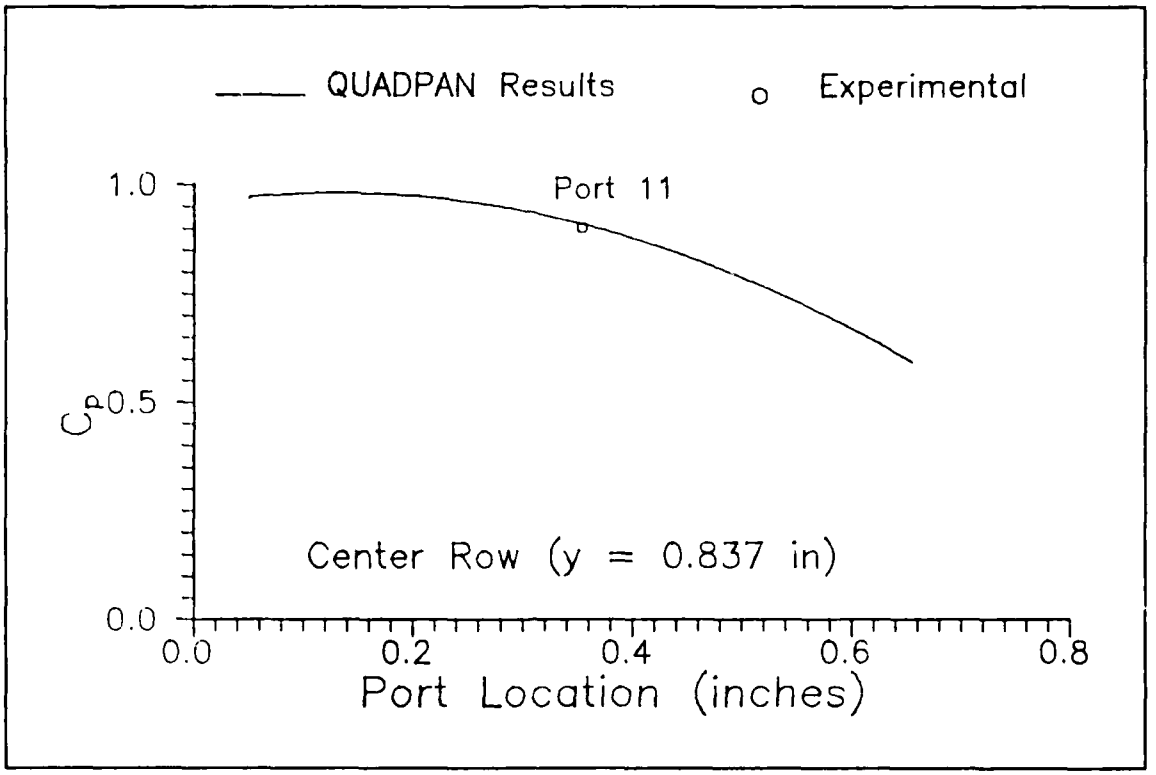

Figure 6.5. QUADPAN/Wind Tunnel Comparison of C_p for Chamfer

and 21). These ports, however, are located in regions where the computational edge effects are locally significant, driving the analytical C_p values down. The one data point on the chamfer (see Figure 6.5) matches the predicted curve quite well. In Figure 6.4, we see that the analytical solution and the wind tunnel results are also almost perfectly matched. Overall, port 12 represents the worst case with an error of $\Delta C_p = 0.1$, which corresponds to a velocity error of 9.7%. It should be noted that port 5 was omitted from the data, because that channel was reporting erroneous pressures, possibly due to debris in the tubing.

It should be noted that the reported experimental results are an average of two test points, thus there is not a large statistical base from which to draw conclusions. In addition, the angle of attack for the experimental data was approximately 51.5 degrees, compared to the 52 degrees for the analytical case. Referring to Figure 4.9, we see that some ports are very sensitive to α at these angles of attack. Therefore, one might conclude that this might

be the reason that the data for the front cowling is predicted too high. However, since the model was at too low an α, one would expect the experimental pressure results to be too high on the front cowling, which is more normal to the flow, and too low on the bottom cowling. This is not the case. Another possible source of error is that the dynamic pressure was not corrected for blockage effects. Again, however, this should affect the pressure data uniformly. Therefore, although these may be factors, there must be other reasons for the discrepancy.

The most probable explanation lies in the construction of the apparent body. If the envelope in the regions of the front cowling were located too far laterally from the seat, the PRESS would appear blunter than normal, which would result in higher pressures. Since only one configuration was analyzed, however, one cannot determine the sensitivity of the QUADPAN results to body shape.

Pressure data comparisons elsewhere on the model are more difficult because QUADPAN can only predict pressures on the surface of the apparent body, and all regions other than the impact surfaces have no physical counterpart. Therefore, one can only compare trends rather than exact points. The pressure coefficients measured by the pressure taps on the upper cowling and the head shield at α = 52 degrees ranged from -0.51 to -0.60. The analytical results in this region were approximately -0.57 to -0.60. Thus, there is a reasonably good correlation for the data in this region. For the tap on the seat pan (port 50), experimental data shows a C_p of -0.77 at α = 52 degrees. This compares to QUADPAN predictions of approximately -0.43. Therefore, it would appear that the pressures behind the cowling where the major flow separation is occurring cannot be predicted with any reliability.

Force And Moment Data QUADPAN uses the pressure coefficients on each panel, the direction of the panel's surface normal vector, and a moment reference center to determine force and moment coefficients on the vehicle. It was a goal of this thesis to determine whether QUADPAN could provide such data for the PRESS using the apparent body approach. Unfortunately, this data was not even close enough to identify trends. There are several possible explanations for this, but the main reason is that the apparent body

approach provides pressure data not on the surface of the seat, but at some point out in the flow where the turbulent flow transitions into laminar flow. Since turbulence is by definition a mixing flow, the flow conditions at the surface of the apparent body are quite different from those found on the model itself. Another reason for the poor correlation is that the analytical model consists of surfaces that have no physical counterparts, such as the extended tail behind the seat. Although QUADPAN is capable of ignoring specified panels for force calculations, the geometry of the problem still left a large amount of excess surface area. Finally, since QUADPAN is a potential code based on inviscid flow theory, there is no friction drag, and since the turbulent region was removed from consideration by being placed inside the body, there was no drag resulting from turbulence, which for the PRESS is a major portion of the overall drag. Thus, the drag was poorly calculated, which in turn contributes to the poor result in the pitching moment calculations. The result of all this is the apparent body approach worked very well for the wetted surface pressures but did not work well for forces and moments for this test case.

VII. Summary Of Results and Conclusions

This chapter will present a summary of the results and conclusions reached in the previous chapters.

Stability Characteristics of the PRESS

Wind tunnel testing showed that the PRESS in the baseline configuration is laterally and directionally stable in ejected flight at low speeds, but exhibits unacceptable pitching moment behavior. However, it was demonstrated that the pitch stability can be greatly improved with the addition of aerodynamic fins. Improvements can also be made in the directional stability of the seat with the addition of yaw fins, but testing showed that the fins cause lateral instabilities.

In addition, the center of pressure was located for the desired trim angle of 35 degrees, and analysis showed that the PRESS could be trimmed and stabilized at this angle by shifting the center of gravity 3.24 inches from its present location. By adding the short tail, a smaller shift of only 1.5 inches can trim and stabilize the PRESS at 35 degrees.

Computer Analysis Results

This study showed that by constructing an apparent body for the PRESS and its flow separation regions, a subsonic paneling code such as QUADPAN is capable of accurately predicting aerodynamic pressure coefficients on the impact surfaces, and those surfaces close to the apparent body surface. However, the program was not able to predict pressures measured at a point on the seat just below the pilot's leg. Therefore, it appears that flow behavior behind the cowling where severe turbulence was occurring cannot be reliably determined with this method. In addition, the code was incapable of accurately determining force and moment coefficients. This was because the code determined the flow characteristics on the apparent body surface only, which are quite different than the characteristics on the surface on the seat itself, with the exception of the cowling which formed the leading edge of the apparent body.

Conclusions

This thesis has proven the aerodynamic feasibility of the Prone Escape System. Although stability and the correct trim was achieved with external fins and/or a shift in the PRESS's center of gravity location, it should be possible to accomplish this with a simple refinement in the external shape of the cowling itself. Therefore,it is recommended that an aerodynamic refinement be performed on the cowling and further wind tunnel testing be performed.

Bibliography

1. Bennet, David. Former Engineer, Deputy for Life Support Systems, ASD, Wright-Patterson AFB, OH 45431. Personal interview, 1988.
2. Burton, Russell R. "A Conceptual Model for Predicting Pilot Group G Tolerance for Tactical Fighter Aircraft". *Aviation, Space and Environmental Medicine*, 57:733–744, August 1986.
3. Chaing, Donald C. *Computer Code for the Determination of Ejection Seat/Man Aerodynamic Parameters.* Technical Report AFOSR-80-0147, Air Force Office of Scientific Research, 1980.
4. Disselkoen, Allen D. et al. *Prone Escape System (PRESS) Design Study.* Master's thesis, School of Engineering, Air Force Institute of Technology (AU), Wright-Patterson AFB, OH, December 1987. AFIT/GSE/AA/87D-2. (AD-B 118011).
5. Gething, Michael J. et al. *The Great Book of Modern Warplanes.* Portland House, New York, 1987.
6. Hubert, James H. Vehicle Equipment Division, Flight Dynamics Laboratory, Wright-Patterson AFB, OH 45431. Personal interview, 1988.
7. Jines, Lanny. Aircrew Escape Branch, Flight Dynamics Laboratory, Wright-Patterson AFB, OH 45431. Personal interview, 1988.
8. Kuethe, Arnold M. and Chuen-Yen Chow. *Foundations of Aerodynamics.* John Wiley & Sons, New York, third edition, 1976.
9. Pope, Alan and William H. Rae Jr. *Low Speed Wind Tunnel Testing.* John Wiley and Sons, New York, 1984.
10. Roskam, Jan. *Airplane Flight Dynamics and Automatic Flight Controls, Part I.* Roskam Aviation and Engineering Corporation, Ottawa, Kansas, 1979.
11. Shereda, Don. Aeromechanics Division, Flight Dynamics Laboratory, Wright-Patterson AFB, Oh 45431. Personal interview, 1988.
12. Youngren, Harold H. et al. *QUADPAN Users Manual Ver 3.2.* Technical Report LR 30563, Lockheed Corporation, 1984.

Appendix A. *Wind Tunnel Program Algorithm*

This section will briefly describe the program used at the AFIT five foot wind tunnel in terms of procedural steps. The program can be separated into four major components: calibration, data collection, tare slope calculation, and data reduction/presentation. The entire program runs from a menu, incorporating all parts into one very user-friendly package.

Calibration

At the beginning of any test program, four types of calibrations must be performed: strain gage, sting bend, angle of attack, and pressure. The computer programs role in these calibrations will be discussed below.

Balance Strain Gage Calibration The strain gage balance consists of six gages: two normal force (*N1* and *N2*), two side force (*Y1* and *Y2*), an axial force gage, (*AX*), and a rolling moment gage (*RM*). The purpose of the strain gage calibration is to determine the relationship between the applied force and the balance voltage output, i.e. pounds per volt for each gage. Each of these gages must be calibrated for both positive and negative loads, with the exception of *AX* which is calibrated in the positive direction only. Positive loads on the balance are defined as follows: normal force is upward ($\approx$ lift), axial is rearward ($\approx$ drag), side force is to the right when looking forward ($\vec{N} \times \vec{AX} = \vec{Y}$), and positive rolling moment is right wing down.

The calibration procedure calls for hanging weights from a calibration body mounted on the balance such that the applied force is aligned with the line of action of the gage in question. The output voltage of all six gages and the applied weight is recorded by the computer. It is important to record the output voltage of all six gages regardless of which gage has the applied weight. Even though 50 lbs is being applied to the *N1* gage, the output voltages of the other five gages will change as well. This behavior is called gage interaction. The weight is incremented throughout the expected range, both positively and negatively.

Next, a least squares linear regression is performed on the voltage data collected to obtain volts per pound values for each gage. This step includes the interaction effects, i.e. the voltage change in *Y1* due to a force applied to, say, *N2*. This results in 72 values (6 gages $\times$ 6 forces $\times$ 2 directions). These values are stored in a file called the balance calibration file.

Sting Bend Calibration As forces are applied to the model during a test, the sting will bend, changing the angle of attack. The purpose of the sting bend calibration is to determine the amount of bend the sting undergoes in degrees per pound of load, as well as sting twist due to external torques. In the above procedure, each incremental weight is applied with the balance at a zero degree angle of attack. As each weight is applied, the sting bends a small amount. This angle is recorded along with the applied force, and the balance is then restored to zero degrees by pitching the yoke. The next weight is then applied, and the process is repeated. Thus, both calibrations are performed simultaneously. Required data is vertical bend due to positive and negative normal loads, horizontal bend due to side forces, and twist due to rolling moments. For this step, it is assumed that the bend is symmetrical, i.e, the sting bends the same for positive forces as it does for negative forces. The positive and negative measurements serve as a check, and if they differ, an average can be use. Tables are created and input into the program that relates total sting bend to applied force for *N1*, *N2*, *Y1*, and *Y2*, and sting twist to *RM*, and stored until needed for data reduction.

Angle of Attack Calibration The previous two calibrations can theoretically be performed only once per balance, although good testing procedures dictate it be done for each test. However, the angle of attack calibration must be done for each model. Since the sting bends with applied force, the weight of the model itself will change it's own angle of attack. To account for this, the model is placed at known angles of attack as measured by an inclinometer, and the voltage from the α potentiometer is recorded. These values will differ, however, if the model is placed in sideslip, β, due to mechanical reasons. Therefore, this procedure must be repeated for various sideslip angles as well. This data is entered into the computer as α versus volts in tabular form for each β. As above, this data is

stored until needed by the data reduction program. In addition, values of β angles versus β voltage is also recorded.

Pressure Calibration The data acquisition system measures two pressure values using voltage levels: dynamic pressure and base pressure. Each must be properly calibrated to produce accurate readings. This is done by using a dead weight tester or similar device to provide known pressures and record output voltages. The data is tabulated and stored in a pressure calibration file for use by the data reduction routines.

Data Collection

The data collection procedure is as follows:

1. The operator inputs several lines of data such as model configuration, roll angle and barometric pressure. The computer labels the data and places it in the resulting raw data file for that particular run.
2. The model is placed at zero α, and strain gage voltages are collected with the wind off. This will be referred to as the zero point. Each data point is actually a statistical set of data returned to the Z-248 computer from the Hewlett-Packard digital data acquisition unit. The unit takes a number of data points (user selectable) and returns to the Z-248 computer the high, low, mean, and standard deviation of that measurement set, which is then presented to the operator. If voltage spikes appear in the data, the operator can abort the run; otherwise the wind is brought up to speed and the model placed in position for the first data point. The zero point can also be used to perform steps such as calibrating the onboard pressure transducer.
3. The model is then incremented through α, typically from low to high, and data is collected at each point. Run data includes air temperature in the tunnel, dynamic and base pressure voltages, strain gage voltages, α and β potentiometer voltages, and any other data the operator chooses to include such as pressure port data from the model. As above, each set of data is presented to the operator for approval or a

retake. This data should include some repeat points with sting movement reversed to check for repeatability and hysteresis effects.

4. At the completion of the run, the operator then inputs a line into the data file indicating repeat points or other problems which occurred during the run. The data file is then stored until needed for data reduction.

Tare Slope Calculation

The purpose of tare data, is to eliminate the model's weight contribution to the total forces and moments measured by the balance. To accomplish this, it is necessary to know the models weight, and the location of it's center of gravity relative to the balance moment center. This is calculated by either direct physical measurement or using the tare slope calculation routines in the computer. This procedure was developed by the author and is outlined in detail in Appendix B.

Data Reduction

The data reduction program, although a small portion of the overall package, is the heart of the wind tunnel data acquisition system. This set of routines takes the raw voltages and creates aerodynamic coefficients in three axis systems: body, stability, and wind. The steps performed by the computer during this process are described below.

1. The first step is to calculate α and β from the voltage levels. This is done by creating two tables of voltages in the form shown in Table A.1. First, a cubic spline function is fit to the β table to determine the sideslip angle from the measured value. Then, using the α table, a column of α voltages for the determined value of β is constructed by interpolating between the existing columns. Then a cubic spline is used to determine the correct value for α.
2. Cubic spline functions are fit to the dynamic pressure and the base pressure calibration files to determine the values from the raw voltages.
3. The raw voltages, E, from the strain gage balance are then analyzed to determine whether a positive or a negative load is being applied to each. Then the appropriate

Table A.1. Angle Spline Tables

β	
Deg	Volts
-6	1.942
-4	2.140
-3	2.237
-2	2.334
0	2.538
2	2.737
3	2.834
4	2.931
6	3.134

α			
Deg	Volts		
α	$\beta = 0$	$\beta = 3$	$\beta = 6$
-6	1.727	1.721	1.706
-4	1.867	1.858	1.843
-2	2.008	2.002	1.985
0	2.149	2.143	2.128
⋮	⋮	⋮	⋮
22	3.725	3.718	3.681
24	3.865	3.854	3.816
26	4.005	3.991	3.990

values are retrieved from the balance calibration file and placed into a sixth order matrix equation of the form

$$\begin{bmatrix} \frac{\partial E_{N1}}{\partial F_{N1}} & \cdots & \frac{\partial E_{N1}}{\partial M_{RM}} \\ \vdots & \ddots & \vdots \\ \frac{\partial E_{RM}}{\partial F_{N1}} & \cdots & \frac{\partial E_{RM}}{\partial M_{RM}} \end{bmatrix} \begin{Bmatrix} F_{N1} \\ \vdots \\ M_{RM} \end{Bmatrix} = \begin{Bmatrix} E_{N1} \\ \vdots \\ E_{RM} \end{Bmatrix} \tag{A.1}$$

The zero point is then subtracted from each measured voltages E. This accounts for any non-zero voltages for zero load inaccuracies and provides a force difference from a known condition, i.e. wind off. The results are the placed into the right side of the Eq (A.1), and the values for the forces and moments are then found using a matrix inversion technique.

4. After the forces are found, the bend corrections are applied. A cubic spline function is fit to the bend calibration data and the measured forces are input to provide the sting bend and twist angles. This procedure was rewritten by the author to account for sting prebend and roll angles. The corrections are then applied to α, β, and ϕ.

5. After the forces and true sting angles are calculated, the tare equations of Appendix B are applied to determine the aerodynamic forces and moments.

6. The program then uses the temperature in the tunnel, the total pressure input by the operator, and the measured dynamic pressure to find such parameters as air density, viscosity, speed of sound, and Mach number. Using the latter two the program then

finds the velocity of the air in the tunnel and the true dynamic pressure, q. This differs from the measured dynamic pressure due to compressibility effects. During this step corrections are applied to q to account for factors such as tunnel skew and model blockage effects.

7. The next step is to use the reference values and dynamic pressure to nondimensionalize the measured forces and moments as described in Chapter III. The buoyancy, induced drag, and base pressure corrections to the drag coefficient are then applied. The data produced here is in body coordinates (see page 3-2). The moment coefficients are calculated at the balance moment center and can be transferred to any point the user wishes, such as the CG of the full scale vehicle. Corrections to α and β due to sting prebend and roll are then applied.

8. Finally, coordinate transformations are performed to put the coefficients in stability and wind coordinate systems (see page 3-3).

When data reduction is complete, the program provides a method of printing out a complete record of the reduced data of any data run, as well as providing direct access to a commercial plotting routine.

Appendix B. *Tare Slope Corrections and Calculations*

A difficulty in all wind tunnel testing is that strain gage balances cannot differentiate between aerodynamic and gravitational forces. Thus, it is necessary to determine the model's weight contribution to the total forces and moments measured for each axis as a function of its orientation. These weight effects are called tare. The following will present the basic form of tare equations, develop the transformation matrix required to convert the weight vector into body axis components, and present the final tare equations as used in the program. Finally, the method of experimentally determining the tare slopes of the model will be presented.

General Form of Tare Equations

Model orientation is provided by mechanizing the model support sting with four possible rotations. First, the yoke can be pitched up and down an angle θ. Second, the yoke can be yawed left or right to an angle, ψ. Rolling the sting in the yoke to an angle, ϕ, is a third possible movement. Lastly, the sting can have a prebend in the balance's $\vec{XY}$ plane of an angle γ. This results in the weight component along any axis being a function of θ, ϕ, and γ. ψ is not a factor because it is measured about an axis parallel to the gravity vector.

The first step is to develop a general equation for the tare forces. We can write the total forces along any axis 'Q' as measured by the balance as

$$F_{Q_T} = F_{Q_A} + F_{Q_0} + F_{Q_W}(\theta, \phi, \gamma) \tag{B.1}$$

where

F_{Q_T}	=	Total force measured along 'Q' axis
F_{Q_A}	=	Aerodynamic force along 'X' axis
F_{Q_0}	=	Forces other than model weight, measured at zero airspeed
$F_{Q_W}(\theta, \phi, \gamma)$	=	Weight component of model as function of θ, ϕ, and γ

The F_{Q_0} term may need further explanation. Due to the inherent nature of strain gage balances, the gages may indicate a voltage due to a non-zero offset of the bridge balance

with no external load present. Since this is not accounted for in the gage coefficient matrix, it will show up in the data reduction as a virtual force. From the discussion on data reduction, we know that we subtract the zero point from each data point. The zero point is the algebraic sum of F_{Q_0} and $F_{Q_W}(0,\phi,\gamma)$. Therefore, subtracting these terms from both sides of Eq (B.1) yields:

$$F_{Q_C} = F_{Q_A} + F_{Q_W}(\theta,\phi,\gamma) - F_{Q_W}(0,\phi,\gamma) \tag{B.2}$$

where

F_{Q_C} = Corrected force $(F_{Q_T} - F_{Q_0} - F_{Q_W}(0,\phi,\gamma))$

The next step is to determine the functional relationship between F_{Q_W} and the rotation angles θ, ϕ, and γ.

Transformation Matrix and Tare Equations

A vector in any coordinate system can be transformed to another system using a maximum of three rotations. In this case, we will transform the weight vector from tunnel coordinates to balance coordinates. We begin with a standard wind axis coordinate system (see page 3-3), and make the following rotations:

1. Rotate an angle θ about the Y_W axis to create an intermediate axis system $X_1Y_1Z_1$. Putting this in matrix form:

$$\begin{Bmatrix} X_1 \\ Y_1 \\ Z_1 \end{Bmatrix} = \begin{bmatrix} \cos\theta & 0 & -\sin\theta \\ 0 & 1 & 0 \\ \sin\theta & 0 & \cos\theta \end{bmatrix} \begin{Bmatrix} X_W \\ Y_W \\ Z_W \end{Bmatrix} \tag{B.3}$$

2. Rotate an angle ϕ about the X_1 axis to create the next intermediate axis system $X_2Y_2Z_2$. In equation form this becomes:

$$\begin{Bmatrix} X_2 \\ Y_2 \\ Z_2 \end{Bmatrix} = \begin{bmatrix} 1 & 0 & 0 \\ 0 & \cos\phi & \sin\phi \\ 0 & -\sin\phi & \cos\phi \end{bmatrix} \begin{Bmatrix} X_1 \\ Y_1 \\ Z_1 \end{Bmatrix} \tag{B.4}$$

3. Rotate an angle γ about the X_2 axis to create the final axis system $X_B Y_B Z_B$. Again, in matrix form:

$$\begin{Bmatrix} X_B \\ Y_B \\ Z_B \end{Bmatrix} = \begin{bmatrix} \cos\gamma & 0 & -\sin\gamma \\ 0 & 1 & 0 \\ \sin\gamma & 0 & \cos\gamma \end{bmatrix} \begin{Bmatrix} X_2 \\ Y_2 \\ Z_2 \end{Bmatrix} \tag{B.5}$$

By performing back substitution, one gets:

$$\begin{Bmatrix} X_B \\ Y_B \\ Z_B \end{Bmatrix} = \begin{bmatrix} \cos\gamma & 0 & -\sin\gamma \\ 0 & 1 & 0 \\ \sin\gamma & 0 & \cos\gamma \end{bmatrix} \begin{bmatrix} 1 & 0 & 0 \\ 0 & \cos\phi & \sin\phi \\ 0 & -\sin\phi & \cos\phi \end{bmatrix} \begin{bmatrix} \cos\theta & 0 & -\sin\theta \\ 0 & 1 & 0 \\ \sin\theta & 0 & \cos\theta \end{bmatrix} \begin{Bmatrix} X \\ Y \\ Z \end{Bmatrix} \tag{B.6}$$

The above expression will transform force vectors from the tunnel coordinate system into balance coordinates. A problem with this is that strain gage coordinate systems typically are not calibrated with this orientation. Standard procedure is to calibrate the balance such that a positive force will generate a positive voltage and vica versa. This results in a positive normal force directed upward $(-\vec{Z})$, a positive axial force rearward $(-\vec{X})$, and a positive side force to the right $(+\vec{Y})$. This is shown along with the tunnel axis system in Figure B.1. Using this convention, the weight vector in balance coordinates is

$$\vec{F}_{B_W}(\theta,\phi,\gamma) = -F_{A_W}(\theta,\phi,\gamma)\vec{X}_B + F_{S_W}(\theta,\phi,\gamma)\vec{Y}_B - F_{N_W}(\theta,\phi,\gamma)\vec{Z}_B \tag{B.7}$$

and the weight vector in the wind axis system is

$$\vec{W} = 0\vec{X} + 0\vec{Y} + W\vec{Z} \tag{B.8}$$

We now substitute Eqs (B.7) and (B.8) into the first and last column vectors of Eq (B.6) respectively:

$$\begin{Bmatrix} X_B \\ Y_B \\ Z_B \end{Bmatrix} \Rightarrow \begin{Bmatrix} -F_{A_W}(\theta,\phi,\gamma) \\ F_{S_W}(\theta,\phi,\gamma) \\ -F_{N_W}(\theta,\phi,\gamma) \end{Bmatrix} \qquad \begin{Bmatrix} X \\ Y \\ Z \end{Bmatrix} \Rightarrow \begin{Bmatrix} 0 \\ 0 \\ W \end{Bmatrix} \tag{B.9}$$

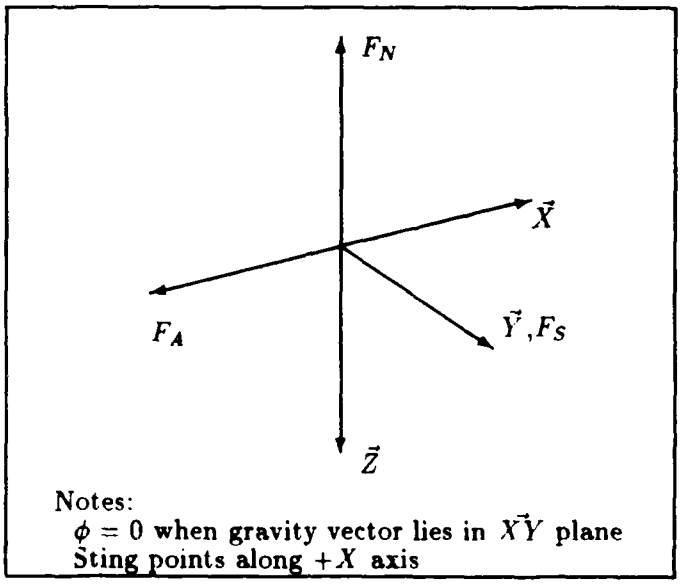

Figure B.1. Balance Coordinate System

Performing the algebra yields the equations we need:

$$\begin{aligned} F_{A_W}(\theta,\phi,\gamma) &= W\cos\gamma\sin\theta - W\sin\gamma\cos\phi\cos\theta \\ F_{S_W}(\theta,\phi,\gamma) &= W\sin\phi\cos\theta \\ F_{N_W}(\theta,\phi,\gamma) &= W\sin\gamma\sin\theta - W\cos\gamma\cos\phi\cos\theta \end{aligned} \tag{B.10}$$

By substituting Eq (B.10) into Eq (B.2), evaluating, and rearranging, the force tare equations become:

$$\begin{aligned} F_{A_A} &= F_{A_C} - W\cos\gamma\sin\theta - W\sin\gamma\cos\phi(\cos\theta - 1) \\ F_{S_A} &= F_{S_C} - W\sin\phi(\cos\theta - 1) \\ F_{N_A} &= F_{N_C} - W\sin\gamma\sin\theta + W\cos\gamma\cos\phi(\cos\theta - 1) \end{aligned} \tag{B.11}$$

Next, we must obtain the moment tare equations. These equations are of the same form as Eq (B.2)

$$M_{Q_C} = M_{Q_A} + M_{Q_W}(\theta,\phi,\gamma) - M_{Q_W}(0,\phi,\gamma) \tag{B.12}$$

They result from the forces in Eq (B.10) acting through the model's center of gravity (CG) located some finite distance from the balance moment center (BMC). Figure B.2

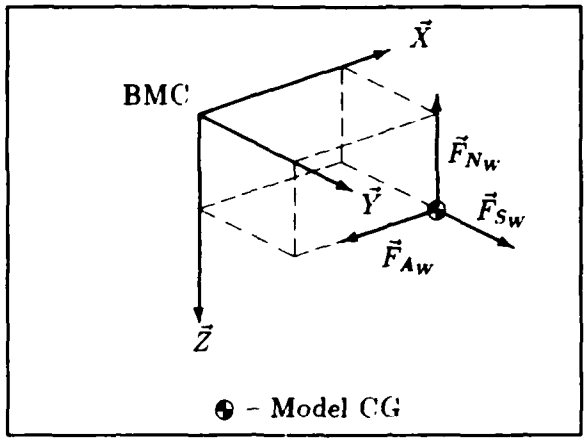

Figure B.2. Weight Induced Moments (Body Coordinates)

shows the relationship between the BMC and the model's weight force components in body coordinates.

Referring to Figure B.2, it is clear that a positive F_{N_W} acting at the CG will result in a negative rolling moment about the X-axis and a positive pitching moment about the Y-axis. Similarly, a positive F_{A_W} will create a negative pitching moment and a positive yawing moment. Defining the location of the model's CG relative to the BMC as scalar values x, y, and z along their respective axis, we can write the roll, pitch, and yaw moments about the BMC due to the model's weight in body coordinates as

$$\begin{aligned} M_{R_W} &= -yF_{N_W} - zF_{S_W} \\ M_{P_W} &= xF_{N_W} - zF_{A_W} \\ M_{Y_W} &= xF_{S_W} + yF_{A_W} \end{aligned} \tag{B.13}$$

Substituting Eq (B.10) into Eq (B.13) yields:

$$\begin{aligned} M_{R_W} &= Wy(\cos\gamma\cos\phi\cos\theta - \sin\gamma\sin\theta) - Wz\sin\phi\cos\theta \\ M_{P_W} &= Wx(\sin\gamma\sin\theta - \cos\gamma\cos\phi\cos\theta) - Wz(\cos\gamma\sin\theta + \sin\gamma\cos\phi\cos\theta) \\ M_{Y_W} &= Wx\sin\phi\cos\theta + Wy(\cos\gamma\sin\theta + \sin\gamma\cos\phi\cos\theta) \end{aligned} \tag{B.14}$$

The final moment tare equations result when Eq (B.14) is substituted into Eq (B.12):

$$\begin{aligned} M_{R_A} &= M_{R_C} + Wz\sin\phi(\cos\theta - 1) \\ &\quad + Wy(\sin\gamma\sin\theta - \cos\gamma\cos\phi(\cos\theta - 1)) \\ M_{P_A} &= M_{P_C} - Wx(\sin\gamma\sin\theta - \cos\gamma\cos\phi(\cos\theta - 1)) \\ &\quad + Wz(\cos\gamma\sin\theta + \sin\gamma\cos\phi(\cos\theta - 1)) \\ M_{Y_A} &= M_{Y_C} - Wx\sin\phi(\cos\theta - 1) \\ &\quad - Wy(\cos\gamma\sin\theta - \sin\gamma\cos\phi(\cos\theta - 1)) \end{aligned} \tag{B.15}$$

Tare Slope Calculation

The preceding sections presented the technique for removing the weight component from the measured forces and moments assuming the weight and moment arms are known. This section will present a method of using the strain gage balance and those equations to determine the weight and location of the model CG. The procedure can be divided into a data collection portion and a data reduction portion.

The tare data is collected in a similar manner as the test data (see Appendix A) with two exceptions. First, the wind is off. This serves the purpose of removing all forces and moments due to aerodynamics from Eqs (B.11) and (B.15). Second, the sting is positioned with no roll ($\phi = 0$). This is a restriction that was imposed to keep the program to reasonable size. With these exceptions, Eqs (B.11) and (B.15) reduce to

$$\begin{aligned} F_{A_C} &= W\sin\theta && \text{(a)} \\ F_{S_C} &= 0 && \text{(b)} \\ F_{N_C} &= -W(\cos\theta - 1) && \text{(c)} \\ M_{R_C} &= Wy(\cos\theta - 1)) && \text{(d)} \\ M_{P_C} &= -Wx(\cos\theta - 1) - Wz\sin\theta && \text{(e)} \\ M_{Y_C} &= Wy\sin\theta && \text{(f)} \end{aligned} \tag{B.16}$$

All of the values in Eq (B.16) are now known except W and the products Wx, Wy, and Wz. These four values are collectively called the tare slopes. W can be found by performing a least squares regression technique to Eq (B.16a) or Eq (B.16c). The program allows the user to use the average of the two or pick one. Similarly, Wy can be determined using a least squares regression on Eq (B.16d) or Eq (B.16f). Again, the user can choose to use either value or the average for Wy. Finally, a two dimensional least squares can be used on Eq (B.16e) to determine both Wx and Wz.

Vita

Captain Lonnie R. Dillon was born on [redacted] He graduated from Lawrence High School in 1980 and began attending the University of Kansas. In 1984 he graduated with a degree of Bachelor of Science in Aerospace Engineering. He received his commission in August 1984 upon graduation from Officer Training School at Lackland AFB, Texas. From September 1984 to April 1987 he served as a munitions test engineer with the 3246 Test Wing, Armament Division, at Eglin AFB, Florida. In April 1987 Captain Dillon transferred to the School of Engineering, Air Force Institute of Technology, Wright-Patterson AFB.

[redacted]

REPORT DOCUMENTATION PAGE

Form Approved
OMB No. 0704-0188

1a. REPORT SECURITY CLASSIFICATION UNCLASSIFIED	1b. RESTRICTIVE MARKINGS
2a. SECURITY CLASSIFICATION AUTHORITY	3. DISTRIBUTION/AVAILABILITY OF REPORT Approved for Public Release; distribution unlimited
2b. DECLASSIFICATION/DOWNGRADING SCHEDULE	
4. PERFORMING ORGANIZATION REPORT NUMBER(S) AFIT/GAE/AA/88D-09	5. MONITORING ORGANIZATION REPORT NUMBER(S)
6a. NAME OF PERFORMING ORGANIZATION School of Engineering 6b. OFFICE SYMBOL (If applicable) AFIT/ENY	7a. NAME OF MONITORING ORGANIZATION
6c. ADDRESS (City, State, and ZIP Code) Air Force Institute of Technology (AU) Wright-Patterson AFB, Ohio 45433-6583	7b. ADDRESS (City, State, and ZIP Code)
8a. NAME OF FUNDING/SPONSORING ORGANIZATION Biomedical Protection Branch 8b. OFFICE SYMBOL (If applicable) AAMRL/BBP	9. PROCUREMENT INSTRUMENT IDENTIFICATION NUMBER
8c. ADDRESS (City, State, and ZIP Code) Wright-Patterson AFB, Ohio 45433-6583	10. SOURCE OF FUNDING NUMBERS PROGRAM ELEMENT NO. / PROJECT NO. / TASK NO / WORK UNIT ACCESSION NO.

11. TITLE (Include Security Classification)
A WIND TUNNEL AND COMPUTER INVESTIGATION OF THE LOW SPEED AERODYNAMIC CHARACTERISTICS OF THE PRONE ESCAPE SYSTEM (PRESS)

12. PERSONAL AUTHOR(S)
Connie R. Dillon, B.S., Capt, USAF

13a. TYPE OF REPORT	13b. TIME COVERED	14. DATE OF REPORT (Year, Month, Day)	15. PAGE COUNT
MS Thesis	FROM _____ TO _____	December 1988	103

16. SUPPLEMENTARY NOTATION

17. COSATI CODES			18. SUBJECT TERMS (Continue on reverse if necessary and identify by block number)
FIELD	GROUP	SUB-GROUP	Ejection seats; Water tunnels; Subsonic wind tunnels; Computerized simulation
01	01		

19. ABSTRACT (Continue on reverse if necessary and identify by block number)

Thesis Advisor: Lt Col Paul King
Assistant Professor
Department of Aeronautics and Astronautics

Approved for Public Release IAW AFR 190-1
12 Jan 1989

20. DISTRIBUTION/AVAILABILITY OF ABSTRACT ☒ UNCLASSIFIED/UNLIMITED ☐ SAME AS RPT. ☐ DTIC USERS	21. ABSTRACT SECURITY CLASSIFICATION UNCLASSIFIED
22a. NAME OF RESPONSIBLE INDIVIDUAL Paul I. King, Assistant Professor	22b. TELEPHONE (Include Area Code) (513) 255-2362 22c. OFFICE SYMBOL AFIT/ENY

DD Form 1473, JUN 86 *Previous editions are obsolete.* SECURITY CLASSIFICATION OF THIS PAGE

Due to new design technology, future fighter aircraft will fly at higher g levels than ever before. As a result, a previous preliminary design study was conducted to develop an ejection seat providing higher g-tolerance for the crewmember during maneuvering as well as improved windblast protection during ejection. This seat utilized the crewmember in a prone, or leaning forward, position. The Prone Ejection System (PRESS) was computer simulated at supersonic conditions in the earlier report and found satisfactory. It was the purpose of this research to perform an experimental low speed study of the aerodynamic characteristics of the PRESS. Wind tunnel testing was performed to determine the static stability of the PRESS and measure pressures over the seat. It was determined that static pitch stability did not occur at the desired angle of attack, but could be easily corrected with aerodynamic fins and/or a shift in the center of gravity. Directional stability was also confirmed. In addition, an analytical experiment was performed to determine whether a potential paneling code could be modified to predict flow conditions about the PRESS. An apparent body was constructed by including the regions of flow separation as part of the seat itself. Water tunnel flow visualization was utilized to determine the shape of the apparent body. The computer analysis showed that a paneling code could accurately predict the pressure coefficients on the cowling.